AN ABSTRACT OF THE THESIS OF

Barbara K. Burkholder for the degree of Masters of Science in Water Resources Science presented on November 26, 2007.
Title: Influence of Hyporheic Flow and Geomorphology on Temperature of a Large, Gravel-bed River, Clackamas River, Oregon, USA.

Abstract approved:

Gordon E. Grant Roy Haggerty

The hyporheic zone influences the thermal regime of rivers, buffering temperature by storing and releasing heat over a range of timescales. We examined the relationship between hyporheic exchange and temperature along a 24-km reach of the lower Clackamas River, a large gravel-bed river in northwestern Oregon (median discharge = 75.7 $m^3/s$; minimum mean monthly discharge = 22.7 $m^3/s$ in August 2006). With a simple mixing model, we estimated how much hyporheic exchange cools the river during hot summer months. Hyporheic exchange was primarily identified by temperature anomalies, which are patches of water that demonstrate at least a 1 °C temperature difference from the main channel. Forty hyporheic temperature anomalies were identified through field investigations and TIR (Thermal-Infrared-Radiometry) in summer 2006. The location of anomalies was associated with specific geomorphic features, primarily bar channels and bar heads that act as preferential pathways for hyporheic flow. Detailed field characterization and groundwater modeling on three Clackamas gravel bars indicate residence times of hyporheic water can vary from hours to weeks and months. This was largely determined by hydraulic conductivity, which is affected by how recently the gravel bar formed or was reworked. Upscaling of modeled discharges and hydrologic parameters from these bars to the other anomalies on the Clackamas network shows that hyporheic discharge from anomalies comprises a small fraction (<< 1 %) of mainstem

discharge, resulting in small river cooling effects (0.012 °C). However, the presence of cooler patches of water within rivers can act as thermal refugia for fish and other aquatic organisms, making the creation or enhancement of hyporheic exchange an attractive method in restoring the thermal regime of rivers.

# Influence of Hyporheic Flow and Geomorphology on Temperature of a Large, Gravel-bed River, Clackamas River, Oregon, USA

by
Barbara K. Burkholder

A THESIS

submitted to

Oregon State University

in partial fulfillment of
the requirements for the
degree of

Master of Science

Presented November 26, 2007
Commencement June 2008

Master of Science thesis of Barbara K. Burkholder

Presented on November 26, 2007

APPROVED:

---

Co-major Professor, representing Water Resources Science

---

Co-major Professor, representing Water Resources Science

---

Director of the Water Resources Science Program

---

Dean of the Graduate School

I understand that my thesis will become part of the permanent collection of Oregon State University libraries. My signature below authorizes release of my thesis to any reader upon request.

---

Barbara K. Burkholder, Author

# ACKNOWLEDGEMENTS

I would like to thank my committee members, Dr. Gordon Grant, Dr. Roy Haggerty, Dr. Tarang Khangaonkar, Dr. Peter Wampler, and Dr. John Bailey for their help and support throughout the project. A special thanks to Gordon Grant and Roy Haggerty for their continual encouragement, helpful suggestions, and patience as they have mentored me along the way.

My sincere appreciation to all those who contributed to my field campaign, especially field assistants Heidi Springer, Shawn Majors, and Roger Lewis who all suffered with me through numerous pebble counts and the pains of piezometer installation. I am indebted to Portland General Electric (PGE) biologists Tim Shibahara and Doug Cramer for shuttling our boat every day and to other PGE crew members who offered technical support. Also, thanks to PGE surveyors Rick Belliveau and Larry McGinnis for their expertise and enthusiasm.

I am also grateful to my colleagues and friends at Oregon State University for their knowledge and support. Thanks to Sarah Lewis for her expansive expertise, guidance, and friendship throughout the research process and Anne Jefferson for her knowledgeable input and help with the cooling calculation. Also, thanks to my family and friends who have been a constant source of encouragement and humor.

This material is based upon work supported under a grant from Portland General Electric (PGE) and a cooperative agreement between Oregon State University and the USDA Forest Service. I am grateful to John Esler and Julie Keil at PGE for supporting the research.

## CONTRIBUTION OF AUTHORS

Gordon Grant, Peter Wampler, and Roy Haggerty created the initial study plan and project focus. Gordon Grant and Roy Haggerty provided continual guidance throughout the field campaign and subsequent data analysis. Tarang Khangaonkar provided knowledge of Clackamas River hydrodynamic model CE-QUAL-W2. All listed authors also contributed several helpful reviews and suggestions in preparation of and during the writing of the manuscript.

TABLE OF CONTENTS

Page

LIST OF APPENDICES

LIST OF FIGURES

LIST OF TABLES

LIST OF APPENDIX FIGURES

LIST OF APPENDIX TABLES

# 1 INTRODUCTION

A river's thermal regime is a key factor in determining the overall health of the river ecosystem. River temperature controls what species can exist within the river, as well as the distribution of those species (Vannote *et al*., 1980; Ebersole *et al*., 2001). It determines growth rates of aquatic organisms and timing of emergence and movement for fish such as salmon (Elliot and Hurley, 1997; Johnston, 1997). Water temperature also influences microbial processing rates, which govern nutrient cycling (Edwards, 1998).

River temperature varies diurnally and seasonally, cycles determined by numerous, interrelated variables and heat exchange processes (Fig. 1.1). Although these drivers may change naturally over time, several studies document how anthropogenic impacts, whether applied directly to a river (e.g. channel diversion, dams, or wastewater discharge) or to the land surrounding a river (e.g. deforestation, urbanization), can affect a river temperature (e.g. Brown, 1970; Webb and Walling, 1993b; Johnson and Jones, 2000; Lowney, 2000; Sinokrot and Gulliver, 2000). This is the case on the 6$^{th}$-order, lower Clackamas River, where reservoir heating from a series of hydroelectric dams has resulted in a 1-3 °C increase in maximum daily temperature during summer low flows.

Regulatory temperature standards, such as those set by the Federal Clean Water Act, are created to maintain high quality aquatic habitat and motivate mitigation when river temperatures are out of compliance. However, mitigating temperature changes in rivers is no easy task. In trying to decrease river temperature, one mitigation approach is to increase shade, although this benefit decreases as rivers get wider and the fraction of effectively shaded river decreases. Floodplain restoration may lead to the development of alcoves or side channels that can provide thermal refugia for aquatic organisms (Bryenton, 2007). This project investigates another thermal mitigation strategy based on increasing hyporheic exchange through a planned program of gravel augmentation.

Hyporheic exchange, where river water downwells into the shallow subsurface and reemerges back into the main channel after a period of time, occurs where there

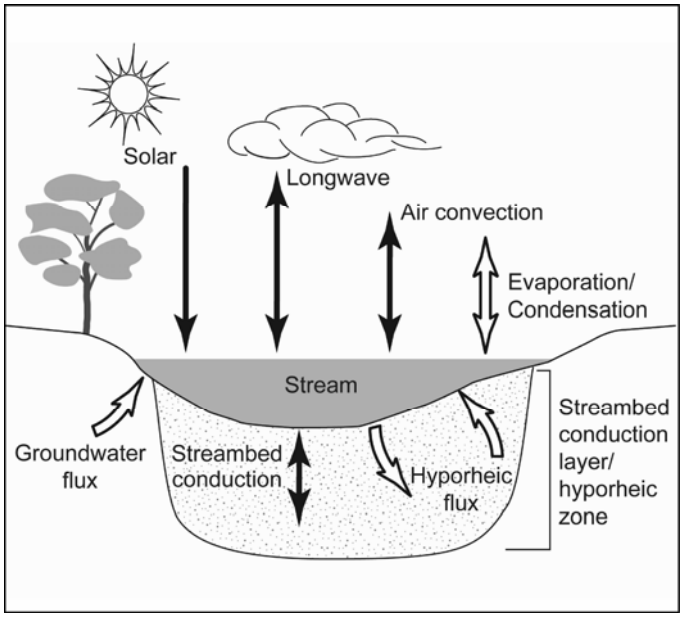


**Figure 1.1 Heat exchange mechanisms that comprise river temperature budgets. From Loheide and Gorelick (2007).**

are changes hydraulic gradient within the river channel. This leads to river water downwelling into the channel bed, banks, or across bar morphology. The residence time of the water within the hyporheic zone can lead to out-of-phase mainstem and hyporheic temperatures, where reemerging hyporheic water is cooler than the mainstem in the middle of the afternoon and warmer than the mainstem at night. This buffers river temperature fluctuations, which could decrease maximum and minimum temperature peaks (Fig. 1.2). This effect is well documented over a range of river sizes and bar morphology. Most studies observe a localized effect associated with bar morphology, where emerging hyporheic water has a different temperature than the mainstem (White *et al*., 1987; Evans and Petts, 1997; Brown *et al*., 2005; Hancock and Boulton, 2005; Moore *et al*., 2005; Sliva and Williams, 2005; Cozzetto *et al*., 2006; Fernald *et al*., 2006), but some studies do document a buffering of overall river temperature (Arscott *et al*., 2001; Johnson, 2004). For example, Johnson (2004)

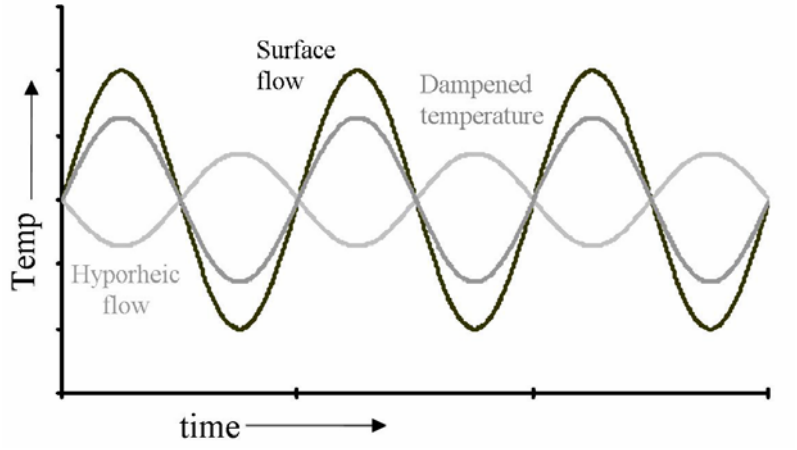


**Figure 1.2 Schematic of idealized out-of-phase mainstem and hyporheic temperature fluctuations and the resulting dampened temperature.**

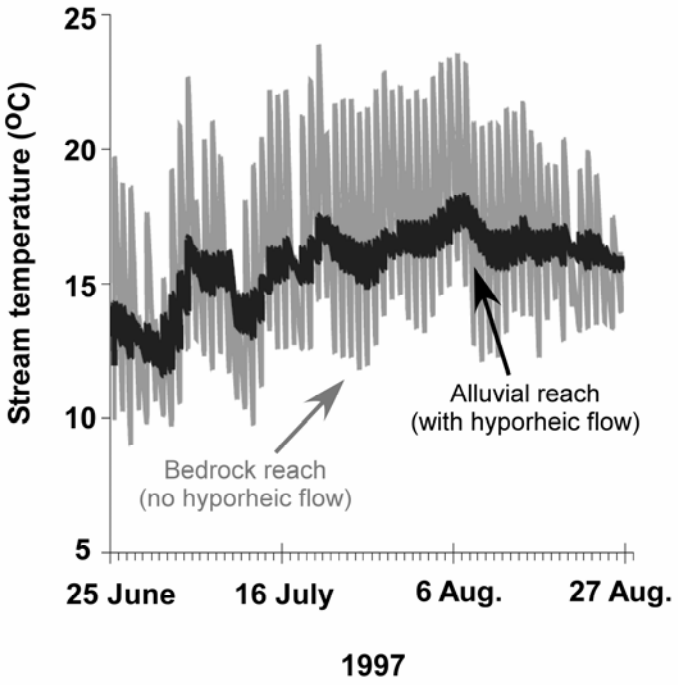


**Figure 1.3 Stream temperature in two adjacent reaches of a stream in the HJ Andrews Experimental Forest, Oregon, USA. Note the large diurnal temperature fluctuations (gray) as water runs through the bedrock reach with no hyporheic zone versus the small temperature fluctuations (black) present in the alluvial reach with large hyporheic zone. Modified from Johnson, 2004.**

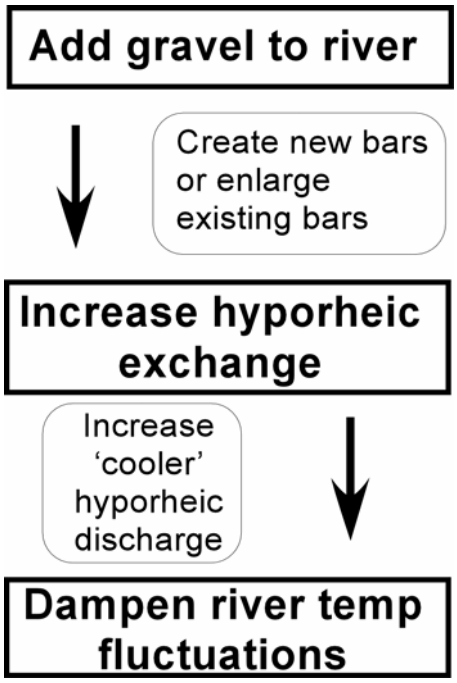


**Figure 1.4 Conceptual diagram describing how gravel augmentation can help thermally restore a river.**

reports that water temperatures are buffered up to 8.7 °C in a 2nd-order stream as it flows through an alluvial reach (Fig. 1.3).

Adding gravel to the river would not only create new bars and/or enhance existing bars, but would also increase the amount of water traveling through the hyporheic zone. Increased hyporheic discharge could lead to more temperature buffering which could affect the overall thermal regime of the river (Fig. 1.4). The owner of the hydroelectric projects on the Clackamas River, Portland General Electric (PGE), is interested in designing a gravel augmentation program below the dams in order to restore sediment transport and enhance fish habitat. Given the elevated temperatures on the lower river, they were also interested in learning about potential thermal benefits from adding gravel. This work addresses that question by qualifying and quantifying the amount of hyporheic exchange that currently affects

temperature on the lower Clackamas River, specifically hyporheic exchange that occurs through gravel bars.

The project approach includes three components: 1) a geomorphic and thermal characterization of the gravel bar population to identify where hyporheic exchange occurs and its connections to bar morphology, 2) a detailed characterization of three representative gravel bars in order to quantify the amount of emerging cooler hyporheic water; and 3) a 1$^{st}$-order mixing model to assess how the quantified hyporheic exchange affects overall river temperature. Appendices A-J include much of the data used and obtained throughout the study, including methodology for collecting and using the data.

Understanding how much hyporheic exchange currently affects the lower Clackamas River will provide insight as to how a gravel augmentation scenario could potentially affect temperatures in a large river and improve aquatic habitat.

# 2 INFLUENCE OF HYPORHEIC FLOW AND GEOMORPHOLOGY ON TEMPERATURE OF A LARGE, GRAVEL-BED RIVER, CLACKAMAS RIVER, OREGON, USA

**Barbara K. Burkholder**

**Department of Geosciences, Oregon State University, Corvallis, OR 97331**

**Hydrological Processes**

**1 Oldlands Way, Bognor Regis, West Sussex PO22 9SA, England**

**Accepted for publication in Hydrological Processes**

## 2.1 Abstract

The hyporheic zone influences the thermal regime of rivers, buffering temperature by storing and releasing heat over a range of timescales. We examined the relationship between hyporheic exchange and temperature along a 24-km reach of the lower Clackamas River, a large gravel-bed river in northwestern Oregon (median discharge = 75.7 $m^3/s$; minimum mean monthly discharge = 22.7 $m^3/s$ in August 2006). With a simple mixing model, we estimated how much hyporheic exchange cools the river during hot summer months. Hyporheic exchange was primarily identified by temperature anomalies, which are patches of water that demonstrate at least a 1 °C temperature difference from the main channel. Forty hyporheic temperature anomalies were identified through field investigations and TIR (Thermal-Infrared-Radiometry) in summer 2006. The location of anomalies was associated with specific geomorphic features, primarily bar channels and bar heads that act as preferential pathways for hyporheic flow. Detailed field characterization and groundwater modeling on three Clackamas gravel bars indicate residence times of hyporheic water can vary from hours to weeks and months. This was largely determined by hydraulic conductivity, which is affected by how recently the gravel bar formed or was reworked. Upscaling of modeled discharges and hydrologic parameters from these bars to the other anomalies on the Clackamas network shows that hyporheic discharge from anomalies comprises a small fraction (<< 1 %) of mainstem discharge, resulting in small river cooling effects (0.012 °C). However, the presence of cooler patches of water within rivers can act as thermal refugia for fish and other aquatic organisms, making the creation or enhancement of hyporheic exchange an attractive method in restoring the thermal regime of rivers.

## 2.2 Introduction

Understanding heat fluxes within rivers is increasingly important as anthropogenic influences and changing climate alter river thermal regimes, which can lead to shifts in aquatic species composition and changing rates of biogeochemical processes (Evans *et al*., 1998; Poole and Berman, 2001). Numerous and inter-related

physical mechanisms influence stream temperature, making it difficult to distinguish the magnitude or impact of individual drivers (Johnson, 2004).

Solar radiation (and shade), air temperature, groundwater inputs, and wind speed are the primary external drivers in most rivers that determine how much heat is added to or removed from the system (Sullivan and Adams, 1991). Internal drivers, which include bed conduction and hyporheic exchange, do not remove heat from the river channel but redistribute it temporally and spatially (Poole and Berman, 2001). Hyporheic exchange, where surface water enters the shallow subsurface (channel bed, banks or morphological features) and then reemerges back into the main channel, has previously been thought to have little impact on river temperature (Brown 1969), but a number of recent studies show that hyporheic exchange plays an important role in the thermal dynamics of some streams (Story *et al*., 2003; Johnson, 2004; Loheide and Gorelick, 2006).

The hyporheic zone serves as transient storage within a river, where river water and heat can be retained for periods of time before being released back into the river (Bencala and Walters, 1983; Bencala, 2005). As surface water downwells into and is transported through the hyporheic zone, the heat within that water is transported and exchanged by several processes (Fig. 2.1). Advection via fluid flow dominates heat transfer (Stallman, 1965; Silliman *et al*., 1993; Silliman *et al*., 1995; Anderson, 2005; Keery *et al*., 2006), although heat exchange may also influence hyporheic heat transfer. Along hyporheic flow paths, heat exchanges with sediment by conduction. This exchange is fast – dimensional analysis for cobbles of typical properties indicate thermal equilibrium is achieved within an hour or two. Heat also exchanges with groundwater by dispersion and conduction, and with the atmosphere by conduction and movement of latent and sensible heat. If the water table is high, solar heating of surface sediments may increase hyporheic water temperatures (Silliman *et al*., 1995, Arrigoni *et al.*, *in press*). Collectively, these processes generally lead to a combination of "buffering, cooling and lagging" (Arrigoni *et al*., *in press*) of temperatures within the hyporheic zone.

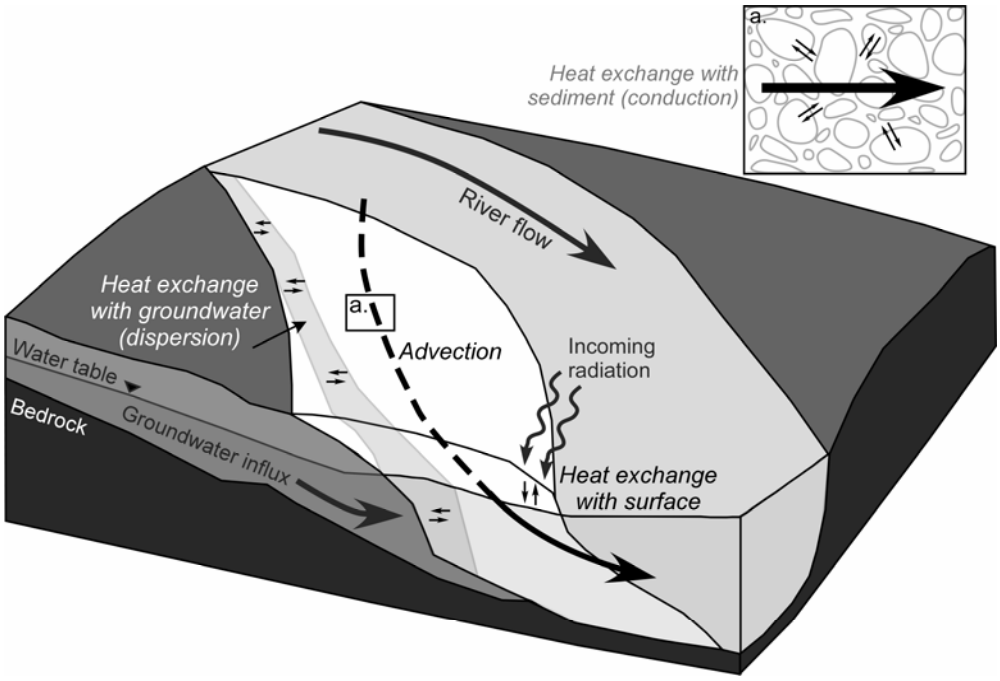


**Figure 2.1: Conceptual diagram showing the different processes that influence hyporheic water temperatures in a gravel bar (white). Advection (large dashed/solid black arrow) transports hear via fluid flow, conduction (small black arrows) transfers heat between sediment and hyporheic water, dispersion and conduction (shaded zone within gravel bar) occur as hyporheic water and groundwater interact, and incoming solar radiation indirectly warms hyporheic water via conduction and transfer of latent and sensible heat.**

Emergent hyporheic temperature may be different than the mainstem temperature. Transport through the hyporheic zone may result in a temporal phase shift between hyporheic and mainstem temperatures, where cooler hyporheic water reemerges back into a warmer mainstem and vice versa. However, the mixing of emerging hyporheic water and mainstem water does not 'cool' a river – mean temperature may stay constant – but it does dampen diurnal temperature fluctuations in the river by decreasing maximum temperatures and increasing minimum temperatures (Johnson, 2004; Arrigoni *et al*., *in press*). This dampening results from

shielding of hyporheic water from changes in solar radiation and air temperature that influence mainstem surface water temperature.

Hyporheic exchange can occur across several spatial scales, from roughness elements on the stream bed to channel-scale riffles and bars to reach-scale meander necks and floodplains (Edwards, 1998; Harvey and Wagner, 2000). Most hyporheic temperature studies to date have focused on examining the relationship between hyporheic exchange and channel-scale morphology. In smaller catchments, several studies report finding cooler water emerging from the bottom of riffles or step-pool structures (Evans and Petts, 1997; Brown *et al*., 2005; Hancock and Boulton, 2005; Moore *et al*., 2005; Sliva and Williams, 2005; Hunt *et al*., 2006). Peterson and Sickbert (2006) studied hyporheic exchange across a meander neck of a 3$^{rd}$-order stream and found that hyporheic temperatures correlate with seasonal temperature variations, suggesting seasonal residence times. Fernald *et al*. (2000, 2006) reported on a larger river (8$^{th}$ order), that cooler water emerges from gravel bars into 'alcoves,' or off-channel lentic water connected at the downstream end to the mainstem. Additionally, hyporheic flows were more pronounced and had a greater impact on river temperature where gravel had been recently reworked by river flows. Arscott *et al.* (2001) found that hyporheic exchange generated significant temperature heterogeneity in higher-order reaches (2$^{nd}$ - 7$^{th}$).

In reach-scale temperature studies, longitudinal trends in temperature demonstrate spatial and temporal thermal heterogeneity. Johnson (2004) compared bedrock and alluvial reaches along the same reach of 1$^{st}$- and 2$^{nd}$-order streams and found maximum daily temperatures were buffered by as much as 8.7°C. Torgersen *et al*. (1999) used thermal imagery along a river reach and found that the general increase in temperature downstream contained several peaks and troughs, reflecting bedrock and alluvial reaches respectively.

There are few hyporheic temperature studies for larger, lower-gradient rivers, and none have quantified the effect of hyporheic exchange on overall longitudinal river temperature. In this study we sought to: 1) identify areas of hyporheic exchange on a large, gravel-bed river and investigate their relationship with channel

morphological features, 2) quantify the amount of hyporheic exchange occurring, and 3) estimate how much hyporheic exchange affects overall river temperatures.

## 2.3 Methods

### *2.3.1 Study Area:*

The Clackamas River is a 6th-order, gravel-bed river in northwestern Oregon, USA that drains approximately 2,430 $km^2$ from its headwaters in the Cascade Range to its confluence with the Willamette River in Oregon City. Our study focused on a 24-km reach on the lower Clackamas River, stretching from River Mill Dam (River km 37 (RKM 37)) to Carver, Oregon (RKM 13) (Fig. 2.2). The dam location marks a change of topography within the drainage basin, with the river moving from a confined canyon into a broad valley. Longitudinal gradients below the dam along the study reach average 0.0029 (Wampler, 2004). The median annual flow is 75.7 $m^3/s$ and the median summer flow is 25.9 $m^3/s$.

Sediment supply to the lower river is generated primarily from periglacial sediment in the Cascade Range. Dam infrastructure on the Clackamas has cut off this supply for almost 100 years, and sediment inputs into the reach are limited to periodic erosion of alluvial Holocene terraces (Wampler, 2004). However, an extensive gravel bar population (> 50 bars) is distributed throughout the study reach, with median grain-size of 7.5 cm (Wampler, 2004). The population is composed primarily of mid-channel bars (55 % of bars by area), with lateral bars (34 %) and point bars (11 %) making up the rest of the network. The bar alluvium, which can range up to 6 m in thickness, rests on cemented, fine-grained Miocene volcanoclastics and mudstones. The Sandy River Mudstone, which underlies the lower 21 km of the study reach, is easily eroded, leading to rapid formation of flutes and potholes when bedrock surfaces are exposed (Wampler, 2004).

Gravel bar stability decreases downstream, with well-vegetated, coarse-grained, skeletal bars, bars without finer sediments (median grain size ($D_{50}$) surface: 15 - 30 cm), in the upper 3 km of the reach grading into unvegetated bars with smaller grain sizes ($D_{50}$ surface = 5 - 7 cm). Wampler (2004) points out that the presence of

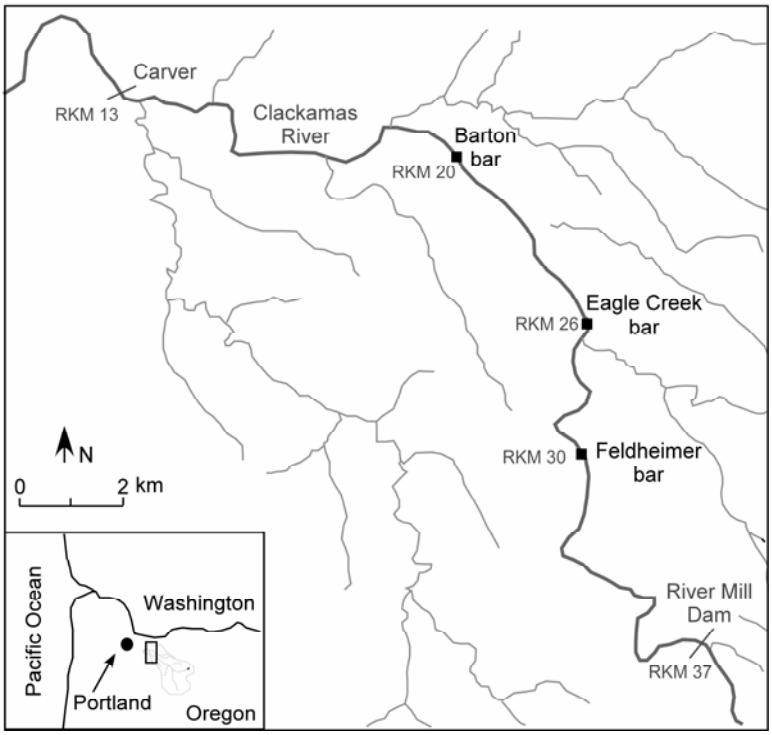


**Figure 2.2 Site location and study reach, lower Clackamas River, Oregon, USA.**

the dam most likely causes this effect, as winter flows (850 - 1130 $m^3/s$) winnow out fines and smaller particles from the upper reaches and transport them downstream. Winter flows influence bar morphology throughout the reach, with most gravel reworking occurring between Feldheimer (RKM 30) and Carver (RKM 13).

The dam also affects the river temperature regime, especially during low flows in the summer months. The magnitude of this change has been modeled with CE-QUAL-W2, a hydrodynamic 2D water quality model, which shows that the Clackamas River currently exceeds state temperature standards by 1 - 3 ˚C from July to September (Portland General Electric, 2005). Current research in association with dam relicensing efforts are exploring natural mechanisms of thermal mitigation, including potential thermal benefits of adding gravel to the river to increase the amount of hyporheic exchange and hyporheic buffering.

### *2.3.2 Field measurements and data collection:*

Our field campaign from July to September 2006 investigated the gravel bars within the study reach, the hypothesized primary location of hyporheic flow that could influence mainstem river temperature. Due to the length of the study reach, hyporheic exchange was identified using techniques that were easy to conduct and replicate over 24 km of river. During early reconnaissance we identified locations with visually observable flow from gravel bars and used a handheld YSI 63 electrical conductivity and temperature probe (Yellow Springs, Ohio, USA) to identify temperature anomalies, which we defined as patches of water that deviate from mainstem water temperatures by at least 1 °C. The handheld probe was used to conduct temperature surveys around bar perimeters and identify anomaly locations. Reference mainstem temperatures were taken during temperature surveys at each site to account for diurnal heating of the river. Once an anomaly was identified, we also recorded electrical conductivity and width and depth along gravel bar edges. Groundwater inputs were distinguished from hyporheic flow by: (1) water emerging from channel edges rather than gravel bars; (2) higher specific conductance (> 80 μS/cm compared to river 55 – 65 μS/cm); (3) iron-stained sediment resulting from groundwater oxidation; and/or (4) consistent temperatures representative of groundwater (10 - 12 °C (Well logs obtained from OWRD)). River discharge decreased throughout the summer (from 28 to 21 $m^3/s$), and to capture how this impacted the hyporheic zone, most identified anomaly sites were revisited several times over the summer to take more temperature measurements and re-measure anomaly dimensions.

Two Thermal-Infrared Radiometry (TIR) surveys were flown over the study reach on August 13$^{th}$, 2006, one at 6 am and the other at 3 pm (Watershed Sciences, Inc., Corvallis, Oregon, USA). This provided a complete 2D map of daily maximum and minimum river surface temperatures, as well as an additional visual method to observe and detect temperature anomalies. Longitudinal temperature profiles were constructed by taking the median temperature for each sampled image per river kilometer. In-stream temperature loggers deployed throughout the study reach before

the flights were used to calibrate and verify the accuracy of TIR data. Pixel resolution of imagery is 0.9 m.

Three gravel bars with temperature anomalies were selected for detailed field characterization and modeling. These three representative bars exhibited geomorphic features and sedimentological textures characteristic of the majority of the gravel bar population on the lower Clackamas River. Field characterization included examination of bar type, location within the reach, sediment size, presence of vegetation, and bar history. Based on comparison of aerial photos from July 2005 (discharge, $Q = 29.3$ m$^3$/s) and August 2006 ($Q = 23$ m$^3$/s), gravel features that did not appear in 2005 photos but were mapped in 2006 are considered 'new' features. We refer to all other features as older, but recognize that these bars also have a distribution of ages. Figure 2.3 shows basic bar morphology and interpreted hyporheic flow paths for each bar. Feldheimer bar (RKM 30) is an older, large lateral bar that is well-vegetated except for a 350-m long unvegetated back-bar channel that becomes active during high flow. Eagle Creek bar (RKM 26) is a new gravel feature that formed along an older bar edge during 2005 winter flows (Fig. 2.4). Barton bar is a mid-channel bar (RKM 20) that has new infillings of gravel among older bar deposits (Fig. 2.4).

Each bar was instrumented with several 3.4-cm inner diameter (1.33-in) galvanized steel piezometers (Maas Midwest Manufacturing, Huntley, Illinois, USA) with 17.8-cm (7-in) screens immediately above a conical drive point (3 piezometers in Feldheimer bar, 3 in Eagle Creek bar, 5 in Barton bar). Given the large diameter of the sediment composing the gravel bars, it was not feasible to install the piezometers by hand-driven methods. A gas-powered jackhammer was used to drive the piezometers into the gravel bars, usually through at least 1 m of sediment to a depth of approximately 0.5 m beneath the water table. We assumed that flow across the gravel bars in the hyporheic zone is predominantly horizontal, which is hydrogeologically reasonable. Consequently, hydraulic head would have negligible changes with depth. Therefore, we put highest priority on horizontal separation of piezometers and did not install any multilevel piezometers. Alexander and MacQuarrie (2005) showed that

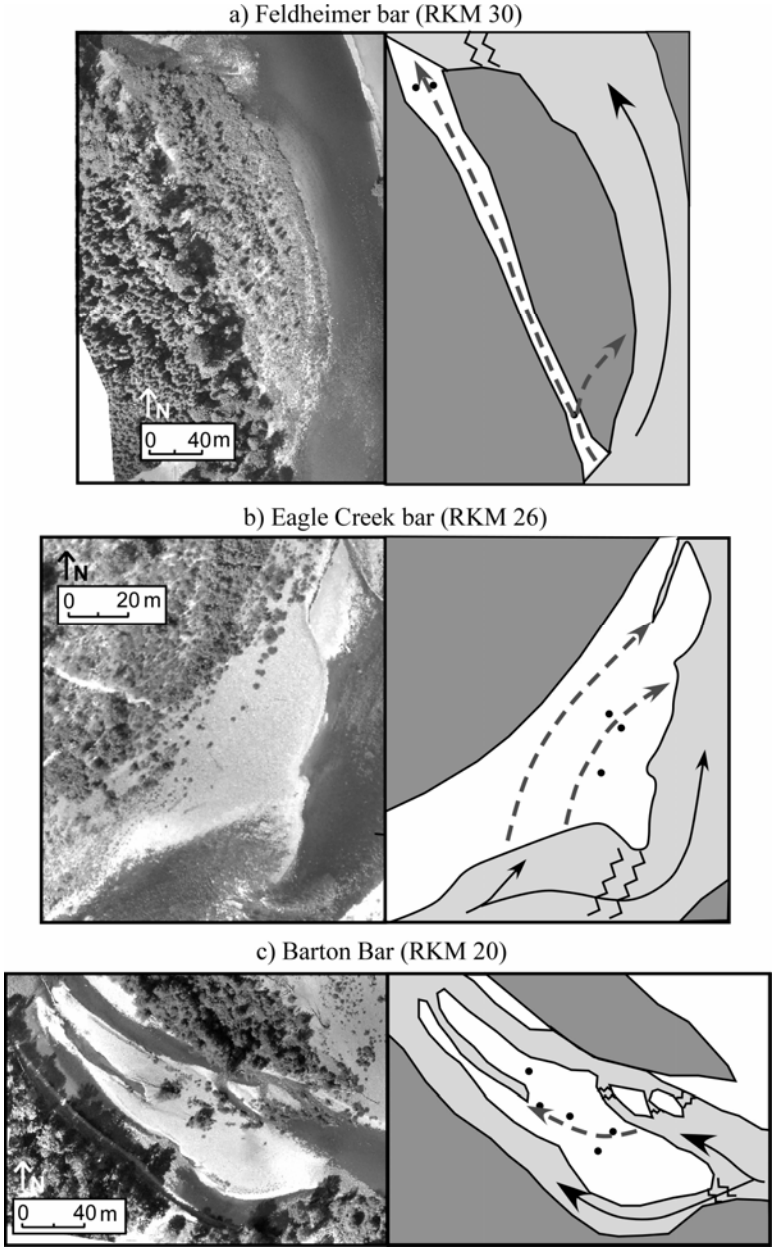


**Figure 2.3 Summer 2006 aerial imagery and schematic diagram for a) Feldheimer, b) Eagle Creek, and c) Barton gravel bars (see Fig. 2.2 for locations). Piezometer locations (black dots) and interpreted subsurface flow paths (dashed gray lines) are overlain on open gravel (white) and vegetated areas (dark gray). Mainstem (light gray) flow direction given by solid black arrows. Riffles represented by zigzag pattern.**

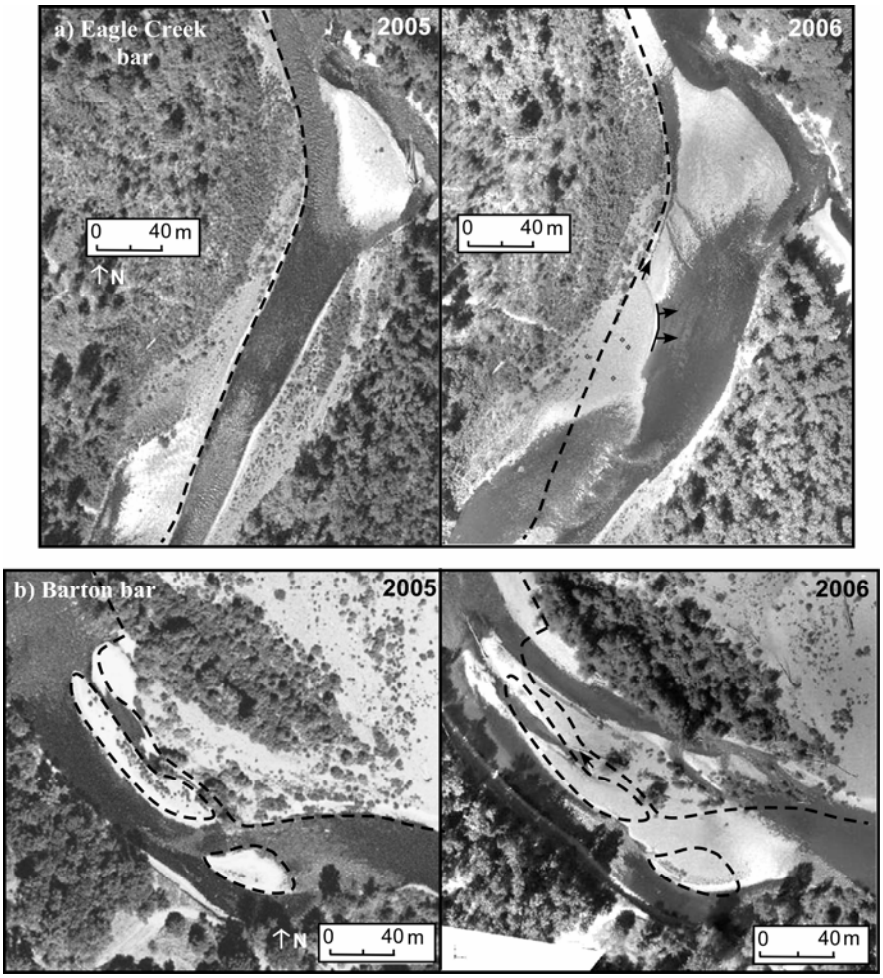


**Figure 2.4 Aerial imagery showing gravel reworking between summers 2005 (left) and 2006 (right) for a) Eagle Creek and b) Barton bars. Dashed black lines follows outline of 2005 gravel bars and solid black arrows indicate flow direction of temperature anomalies.**

temperature measurements within steel piezometers have less than 0.1 °C error and are perfectly correlated to in-situ measurements.

Topographic surveys were conducted at each bar, using both a Leica TCRP 1201 total station (Heerbrugg, Switzerland) and a Trimble 4700 RTK GPS (Sunnyvale, California, USA). We mapped water edges, notable topographic features, and piezometer locations. Heads within piezometers were obtained through surveying

the elevation of the top of the piezometer and subtracting the distance to the water table (2 cm vertical accuracy). Tidbit Stowaway thermistors (0.2 °C accuracy, Onset, Bourne, Massachusetts, USA) were checked against a 0.1 °C resolution NIST-traceable thermometer (Cole-Parmer, Vernon Hills, Illinois, USA) and placed within the screened section of the piezometers where they recorded temperature every 15 min for 7 - 10 days. Tidbits were also placed at head of the bar to record mainstem temperatures of water entering the bar and also placed in areas of emerging hyporheic flow. Slug tests were conducted within each piezometer, and results were analyzed using methods outlined by Bouwer and Rice (1976) and Butler and Garnett (2000).

### *2.3.3 Model simulations of hyporheic exchange within gravel bars:*

Topographic surveys, slug tests, and temperature mapping from the selected gravel bars were used to build and parameterize steady-state groundwater flow models using MODFLOW (McDonald and Harbaugh, 1988) implemented via the GMS interface (Environmental Monitoring Systems, Inc., South Jordan, Utah, USA). Model domains were one-layer thick finite difference grids with square cells, generally ranging between 0.2 m and 0.5 m (depending on the size of the bar being modeled). Models were calibrated to water table elevations in piezometers and anomaly outflow dimensions. On two bars, residence time distributions from detailed Tidbit temperature surveys, simulated with the particle tracking package MODPATH (Pollack, 1994), were also used to calibrate the models. A flow-budget module within MODFLOW was used to calculate the hyporheic discharge emerging from the anomalies, and MODPATH provided a distribution of water residence times.

### *2.3.4 Upscaling hyporheic exchange to the reach scale:*

To assess how hyporheic exchange from gravel bars affects overall river temperatures, we calculated discharges for all anomalies interpreted to be driven by primarily hyporheic flow. We intentionally excluded anomalies that were interpreted to be due to groundwater. We estimated flux through each representative anomaly using Darcy's law ($Q_h = - K \nabla h \; A_h$). While technically valid at a point, we applied

Darcy's law across temperature anomalies by assuming uniform parameters; the accuracy of this is discussed below. $Q_h$ is hyporheic discharge ($L^3/T$) (as defined it is a vector, but we used only the magnitude), $A_h$ is the cross-sectional area of the hyporheic discharge ($L^2$), $K$ is the hydraulic conductivity of the sediment (L/T), and $\nabla h$ is hydraulic gradient (L/L). $A_h$ was calculated by field measurement of the length across the edge of a gravel bar where we could detect a temperature difference and an estimate of the depth of gravel contributing to hyporheic flow. Hydraulic gradient across bars, in most cases, was measured in the field ($N = 27$). On bars where hydraulic gradient was not directly measured (N = 13), we used the average of the field measurements of cross-bar gradients.

Using aerial photographs from 2005 and 2006, we estimated $K$ for each anomaly based on how recently a gravel bar has been created or significantly reworked. From our observations, we assumed that new gravel bars or portions of pre-existing bars that formed during the previous year's high flows were likely to have a higher $K$ than older bars, inferring that these deposits will not have been substantially infiltrated by fines. Older gravel bars, on the other hand, were interpreted as more likely to have had finer sediments infiltrating the sediment matrix, leading to lower $K$ values (Packman and Salehin, 2003). Some bars are a combination of both older and newer gravel deposits, which can lead to large differences in $K$ over a limited area. Model data from our three representative bars helped us constrain hydraulic conductivities by giving us a $K$ estimate for newer and older bars, as well as bars with both newer and older deposits. The limitations of this approach will be discussed in results.

We checked the accuracy of the Darcy's law discharge estimates against the discharge calculated by the groundwater flow models. We estimated parameters for Darcy's law using field estimates of average hydraulic gradient and hyporheic area. We also used a spatially-averaged $K$ value from the groundwater models. Darcy's law and a full groundwater flow model yield nearly the same discharges: the relationship is approximately 1:1 and the mean difference between them is 25 % (Fig. 2.5). The discharges are nearly the same for the following reasons: changes in gradient (both

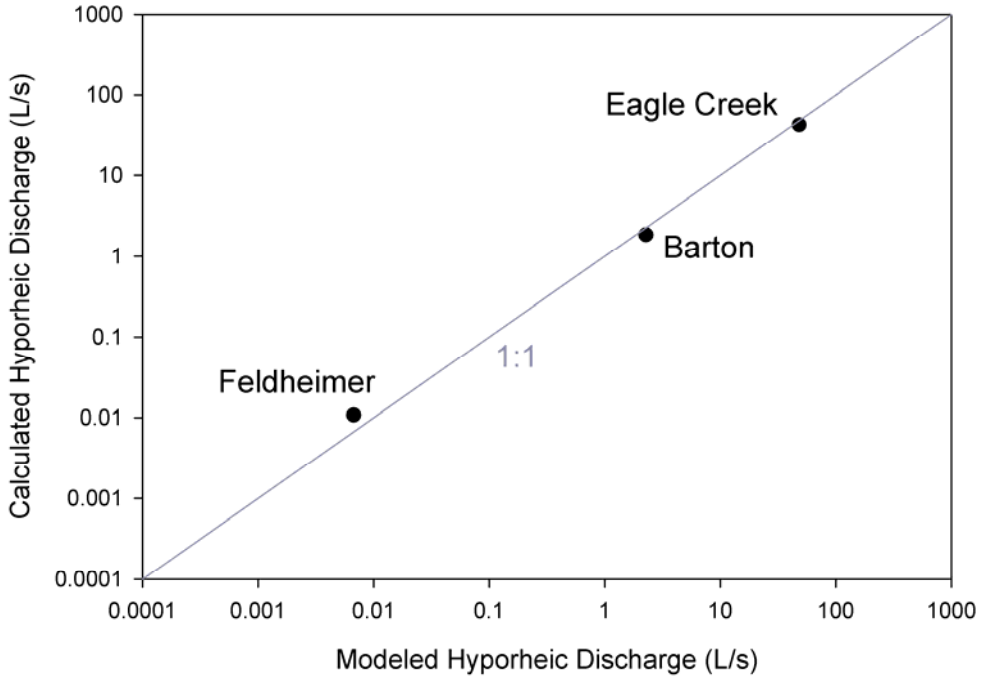


**Figure 2.5 Comparison of calculated (Darcy's law) and modeled (MODFLOW) hyporheic discharge for temperature anomalies on gravel bars. 1:1 line shown for reference.**

direction and magnitude) along the flow paths are small; we assumed *K* and cross-sectional area of hyporheic discharge are homogeneous along flow paths in both the Darcy's law and groundwater flow model calculations; and no sources or sinks of water exist along the flow paths. While there are significant heterogeneities in *K* within and between gravel bars, these within bar heterogeneities are at a large scale in comparison to the gravel bar, meaning that individual flow paths have relatively homogeneous *K*. Consequently, the Darcy's law approach provides a reasonable and feasible estimate of hyporheic discharge, and we confidently employ it for the other temperature anomalies on the Clackamas.

All field and model data can be obtained from appendices in Burkholder (2008).

## 2.4 RESULTS

### *2.4.1 Thermal Infrared Radiometry (TIR):*

TIR was used to construct a reach-scale longitudinal profile of stream temperatures as recorded at two points in time (Fig. 2.6). Comparison between thermal images and in-stream temperature loggers suggests that thermal images are within 0.5 °C of directly measured mainstem temperatures. Water released from the dam had a constant temperature of approximately 17.4 °C. Water warmed downstream during the day and cooled during the night, with rates of warming and cooling decreasing downstream, presumably either because stream temperatures are closer to thermal equilibrium with the atmosphere and/or because increased discharge downstream (from groundwater and tributary inputs) creates a larger volume of water to be heated/cooled. Consequently, the warmest point in the reach during the day was near Barton (RKM 21), which approximately corresponds to the distance water traveled in daylight hours from the dam (16 km) (see analysis in Khangaonkar and Yang, *in press*). Further downstream, water was cooler because this water traveled some distance downstream from the dam during the night. An inverse pattern was observable in the early morning, with minimum temperatures recorded at Barton (Fig. 6). This modulation of temperature amplitudes below a dam is well documented (Polehn and Kinsel, 1997; Lowney, 2000) and was recently re-visited for the Clackamas River by Khangaonkar and Yang (*in press*).

TIR demonstrates that significant spatial and temporal thermal heterogeneity exists within the study reach. TIR morning imagery detected 34 temperature anomalies using the 1 °C rule, 16 of which were not previously identified in the field. These warmer patches of water emerged from gravel bars into a cooler mainstem (Figs. 2.7, 2.8). Anomalies with temperatures cooler than the mainstem were also detected in morning imagery, suggestive of groundwater influx rather than hyporheic exchange. Afternoon flight imagery was not useful in identifying cooler hyporheic patches. TIR measures temperatures at the surface, which masked the denser, cooler water that emerged below the warmer surface water surface. The resolution of the

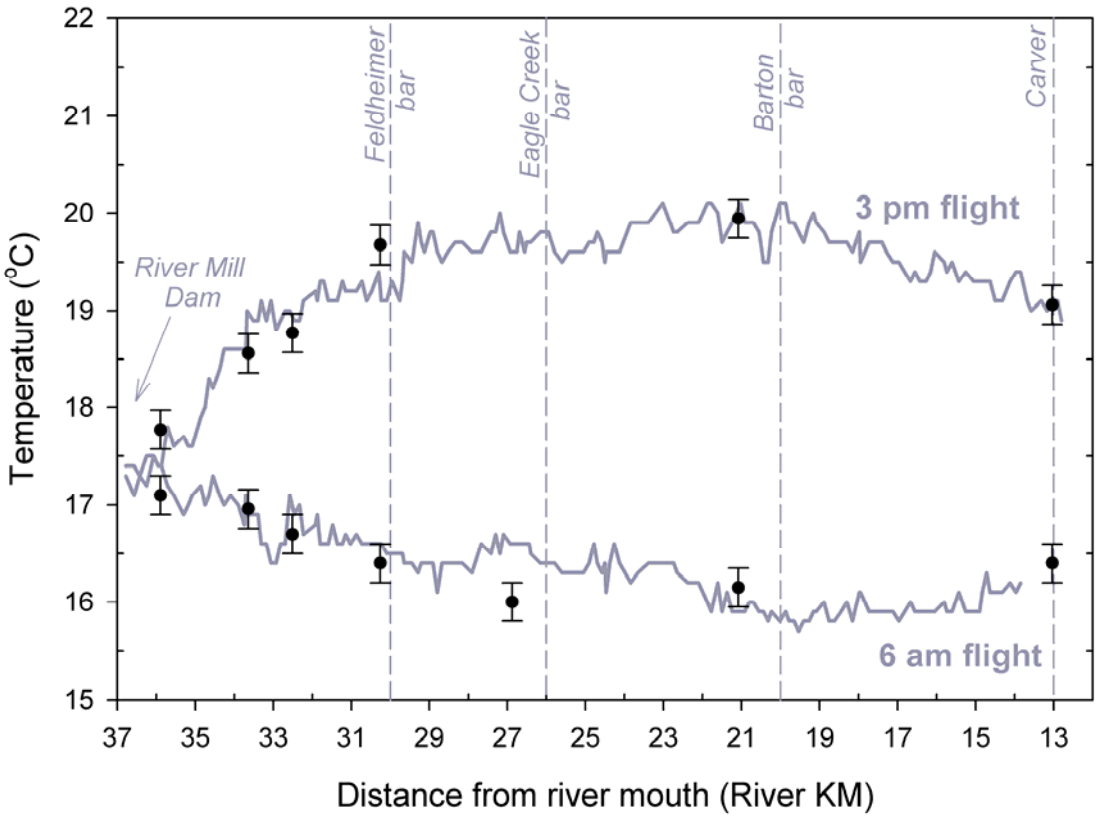


**Figure 2.6 Longitudinal temperature profiles of the lower Clackamas River from River Mill Dam (RKM 37) to Carver, Oregon (RKM 13) recorded by TIR on August 13th, 2006. In-stream data loggers (black circles) indicate river temperature with measurement error.**

imagery may also play a role in masking anomalies by averaging the much warmer gravel shoreline with cooler water temperatures in a single pixel.

### *2.4.2 Bar geomorphology controls on hyporheic exchange:*

A total of 52 temperature anomalies were identified by a combination of field investigations and TIR imagery over summer 2006. Depending on time of day, these features discharged water that generally ranged from 1 to 4 °C different than the mainstem. The anomalies were distributed along the entire 24-km study reach, with the greatest anomaly density (3.0 anomalies/km) in the 6.4-km reach between the

Eagle Creek confluence to just below Barton (RKM 26.4 to RKM 20). The lowest density (1.4 anomalies/km) was in the 8-km reach immediately below River Mill Dam. This is consistent with previously interpreted levels of bar activity and presence of skeletal bars (bars without finer gravel) in the reaches immediately below the dam (Wampler, 2004).

Twelve anomalies were interpreted as primarily due to groundwater seepage rather than hyporheic exchange, based on the criteria outlined in methods. The remaining 40 anomalies are interpreted to be primarily driven by downwelling of river water, although we recognize they may also be influenced by some heat exchange with groundwater. This is supported by the fact that groundwater and hyporheic anomalies tended to occur adjacent to one another on individual gravel bars (6 of 12 identified groundwater seeps). One anomaly demonstrated warmer temperatures in the late afternoon, but the water table was near the uppermost gravel surface and was likely influenced by heat of the gravel.

All hyporheic temperature anomalies occur on the edges of gravel bars. However, in most cases, they do not extend across the entire downstream edge of a gravel bar. Instead, they occur in association with specific geomorphic features present on gravel bars, features whose hydraulic gradient and hydraulic conductivity promote hyporheic residence times that result in offset hyporheic and mainstem temperature signals.

Twenty-four hyporheic anomalies (60 %) occur at the downstream end of bar channels, which are unvegetated pathways that are active during high flows (e.g., Feldheimer and Barton bars). These channels occurred along the back margin of bars (i.e., away from the mainstem), across bars, or as paleochannels that have been infilled by new gravel. Gradients along bar channels were higher than the longitudinal river gradient (mean cross-bar gradient: 0.007 compared to mean longitudinal gradient: 0.0029). Temperature anomalies associated with bar channels formed discrete, small patches (< 0.5 to 1 m in length as measured along the bar margin), due to the more defined structure of the feature (Fig. 2.7).

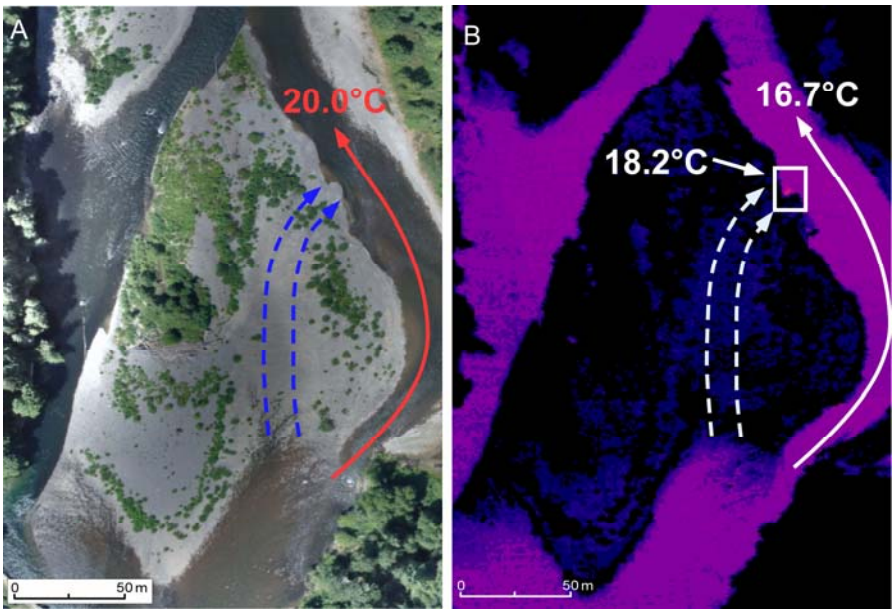


**Figure 2.7 Hyporheic exchange across a mid-channel bar (RKM 27). A) Dashed arrows on 2006 aerial photography indicate likely hyporheic flow paths through cross-bar channel feature. B) Small, discrete temperature anomaly identified on 6 am TIR photography.**

Sixteen hyporheic anomalies (40 %) were located downstream from bar heads, where hyporheic exchange follows a cross-bar gradient from hydraulically pooled water at the bar head to upwelling at the bar tail. (e.g. Eagle Creek bar) (Fig. 2.8). Unlike bar channels, we interpret hyporheic flow through this geomorphic feature as not being confined to discrete subsurface channels, but occurring across riffle structures, large sections of bars, or entire bars. Downstream temperature anomalies associated with this feature were laterally extensive (up to 25 m along gravel bar edges). Bar heads were primarily found on mid-channel bars, where branching of the mainstem creates higher hydraulic gradients (0.005 - 0.012) due to elevation differences between channels.

Decreases in river discharge throughout the summer, particularly from July to August, did influence the size of temperature anomalies. Generally, as discharge

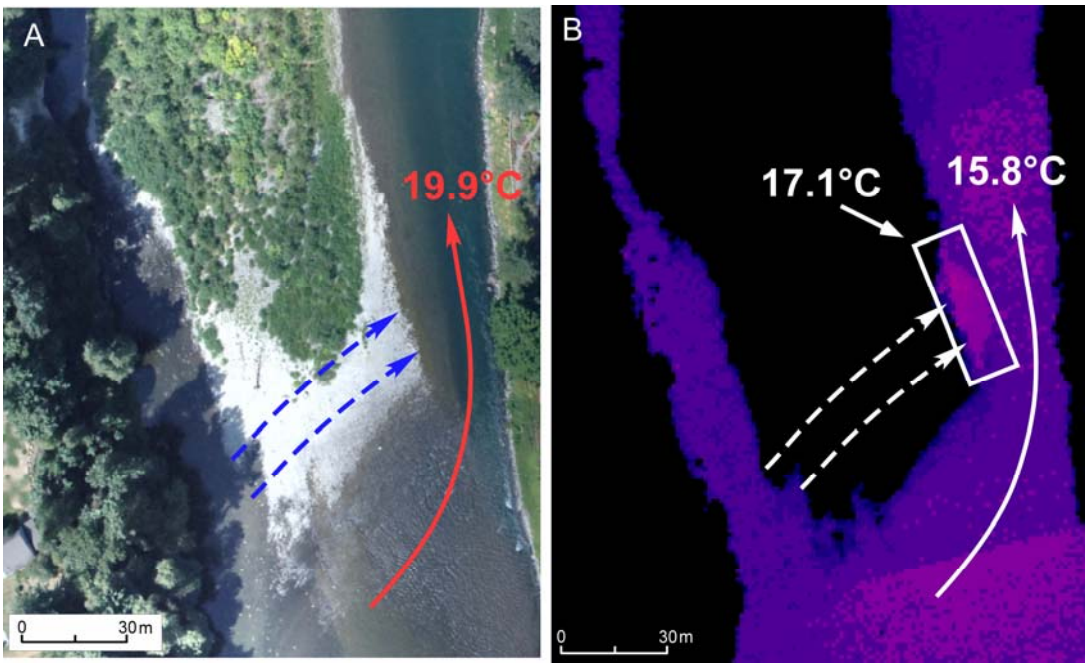


**Figure 2.8 Hyporheic exchange across unvegetated section of mid-channel bar (RKM 15). A) Dashed arrows indicate likely hyporheic flow paths through bar head feature. B) Laterally extensive temperature anomaly identified on TIR 6 am photography.**

decreased, the width of several temperature anomalies along gravel bar edges also decreased (up to 1 – 2 m). However, all except 2 hyporheic anomalies persisted through late July and August when river temperatures were highest in the channel.

### *2.4.3 Bar-scale data and model analysis:*

We summarize field and model data for each of the gravel bars selected for further characterization in Table 1. Changes in piezometer head elevations from upper to lower ends of the gravel bars varied, with about 0.1 - 0.2 m change across Eagle Creek and Barton bars and 0.682 m across the larger Feldheimer bar. Slug tests within piezometers demonstrated different behaviors between new and older gravel bars. In older bars (Feldheimer bar and sections of Barton bar), $K$ ranges from $1.1 \times 10^{-6}$ m/s to $7.7 \times 10^{-5}$ m/s. In gravel that had been recently reworked (Eagle Creek bar and

**Table 2.1: Field and model data for representative Clackamas gravel bars.**

| Parameter | Feldheimer bar RKM 30 | Eagle Creek bar RKM 26 | Barton bar RKM 20 |
|---|---|---|---|
| **Bar type** | Lateral | Point Bar | Mid-channel |
| **Geomorphic feature** | Back-bar channel | Bar head | Remnant channel |
| **Gradient (m/m)** | 0.010 | 0.012 | 0.015 |
| **$D_{50}$ surface (cm)** | 6.4 | 5.8 | 6.9 |
| **$D_{50}$ subsurface (cm)** | 1.2 | 3.4 | 2.2 |
| **Hyporheic area ($m^2$)** | 34 | 66 | 8 |
| **Average *K* (m/s)** | $1.99 \times 10^{-5}$ | $6.19 \times 10^{-2}$ | $1.93 \times 10^{-3}$ |
| **Residence time (d)** | ~1040 d | 0.49 | ~12 |
| **Discharge ($m^3/s$)** | $6.73 \times 10^{-6}$ | $4.28 \times 10^{-2}$ | $1.85 \times 10^{-4}$ |

sections of Barton bar), 5 - 10 second recovery to static water levels with atypical recovery curves made it difficult to assess hydraulic conductivity using established high-*K* slug test analysis methods. Estimates of *K* were obtained by calibrating the appropriate MODFLOW models to travel time measured in offset temperature fluctuations. Hydraulic conductivity estimates average $6.19 \times 10^{-2}$ m/s from the calibrated Eagle Creek bar model and $1.93 \times 10^{-3}$ m/s from the calibrated Barton bar model.

Week-long temperature surveys also showed important differences between the older and newer gravel bars (Fig. 9). Temperatures in Eagle Creek bar showed a diurnal variation in temperature. As water from the mainstem moves through the bar, diurnal peaks in temperature were reduced to 20 % of their original peak height when they emerged back into the main channel, reflective of advective and conductive heat transfer. The phase lag in emerging hyporheic temperature indicates an 11.5 - 11.8 h water residence time, which approaches the maximum phase shift possible.

Temperature surveys from within Feldheimer and Barton bars did not fluctuate diurnally, but temperatures measured in downgradient piezometers were cooler than in upgradient piezometers (Fig. 2.9). The lack of diurnal temperature fluctuations is more indicative of groundwater rather than hyporheic exchange, but water temperatures

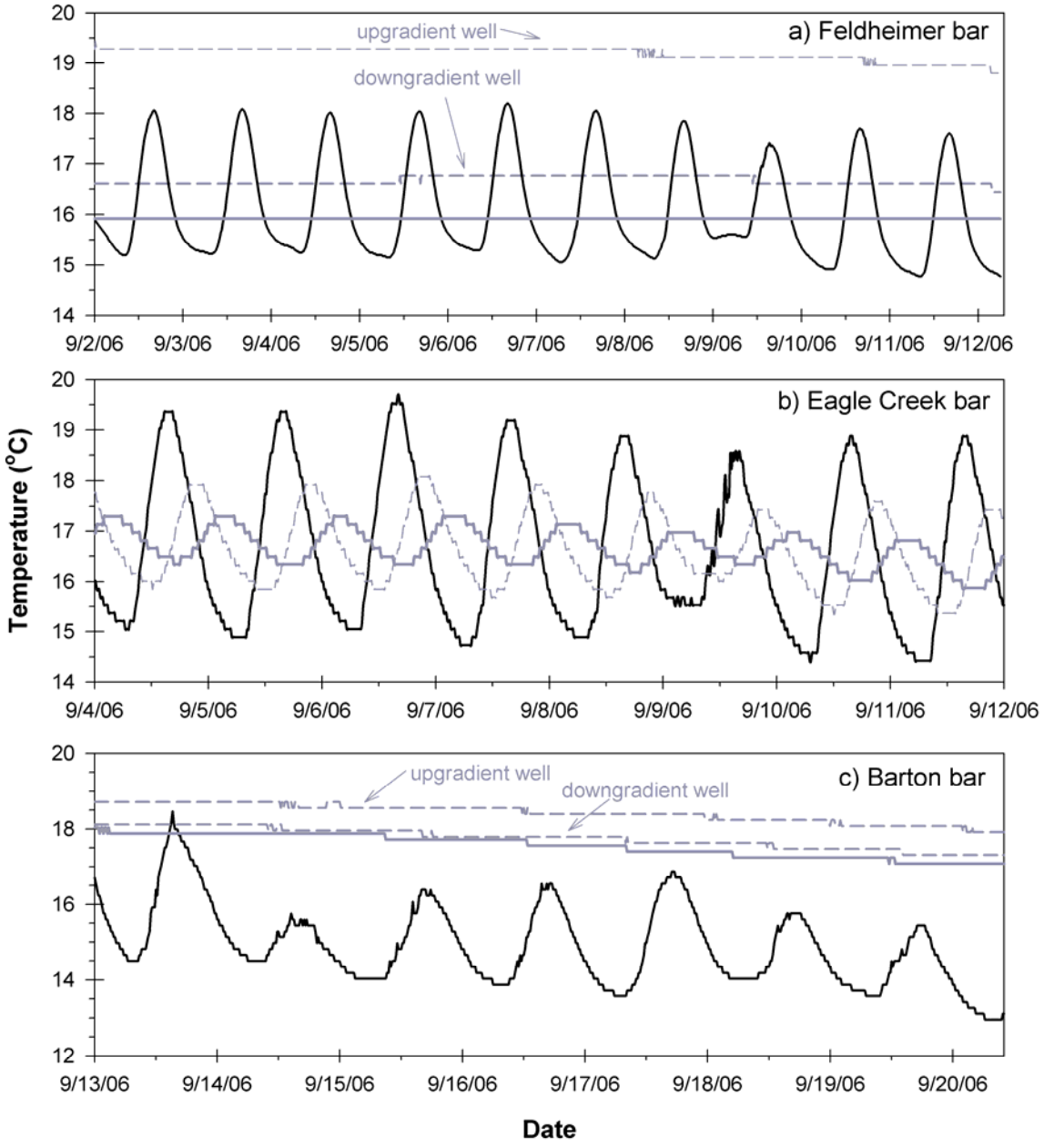


**Figure 2.9 Week-long temperature profiles for a) Feldheimer, b) Eagle Creek, and c) Barton bars. Surface mainstem temperatures (solid black lines) show dampening of diurnal fluctuations in emerging hyporheic flow (solid gray lines). Dashed gray lines represent within bar well temperatures.**

within the piezometers are well above ambient groundwater temperatures, suggesting that the water originated from the river channel. The loss of diurnal fluctuation is likely due to longer residence times (weeks to months), which is consistent with the much lower *K* values within the bars as estimated from slug tests and MODFLOW. Longer residence time can buffer and lag temperatures on a seasonal basis. For example, the temperature of emerging hyporheic water at Barton was consistently warmer than the mainstem channel in mid-September (Fig. 2.9) because cloudy, cooler weather reduced the amount of heat gained by the mainstem. Groundwater contributions may still be significant in emerging hyporheic temperatures, especially on Feldheimer bar which is connected to the channel edge.

Estimates of discharge emerging from each temperature anomaly are dependent on hydraulic gradient, hyporheic cross-sectional area, and *K* (Table 1). Of these variables, *K* has the most influence over hyporheic discharge. Eagle Creek bar, with the highest average *K* ($6.19 \times 10^{-2}$ m/s) and largest hyporheic area (66 $m^2$), has the greatest calculated discharge of 42.5 L/s (0.0425 $m^3$/s), or 0.002 % of the mainstem discharge. Feldheimer bar, with the lowest average *K* ($1.99 \times 10^{-5}$ m/s) and relatively large hyporheic area (34 $m^2$), has the lowest discharge of 0.00673 L/s ($6.73 \times 10^{-6}$ $m^3$/s), almost four orders of magnitude lower than Eagle Creek. Barton bar, with an intermediate *K* ($1.93 \times 10^{-3}$ m/s) but small hyporheic area (8 $m^2$) has an anomaly discharge of 1.85 L/s ($1.85 \times 10^{-4}$ $m^3$/s), which is two orders of magnitude lower than Eagle Creek.

### *2.4.4 Hyporheic effect from anomalies on river temperature:*

Estimates of *K* for the three representative bars were used to estimate *K* values for the larger population of hyporheic temperature anomalies, using an inferred association between recent gravel reworking and *K*. Using aerial photo analysis to assess the degree of gravel reworking that occurred on bars during 2005-2006 winter flows, we assigned an Eagle Creek *K* value of $6.19 \times 10^{-2}$ m/s to new bars or bars that were extensively reworked, a Barton *K* value of $1.93 \times 10^{-3}$ m/s to bars that showed some degree of reworking, and a Feldheimer *K* value of $1.99 \times 10^{-5}$ m/s to older bars

with little to no gravel reworking. We recognize that *K* is a highly variable and sensitive parameter, and our approach does not address downstream fining of sediments and changes in sediment packing. We view this approach as providing a rough estimate of the overall order-of-magnitude effect of anomaly-based hyporheic flow on stream temperatures that is consistent with the limited data available.

The change in river temperature due to hyporheic discharge can be approximated using a mixing equation

$$T_c = \frac{Q_m T_m + \sum (Q_h T_h)}{Q_c} \qquad (2)$$

where $Q_m$ is mainstem discharge ($L^3/T$), $T_m$ is mainstem temperature (˚C), $Q_h$ is hyporheic discharge ($L^3/T$), $T_h$ is hyporheic temperature (˚C), $Q_c$ is combined discharge ($L^3/T$), and $T_c$ is combined river temperature (˚C). This equation neglects other sources and sinks of heat, offsets in time due to travel time from one anomaly to the next, and dispersion. These effects are discussed below. We emphasize that we investigated only hyporheic exchange, and not the effects of groundwater inputs on river temperature, so groundwater seeps were not included. Solving for $T_c$ and subtracting it from mainstem temperature, $T_m$, gives the amount of river cooling expected from hyporheic exchange. To check the accuracy of the mixing equation approach, we compared it to results from a 2D hydrodynamic temperature model of the lower Clackamas River. We used CE-QUAL-W2 (Coles and Wells, 2004), a 2-D hydrodynamic model which incorporates the full spectrum of heat sources and sinks, to estimate river temperature sensitivity to hyporheic exchange. The CE-QUAL-W2 model was parameterized with a network of meteorological sensors that provided air temperature (2 points), short- and long-wave radiation (1 point), cloud cover (1 point), wind speed (4 points), and humidity (3 points). Other details on the model are provided by Battelle (2004) and Khangaonkar and Yang (*in press*). We used anomaly discharge, residence time, and temperature from the Eagle Creek bar and added 40 additional Eagle Creek-like anomalies throughout the river (in effect, doubling the number of current hyporheic anomalies), maintaining the same degree of anomaly density between different stretches of river. The model estimates river cooling of

0.16 ˚C. Using the mixing model, we estimated the cooling associated with the Eagle Creek anomaly (0.006 ˚C) and to simulate gravel augmentation, multiplied that effect by 40. This gives a river cooling estimate of 0.24 ˚C, an overestimate of 50%.

Using parameters shown in Table 2, the mixing equation estimates that existing hyporheic anomaly-based hyporheic discharge (0.07 % of total mainstem discharge) provides a local cooling of the summer time maximum daily temperature in lower Clackamas River by 0.012 °C.

Table 2.2: Values entered into mixing calculation.

| Parameter | Value | Source |
|---|---|---|
| $Q_m$ | 22.547 $m^3/s$ | $Q_c$-$Q_h$ |
| $T_m$ | 19.20 °C | Mean temperature for August 13th, 2006 |
| $Q_h$ | 0.153 $m^3/s$ | Sum of all temperature anomaly discharges |
| $T_h$ | depends | $T_m$ - magnitude of cooling for each anomaly |
| $\Sigma(Q_hT_h)$ | 2.660 | |
| $Q_c$ | 22.7 $m^3/s$ | USGS River Gauge at Estacada, Oregon |
| $T_c$ | 19.187 ˚C | $Q_mT_m+\Sigma(Q_hT_h)/Q_c$ |
| Cooling | 0.012 ˚C | $T_m$-$T_c$ |

## 2.5 DISCUSSION

We estimate that existing hyporheic flow in the Clackamas has a minimal impact on daily maximum temperature. This estimate is subject to three significant sources of uncertainty detailed below: the estimate of *K;* the calculation of discharge; and unaccounted for hyporheic exchange.

First, determining *K* for each of the gravel bars with temperature anomalies is difficult. We assigned *K* values using data from our 3 intensively studied bars to all anomalies in the study reach based on whether a bar was new, older, or a combination of new and older deposits. We do not know if this approach over- or under-predicts *K* values, but overall temperature effects in the mainstem are very sensitive to assignment of *K* values. By way of sensitivity analysis, if all gravel bars are assigned the maximum measured value of *K* (Eagle Creek), the mixing model estimates an overall reduction in maximum daily temperatures in the summer of 2006 as 0.021 °C.

If all gravel bars are assigned the minimum measured value of *K* (Feldheimer), the mixing model estimates a reduction in maximum daily temperatures of $7.14 \times 10^{-6}$ °C.

Secondly, we used a simple mixing equation to estimate the effect of hyporheic discharge on mainstem temperature. The steady state simplification assumes that the cooling over multiple anomalies is cumulative and neglects decay and phase effects due to travel time (i.e., temperature is treated conservatively). This model may overestimate the temperature effect. Our comparison with CE-QUAL-W2, which accounts for longitudinal heat loss/gain, demonstrates that if we added 40 Eagle Creek bars on the lower Clackamas by gravel augmentation and make the same calculation with the mixing model as outlined above, the mixing model overestimates the cooling effect by 50 %.

Finally, our study has focused on quantifying hyporheic exchange over summer 2006 on gravel bars that consistently demonstrated different temperatures from the mainstem, due to buffering and lagging of heat resulting from advection and conduction. We did not quantify the thermal effects of diffuse hyporheic discharge through gravel bars where we did not detect a temperature difference, nor did we attempt to assign cooling associated with the simple downwelling of water into gravel bars (where water is not exposed to solar radiation or ambient air temperature). Also, we did not take other hyporheic spatial scales into account, including flow through submerged gravel bedforms (e.g., bed roughness elements), meander necks or floodplains. Exclusion of these effects underestimates the total amount of hyporheic cooling.

Reconciling these sources of error, which point in different directions, is difficult. Obtaining more refined estimates of *K* and hyporheic anomaly discharge would require building additional groundwater models for many more gravel bars on the lower Clackamas. Additional field studies and modeling exercises would examine other spatial scales of hyporheic flow and the thermal benefit afforded by water simply being shielded from solar radiation as it downwells into gravel.

Even within the constraints imposed by the uncertainties in our study, however, we believe our estimate of cooling is not likely to change drastically. Unlike

smaller streams that may see several degrees of cooling from hyporheic buffering (Johnson, 2004), our results suggest that hyporheic exchange will cool larger rivers only a fraction of a degree. This is likely due to diminishing opportunities for hyporheic exchange as channel size increases (D'Angelo et al., 1993; Boulton et al., 1998). We found that in the Clackamas River, hyporheic discharge comprised only a fraction of mainstem summer discharge (<< 1 %). It is therefore difficult for hyporheic exchange to exert significant effect on stream temperature, because any hyporheic buffering present is diluted by large mainstem discharges.

Although hyporheic discharge may not have a large effect on overall river temperature in a large river, we found that it can effectively create localized patches of water that have different temperatures from the mainstem. These patches increase thermal heterogeneity within the river channel and can provide thermal refugia (up to 4 ˚C cooler) for aquatic species that are stressed by conditions in the mainstem channel (Fernald *et al.*, 2006 and Arscott *et al.*, 2001).

Similar to previous studies (e.g., Kasahara and Wondzell, 2003; Poole *et al.*, 2006), we found that channel-scale morphology controls hyporheic exchange in the Clackamas River, which in turn influences thermal heterogeneity (Arscott *et al.*, 2001; Fernald *et al.*, 2006). All anomalies were associated with gravel bars, with the largest discharges emerging from anomalies located downstream from bar heads. The largest number of anomalies was associated with bar channels, but these produced only modest hyporheic discharges.

In most cases, the link between channel morphology and hyporheic flow reflects morphologic control on the distribution and hydraulic properties of preferential flow paths in bars. Temperature anomalies were consistently located downstream from observed or inferred flow paths, which are assumed to feed subsurface channels. Although these geomorphic features usually comprise only a fraction of a gravel bar's area, they generally have higher $K$ values than other parts of the same bar (Wondzell and Swanson, 1999; Fernald *et. al*., 2006). The bar channels and heads that had associated anomalies with the greatest hyporheic discharges had been reworked recently during recent high winter flows and presumably had fewer

fines than older and less reworked parts of the bar. These older bar surfaces tended to be well-vegetated and have likely accumulated fines for longer periods of time. Our slug tests also suggested that *K* values can vary dramatically between newer and older bar features.

Bar channels and bar heads also have hydraulic gradients greater than the longitudinal river gradient due to downstream hydraulic controls and backwater effects. The slope transition at the head of the bar in effect acts as a broad-crested weir, slowing upstream flows. The water that does infiltrate the head of the bar will generally follow a shorter flow path directly through the bar; this will be the steepest gradient across the bar. Together, higher *K* and steeper hydraulic gradient create preferential flow paths, concentrating hyporheic flow. At Eagle Creek, we estimate that 76 % of the total hyporheic flow in the bar was focused along a preferential flow path, giving rise to the downstream temperature anomaly.

On some bars, we found recently reworked bar channels and bar heads that appeared ideal candidates for preferential hyporheic flow, but no temperature anomaly was found. We speculate that in these cases hyporheic flow was present but in phase with mainstem temperature. For a maximum temperature difference to occur, the travel time across the bar must be $24(N\text{-}1/2)$ h where $N$ is a positive integer. A minimum temperature difference occurs, regardless of hyporheic discharge, at $24\ N$ h. This means that certain bar sizes and *K* values can produce significant hyporheic flow but have no appreciable effect on the river temperature.

This study reveals the close coupling among channel morphology, hyporheic flow, and thermal heterogeneity. The relationship among these processes will be affected by channel dynamics in both natural rivers and those located downstream from dams or other anthropogenic influences. In the case of the Clackamas, long-term reduction in sediment supply and transport due to upstream dams has resulted in at least some reaches with limited gravel and skeletal coarse bars. The proposed artificial introduction of gravel to the river below the lowest dam has the potential to increase sediment transport, thereby affecting rates of bar construction, reworking, and channel migration. By the results presented here, there should be at least some local

effects on stream temperatures due to this increased channel activity. It remains to be seen what the magnitude and location of this effect is likely to be, but the opportunity to examine the relationships among channel morphology, stream temperature and hyporheic flow represents an ideal field experiment.

## 2.6 CONCLUSIONS

Our field investigation identified 40 temperature anomalies over a 24-km reach on the lower Clackamas River, a low gradient, gravel-bed river. Temperature anomalies are the result of hyporheic exchange deviating from mainstem temperatures throughout the day, largely due to buffering and lagging of advected heat. The occurrence of temperature anomalies depends strongly on the presence of bar morphology. More specifically, hyporheic exchange that directly influences river temperature is associated with geomorphic features on bars like bar channels and bar heads that exhibit higher gradients (versus river gradient) and higher hydraulic conductivities. The flow emerging from these anomalies is largely controlled by the hydraulic conductivity of the sediments, meaning that gravel bars that have recently formed or been reworked will have greater hyporheic discharges.

A simple mixing model demonstrates that the overall cooling effect associated with these temperature anomalies is small (0.012˚C) due to the fact that hyporheic discharge emerging from these anomalies is only a small fraction (< 0.07 %) of mainstem discharge in a large river. However, these patches of cooler water can benefit cold water species such as salmon, providing local habitat and refugia from warmer mainstem temperatures. With emerging interest in river restoration and incorporating natural river processes into restoration projects (Boulton, 2007), the creation or enhancement of cool patches resulting from hyporheic exchange is a viable method that could be used to offset the harmful effects of thermal degradation.

# 3 CONCLUSIONS

The motivation behind this project was to determine the sensitivity of a large, gravel-bed river to the temperature buffering effects of hyporheic exchange and postulate how gravel augmentation could cool a river by increasing hyporheic exchange.

Temperature surveys and TIR demonstrated that significant thermal heterogeneity exists on the lower Clackamas River, especially with regard to the gravel bar population. A large driver of this heterogeneity is due to patches of hyporheic water that demonstrate out-of-phase temperatures with the mainstem, referred to as temperature anomalies in this study. These anomalies are intimately connected with geomorphic features on gravel bars (bar channels and heads) that focus flow along preferential pathways. This anomaly network is reset each year with high flows, where flow path lengths, hydraulic conductivities, and hydraulic gradients of gravel bars may change as gravel is reworked.

The hyporheic discharges emerging from anomalies result from zones of high hydraulic conductivity, which occurs in gravel that has been recently reworked. However, the cumulative anomaly discharge on the lower Clackamas, in comparison with the large mainstem discharge, is small. Estimates of river cooling reflect this, composing only a fraction of a degree rather than several degrees observed in smaller rivers (Johnson, 2004). Our estimate does not include other potential thermal benefits governed by hyporheic exchange, including buffering effects from other hyporheic pathways (e.g. meander necks or submerged gravel), and thermal shielding resulting from water downwelling into the subsurface and not being exposed to solar radiation. Further studies would have to be developed to investigate these other effects. However, these other effects are not likely to drastically alter the amount of river cooling.

Adding gravel to a river will form new bars or enhance older bars, which will increase the amount of hyporheic exchange occurring throughout the river. This can lead to the development of new temperature anomalies that buffer river temperature. Still, this will not likely significantly affect overall river temperature (as modeled by

CE-QUAL-W2 and our mixing equation) but will provide localized fish habitat and refugia.

**BIBLIOGRAPHY**

Alexander MD, MacQuarrie, KTB. 2005. The measurement of groundwater temperature in shallow piezometers and standpipes. *Canadian Geotechnical Journal* **42**: 1377–1390.

Anderson MP. 2005. Heat as a ground water tracer. *Ground Water* **43**: 951-968.

Arrigoni A, Poole GC, Mertes LAK, O'Daniel SJ, Woessner, WW, Thomas SA. *In-press.* Buffering, lagging, or cooling? Disentangling mechanisms of hyporheic influence on stream channel temperature. *Water Resources Research*.

Arscott DB, Tockner K, Ward JV. 2001. Thermal heterogeneity along a braided floodplain river (Tagliamento River, northeastern Italy). *Canadian Journal of Fisheries and Aquatic Science **58***: 2359–2373.

Battelle, Clackamas River Hydroelectric Project (FERC No. 2195) Water Quality Model of the Clackamas River, Appendix H, report to Portland General Electric, 34 p., August, 2004.

Bencala KE, Walters RA. 1983. Simulation of solute transport in a mountain pool-and-riffle stream: A transient storage model. *Water Resources Research* **19**: 718-724.

Bencala KE. 2005. Hyporheic exchange flows. In *Encyclopedia of Hydrological Sciences*. Anderson MG (ed). Chichester, UK: John Wiley and Sons, Ltd; 1733-1740.

Boulton AJ, Findlay S, Marmonier P, Stanley EH, Valett HM. 1998. The functional significance of the hyporheic zone in streams and rivers. *Annual Review of Ecology and Systematics* **29**: 59-81. DOI: 10.1146/annurev.ecolsys.29.1.59.

Boulton AJ. 2007. Hyporheic rehabilitation in rivers: restoring vertical connectivity. *Freshwater Biology* **52**: 632-650. DOI: 10.1111/j.1365-2427.2006.01710.x.

Bouwer H, Rice RC. 1976. A slug test for determining hydraulic conductivity of unconfined aquifers with completely or partially penetrating wells. *Water Resources Research* **12**: 423-428.

Bouwer H. 1989. The Bouwer and Rice Slug Test – An Update. *Ground Water* **27**: 304-309.

Brown GW. 1969. Predicting temperatures of small streams. *Water Resources Research* **5**: 68-75.

Brown GW. 1970. Predicting the effect of clearcutting on stream temperature. *Journal of Soil and Water Conservation* **25**: 11-13.

Brown LE, Hannah DM, Milner AM. 2005. Spatial and temporal water column and streambed temperature dynamics within an alpine catchment: implications for benthic communities. *Hydrological Processes* **19***:* 1585–1610.

Bryenton AG. 2007. Heat balance of alcoves on the Willamette River, Oregon. MS thesis. Oregon State University. 92p.

Burkholder BK. 2008. Influence of hyporheic flow and geomorphology on temperature of a large, gravel-bed river, Clackamas River, Oregon, USA. MS thesis. Oregon State University. 180p.

Butler Jr. JJ. 1998. *The Design, Performance and Analysis of Slug Tests.* CRC Press, LLC: Boca Raton; 149-169.

Butler Jr. JJ, Garnett EJ. 2000. Simple procedures of analysis of slug tests in formations of high hydraulic conductivity using spreadsheet and scientific graphics software. KGS Open File Report 2000-40. Kansas Geological Survey: Lawrence, Kansas, USA. http://www.krewg.org/Hydro/Publications/OFR00_4-/index.html Date of Access: February 15, 2007.

Cole TM, Wells SA. 2004. CE-Qual-W2: *A Two-Dimensional, Laterally Averaged, Hydrodynamic and Water Quality Model, Version 3.2. User Manual*. Instruction Report E-95-1. U.S. Army Corps of Engineers: Washington, DC.

Cozzetto K, McKnight D, Nylen T, and Fountain A. 2006. Experimental investigations into processes controlling stream and hyporheic temperatures, Fryxell Basin, Antarctica. *Advances in Water Resources* **29**: 130-153.

D'Angelo DJ, Webster JR, Gregory SV, Meyer JL. 1993. Transient storage in Appalachian and Cascade mountain streams as related to hydraulic characteristics. *Journal of the North American Benthological Society* **12**: 223-235.

Ebersole JL, Liss WJ, Frissell CA. 2001. Relationship between stream temperature, thermal refugia and rainbow trout *Oncorhynhus mykiss* abundance in arid-land streams in the northwestern United States. *Ecology of Freshwater Fish* **10**: 1-10.

Edwards RT. 1998. The hyporheic zone. In *River Ecology and Management: Lessons from the Pacific Coastal Ecoregion*, Naiman RJ, Bilby RE (eds). Springer Verlag: New York; 399-429.

Elliot JM, Hurley MA. 1997. A functional model for maximum growth of Atlantic salmon parr, *Salmo salar*, from two populations in northwest England. *Functional Ecology* **11**: 592-603.

Evans EC, and Petts GE. 1997. Hyporheic temperature patterns within riffles. *Hydrological Processes* **42**: 199-213.

Evans EC, McGregor GR, Petts GE. 1998. River energy budgets with special reference to river bed processes. *Hydrological Processes* **12**: 575-595.

Fernald AG, Landers DH, Wigington, PJ. 2000. Water quality effects of hyporheic processing in a large river. International Conference on Riparian Ecology and Management in Multi-Land US Watersheds, Portland, Oregon, USA: American Water Resources Association; 167-172,

Fernald AG, Landers DH, Wigington, PJ. 2006. Water quality changes in hyporheic flow paths between a large gravel bed river and off-channel alcoves in Oregon, USA. *River Research and Applications* **22**: 1111-1124. DOI: 10.1002/rra.961.

Hancock PJ, and Boulton AJ. 2005. The effects of an environmental flow release on water quality in the hyporheic zone of the Hunter River, Australia. *Hydrobiologia* **552**: 75-85.

Harvey JW, Wagner BJ. 2000. Quantifying hydrologic interactions between streams and their subsurface hyporheic zones. In *Streams and Ground Waters*, Jones JB, Mullholland PJ (eds). Academic Press: San Diego; 425.

Hunt RJ, Strand M, Walker JF. 2006. Measuring groundwater-surface water interaction and its effect on wetland stream benthic productivity, Trout Lake watershed, northern Wisconsin, USA. *Journal of Hydrology* **320**: 370-384.

Johnson SL, Jones JA. 2000. Stream temperature response to forest harvest and debris flows in western Cascades, Oregon. *Canadian Journal of Fisheries and Aquatic Sciences* **57**: 30-39.

Johnson SL. 2004. Factors influencing stream temperatures in small streams: substrate effects and a shading experiment. *Canadian Journal of Fisheries and Aquatic Sciences* **61**: 913-923. DOI: 10.1139/F04-040.

Johnston TA. 1997. Downstream movement of young-of-the-year fishes in Catamaran Brook and the Little Southwest Miramichi River, New Brunswick. *Journal of Fish Biology* **51**: 1047-1062.

Kasahara T, Wondzell SM. 2003. Geomorphic controls on hyporheic exchange flow in mountain streams. *Water Resources Research* **39**: 1005. DOI: 10.1029/2002WR001386.

Keery J, Binley A, Crook N, Smith JWN. 2006. Temporal and spatial variability of groundwater-surface water fluxes: Development and application of an analytical method using temperature time series. *Journal of Hydrology* **336**: 1-16.

Khangaonkar T, Yang Z. 2007. Dynamic Response of Stream Temperatures to Boundary and Inflow Perturbation due to Reservoir Operations. *River Research and Applications* **in press**:

Loheide II SP, Gorelick, SM. 2006. Quantifying stream-aquifer interactions through the analysis of remotely sensed thermographic profiles and in situ temperature histories. *Environmental Science and Technology* **40**: 3336-3341. DOI: 10.1021/es0522074.

Lowney CL. 2000. Stream Temperature Variation in Regulated Rivers: Evidence for a Spatial Pattern in Daily Minimum and Maximum Magnitudes. *Water Resources Research* **36**: 2947–2955.

McDonald MG, Harbaugh AW. 1988. A modular three-dimensional finite difference groundwater flow model. OR-83-875 U.S. Geological Survey. Reston, Virginia.

Moore RD, Sutherland P, Gomi T, Dhakal A. 2005. Thermal regime of a headwater stream within a clear-cut, coastal British Columbia, Canada. *Hydrological Processes* **19**: 2591-2608.

Packman AI, Salehin M. 2003. Relative roles of stream flow and sedimentary conditions in controlling hyporheic exchange. *Hydrobiologia* **494**: 291-297.

Peterson EW, Sickbert TB. 2006. Stream water bypass through a meander neck, laterally extending the hyporheic zone. *Hydrogeology Journal* **14**:1443-1451. DOI: 10.1007/s10040-006-0050-3

Portland General Electric (PGE). 2005. Application for Certification Pursuant to Section 401 of the Federal Clean Water Act. FERC No. 2195. Portland General Electric: Portland, Oregon USA.

Polehn RA, Kinsel WC. 1997. Transient temperature solution for streamflow from a controlled temperature source. *Water Resources Research* **33**: 261–265.

Pollock DW. 1994. User's guide for MODFLOW/MODPATH-PLOT, version 3, A particle tracking post-processing package for MODFLOW, the U.S. Geological

Survey finite-difference ground-water flow model. U.S. Geological Survey, Reston, Virginia.

Poole GC, Berman, CH. 2001. An ecological perspective on in-stream temperature: Natural heat dynamics and mechanisms of human-caused thermal degradation. *Environmental Management* **27**: 787-802. DOI: 10.1007/s002670010188.

Poole GC, Stanford JA, Running SW, Frissell CA. 2006. Multiscale geomorphic drivers of groundwater flow paths: Subsurface hydrologic dynamics and hyporheic habitat diversity. *Journal of the North American Benthological Society* **25**: 288–303.

Savant SA, Reible DD, Thibodeaux LJ. 1987. Convective transport within stable river sediments. *Water Resources Research* **23**: 1763-1768.

Silliman SE, Booth DF. 1993. Analysis of time-series measurements of sediment temperature for identification of gaining vs. losing portions of Juday Creek, Indiana. *Journal of Hydrology* **146**: 131-148.

Silliman SE, Ramirez J, McCabe RL. 1995. Quantifying downflow through creek sediments using temperature time series: one-dimensional solution incorporating measured surface temperature. *Journal of Hydrology* **167**: 99-119.

Sliva L, Williams DD. 2005. Exploration of riffle-scale interactions between abiotic variables and microbial assemblages in the hyporheic zone. *Canadian Journal of Fisheries and Aquatic Sciences* **62**: 276-290.

Sinokrot BA, Gulliver JS. 2000. In-stream flow impact on river water temperatures. *Journal of Hydraulic Research* **28**: 339-349.

Stallman RW. 1965. Steady one-dimensional fluid flow in a semi-infinite porous medium with sinusoidal surface temperature. *Journal of Geophysical Research* **70**: 2821-2827.

Story A., Moore RD, Macdonald JS. 2003. Stream temperatures in two shaded reaches below cutblocks and logging roads: downstream cooling linked to subsurface hydrology. C*anadian Journal of Forest Research **33*:** 1383–1396. DOI: 10.1139/X03-087.

Sullivan K, Adams TN. 1991. The physics of stream heating: 2) An analysis of temperature patterns in stream environments based on physical principles and field data. Technical Report 044-5002/89/2. Weyerhaeuser Company: Tacoma, Washington, USA.

Torgersen CE, Price DM, Li HW, McIntosh BA. 1999. Multiscale thermal refugia and stream habitat associations of Chinook salmon in northeastern Oregon. *Ecological Applications* **9**: 301-319.

Vannote RL, Minshall GW, Cummins KW, Sedell JR, Cushing CE. 1980. The river continuum concept. *Canadian Journal of Fisheries and Aquatic Sciences* **37**: 130-137.

Wampler PJ. 2004. *Contrasting geomorphic responses to climatic, anthropogenic, and fluvial change across modern to millennial time scales, Clackamas River, Oregon*. PhD Dissertation, Oregon State University. 398p.

Webb BW, Walling DE 1993b. Temporal variability in the impact of river regulation on thermal regime and some biological implications. *Freshwater Biology* **29**: 167-182.

Wentworth CK. 1922. A scale of grade and class terms for clastic sediments. *Journal of Geology* **30**: 377–392.

White DS, Elzinga CH, Hendricks SP. 1987. Temperature patterns within the hyporheic zone of a northern Michigan river. *Journal of North American Benthological Society* **6:** 85-91.

Wolman MG. 1954. A Method of Sampling Coarse River-Bed Material. *Transactions of the American Geophysical Union* **35**: 951–956.

Wondzell SM, Swanson FJ. 1999. Flood, channel change, and the hyporheic zone. Water *Resources Research* **35**: 555-567.

# APPENDICES

# APPENDIX A

## AERIAL ANALYSIS OF LOWER CLACKAMAS RIVER BAR POPULATION

## A.1 Qualitative and semi-quantitative geomorphic description of lower Clackamas River gravel bar population

We used aerial photos from summer 2005 and summer 2006 to help describe the lower Clackamas River gravel bar population. Lengths, widths are bar areas were calculated using measuring tools within ArcGIS. Field reconnaissance provided further insights on bar stability, including recency of gravel reworking and vegetation.

Table A.1 lists the parameters for the gravel bars.

## Table A.1: Location and brief description of gravel bars on lower Clackamas River

| RKM | Northing (ft)[1] | Easting (ft) | Bar Type[2] | Longitudinal Length (m) | Average Width (m) | Maximum Width (m) | Area ($m^2$) | Vegetation | Reworked over 2005/2006? | Percent of Bar Network |
|---|---|---|---|---|---|---|---|---|---|---|
| 36.4 | 601288 | 7724245 | L | 146 | 17 | 35 | 4168 | mature | N | 0.39 |
| 36.1 | 601254 | 7725196 | L | 162 | 19 | 29 | 3357 | mature | N | 0.31 |
| 35.8 | 600900 | 7723174 | L | 314 | 44 | 69 | 13320 | zonation (immature to mature) | N | 1.23 |
| 35.6 | 600808 | 7722913 | L | 323 | 71 | 87 | 19918 | mature | N | 1.84 |
| 35.2 | 599860 | 7721986 | MC | 186 | 26 | 31 | 3124 | zonation | N | 0.29 |
| 35.0 | 600588 | 7721070 | MC | 113 | 30 | 43 | 3028 | zonation | N | 0.28 |
| 34.7 | 601811 | 7721180 | MC | 456 | 94 | 136 | 41452 | zonation | N | 3.83 |
| 35.0 | 601017 | 7721399 | L | 207 | 41 | 63 | 8881 | mature | N | 0.82 |
| 34.3 | 602478 | 7721906 | PB | 271 | 33 | 56 | 9573 | immature/none | N | 0.89 |
| 33.8 | 604135 | 7722922 | MC | 211 | 44 | 60 | 9089 | mature | N | 0.84 |
| 33.5 | 604198 | 7722087 | L | 510 | 137 | 197 | 71396 | mature | N | 6.60 |
| 33.3 | 604388 | 7721397 | MC | 69 | 15 | 21 | 1045 | zonation | N | 0.10 |
| 33.3 | 604190 | 7721054 | MC | 32 | 14 | 22 | 485 | immature/none | N | 0.04 |
| 33.3 | 604932 | 7721631 | MC | 63 | 16 | 16 | 894 | none | N | 0.08 |
| 33.3 | 604808 | 7721361 | MC | 36 | 14 | 14 | 382 | immature | N | 0.04 |
| 33.1 | 604574 | 7721105 | MC | 547 | 105 | 146 | 45094 | immature/mature | N | 4.17 |
| 33.0 | 604744 | 7720297 | MC | 77 | 26 | 31 | 1715 | zonation | N | 0.16 |
| 32.8 | 605224 | 7720208 | MC | 166 | 55 | 56 | 8183 | mature | N | 0.76 |
| 32.6 | 605317 | 7719454 | MC | 784 | 77 | 125 | 60290 | mature | N | 5.58 |
| 32.5 | 605209 | 7719004 | L | 304 | 35 | 43 | 8759 | mature | N | 0.81 |
| 32.4 | 606034 | 7718909 | L | 198 | 37 | 37 | 7516 | immature | N | 0.70 |
| 32.1 | 605912 | 7717799 | MC | 315 | 65 | 81 | 16782 | immature/mature | N | 1.55 |
| 31.9 | 606346 | 7717301 | PB | 237 | 56 | 62 | 9259 | immature | N | 0.86 |
| 31.9 | 606080 | 7717152 | L | 151 | 19 | 24 | 3065 | mature | N | 0.28 |

## Table A.1: Location and brief description of gravel bars on lower Clackamas River

| RKM | Northing (ft)[1] | Easting (ft) | Bar Type[2] | Longitudinal Length (m) | Average Width (m) | Maximum Width (m) | Area ($m^2$) | Vegetation | Reworked over 2005/2006? | Percent of Bar Network |
|---|---|---|---|---|---|---|---|---|---|---|
| 31.6 | 607110 | 7716775 | PB | 287 | 76 | 76 | 11114 | immature/mature | N | 1.03 |
| 31.1 | 608169 | 7717663 | L | 265 | 27 | 52 | 9100 | immature/mature | N | 0.84 |
| 30.6 | 610108 | 7718182 | L | 294 | 27 | 53 | 9401 | immature/mature | N | 0.87 |
| 29.7 | 612816 | 7718130 | L | 326 | 69 | 85 | 21810 | immature/mature | N | 2.02 |
| 29.3 | 613634 | 7717603 | MC | 279 | 51 | 54 | 12589 | immature/none | N | 1.16 |
| 29.1 | 613973 | 7717170 | L | 245 | 62 | 139 | 18102 | zonation | Y | 1.67 |
| 28.9 | 614651 | 7716330 | PB | 77 | 49 | 49 | 8125 | zonation | Y | 0.75 |
| 28.7 | 615137 | 7716500 | L | 120 | 32 | 35 | 3967 | immature | Y | 0.37 |
| 28.4 | 616099 | 7716864 | L | 155 | 23 | 29 | 3167 | zonation | N | 0.29 |
| 28.0 | 616567 | 7717105 | L | 133 | 19 | 19 | 2298 | mature | N | 0.21 |
| 27.4 | 618107 | 7717641 | MC | 294 | 104 | 139 | 24217 | zonation/none | N | 2.24 |
| 27.2 | 618559 | 7717780 | L | 126 | 27 | 32 | 3122 | none | Y | 0.29 |
| 27.2 | 618674 | 7717484 | MC | 208 | 47 | 67 | 9247 | immature/none | N | 0.86 |
| 26.5 | 620328 | 7718141 | L | 213 | 62 | 82 | 11259 | zonation | Y | 1.04 |
| 26.4 | 620945 | 7718102 | MC | 534 | 183 | 234 | 61106 | mature/none | Y | 5.65 |
| 26.1 | 621420 | 7717932 | PB | 217 | 60 | 60 | 12448 | zonation | Y | 1.15 |
| 26.4 | 620667 | 7718281 | MC | 86 | 22 | 34 | 2282 | immature/none | Y | 0.21 |
| 26.0 | 621799 | 7718134 | MC | 70 | 40 | 63 | 3908 | none | Y | 0.36 |
| 25.7 | 623891 | 7716574 | L | 260 | 17 | 29 | 6800 | immature | N | 0.63 |
| 24.9 | 624536 | 7715811 | L | 435 | 32 | 41 | 11407 | immature | N | 1.05 |
| 24.5 | 625483 | 7714889 | L | 215 | 29 | 29 | 7110 | none | Y | 0.66 |
| 23.7 | 627385 | 7714015 | L | 481 | 169 | 206 | 65015 | immature/mature | Y | 6.01 |
| 24.2 | 626724 | 7714372 | MC | 283 | 64 | 78 | 12997 | zonation | N | 1.20 |
| 24.1 | 626774 | 7713852 | L | 76 | 11 | 14 | 1593 | none | Y | 0.15 |
| 24.1 | 626785 | 7713554 | L | 73 | 14 | 19 | 1304 | none | Y | 0.12 |

## Table A.1: Location and brief description of gravel bars on lower Clackamas River

| RKM | Northing (ft)[1] | Easting (ft) | Bar Type[2] | Longitudinal Length (m) | Average Width (m) | Maximum Width (m) | Area ($m^2$) | Vegetation | Reworked over 2005/2006? | Percent of Bar Network |
|---|---|---|---|---|---|---|---|---|---|---|
| 22.9 | 628167 | 7713893 | L | 70 | 29 | 29 | 1728 | none | Y | 0.16 |
| 22.3 | 629146 | 7713496 | MC | 253 | 70 | 102 | 17552 | immature/none | N | 1.62 |
| 21.9 | 629353 | 7712093 | L | 545 | 38 | 73 | 23148 | immature/none | N | 2.14 |
| 21.5 | 630326 | 7711139 | L | 554 | 33 | 49 | 1649 | zonation | N | 0.15 |
| 21.2 | 630807 | 7710608 | L | 216 | 36 | 37 | 5967 | zonation | N | 0.55 |
| 20.6 | 632425 | 7709709 | MC | 398 | 76 | 97 | 26906 | zonation | N | 2.49 |
| 20.6 | 632281 | 7709246 | L | 369 | 81 | 141 | 33873 | zonation | N | 3.13 |
| 20.5 | 632879 | 7709420 | MC | 59 | 34 | 36 | 1834 | immature/none | Y | 0.17 |
| 20.1 | 633208 | 7708721 | MC | 407 | 124 | 142 | 42214 | zonation/none | Y | 3.90 |
| 20.0 | 633747 | 7708382 | MC | 126 | 21 | 32 | 3204 | immature/none | N | 0.30 |
| 19.9 | 633782 | 7708037 | PB | 244 | 77 | 77 | 11625 | zonation | N | 1.08 |
| 20.2 | 632831 | 7708596 | MC | 196 | 46 | 48 | 7801 | immature/none | Y | 0.72 |
| 20.2 | 632935 | 7708710 | MC | 20 | 11 | 11 | 240 | immature/none | Y | 0.02 |
| 20.2 | 632931 | 7708781 | MC | 25 | 13 | 13 | 200 | immature/none | Y | 0.02 |
| 19.6 | 633839 | 7707092 | L | 169 | 14 | 16 | 2790 | none | Y | 0.26 |
| 19.1 | 633866 | 7705329 | PB | 318 | 137 | 156 | 35351 | zonation | N | 3.27 |
| 18.7 | 633285 | 7705151 | L | 178 | 26 | 58 | 6499 | immature/mature | N | 0.60 |
| 18.9 | 632935 | 7704733 | L | 28 | 14 | 16 | 621 | none | Y | 0.06 |
| 18.0 | 631409 | 7702850 | MC | 101 | 54 | 54 | 4655 | zonation | Y | 0.43 |
| 18.5 | 632454 | 7704302 | L | 193 | 23 | 24 | 3476 | zonation | N | 0.32 |
| 17.6 | 632019 | 7701353 | L | 127 | 54 | 93 | 23657 | immature/mature | N | 2.19 |
| 17.7 | 632024 | 7701964 | L | 140 | 10 | 12 | 2449 | zonation | N | 0.23 |
| 17.9 | 631657 | 7702595 | PB | 140 | 42 | 54 | 4163 | zonation | N | 0.39 |
| 16.7 | 632456 | 7698622 | L | 283 | 30 | 37 | 7609 | immature | N | 0.70 |
| 15.7 | 632818 | 7696007 | PB | 311 | 38 | 80 | 12767 | none | N | 1.18 |

## Table A.1: Location and brief description of gravel bars on lower Clackamas River

| RKM | Northing (ft)[1] | Easting (ft) | Bar Type[2] | Longitudinal Length (m) | Average Width (m) | Maximum Width (m) | Area ($m^2$) | Vegetation | Reworked over 2005/2006? | Percent of Bar Network |
|---|---|---|---|---|---|---|---|---|---|---|
| 15.8 | 632592 | 7695733 | MC | 44 | 18 | 25 | 742 | immature | N | 0.07 |
| 15.0 | 634555 | 7695692 | MC | 700 | 45 | 83 | 36737 | mature | Y | 3.40 |
| 14.8 | 635550 | 7695072 | PB | 247 | 17 | 25 | 4109 | zonation | N | 0.38 |
| 14.6 | 635910 | 7694702 | MC | 27 | 51 | 51 | 1907 | immature/none | Y | 0.18 |
| 14.0 | 635782 | 7692740 | MC | 326 | 178 | 274 | 52282 | zonation | Y | 4.84 |
| 13.8 | 635310 | 7692126 | PB | 58 | 67 | 98 | 5237 | none | Y | 0.48 |
| 13.4 | 635600 | 7690981 | MC | 228 | 54 | 73 | 11294 | immature/mature | N | 1.04 |
| 13.2 | 635943 | 7690270 | L | 38 | 93 | 74 | 2260 | none | Y | 0.21 |
| 13.5 | 635552 | 7690806 | MC | 9 | 6 | 6 | 76 | immature | N | 0.01 |
| 13.3 | 635887 | 7690611 | MC | 13 | 26 | 32 | 411 | none | Y | 0.04 |

[1] Northings and Eastings are in NAD83 Oregon North State Plane Projection.
[2] MC = mid-channel; L = lateral; PB = point bar

# APPENDIX B

## SURFACE AND SUBSURFACE PEBBLE COUNT DATA

## B.1 Pebble Count Procedure

Pebble counts were conducted using a method similar to Wolman (1954). Transects were laid out across gravel bars (ranging from 30 to 100 m), and pebbles were randomly picked along regular intervals of that transect. Subsurface pebble counts were conducted by throwing a Frisbee 10 times randomly along the transect, removing the upper layer of pebbles, and counting the first 10 pebbles touched.

The fine fraction (< 1 mm) was qualitatively described (coarse sand/fine sand/silt/clay), and when entered into results, assigned a grain size according to the Udden-Wentworth scale (Wentworth, 1922). There were no attempts to further quantify these smaller grains.

Table B.1 shows the locations where pebble counts were conducted.

## Table B.1 Pebble Count Data

| Pebble Count Number | Date | RKM | Northing (ft) | Easting (ft)[1] | Transect Length (m) | D50 (cm) | D50sub (cm) | Notes |
|---|---|---|---|---|---|---|---|---|
| 1 | 7/21/2006 | 34.6 | 602063 | 7721618 | 66 | 10.0 | 1.0 | Across bar tail |
| 2 | 7/21/2006 | 34.6 | 601946 | 7721388 | 66 | 19.5 | 2.4 | Down cross bar channel |
| 3 | 7/21/2006 | 34.5 | 602339 | 7721831 | 66 | 12.2 | 1.7 | Across bar head |
| 4 | 7/21/2006 | 34.4 | 602496 | 7721907 | 66 | 11.8 | 1.2 | Remnant channel |
| 5 | 7/21/2006 | 32.1 | 605931 | 7717896 | 76 | 9.5 | 1.1 | Unvegetated channel |
| 6 | 7/18/2006 | 27.3 | 618028 | 7717713 | 87 | 4.8 | 0.8 | Down cross bar channel |
| 7 | 7/24/2006 | 27.5 | 617692 | 7717439 | 66 | 13.9 | 1.6 | Across bar tail |
| 8 | 7/18/2006 | 29.5 | 613191 | 7717806 | 35 | 7.9 | 1.4 | Tail of back bar channel |
| 9 | 7/18/2006 | 29.7 | 612465 | 7718101 | 33 | 10.4 | 1.1 | Head of back bar channel |
| 10 | 8/1/2006 | 29.7 | 612771 | 7717990 | 66 | 9.4 | 1.2 | Middle of back bar channel |
| 11 | 7/24/2006 | 27.1 | 618537 | 7717397 | 40 | 10.4 | 1.2 | Across bar between hf and pool |
| 12 | 7/24/2006 | 26.6 | 620392 | 7718132 | 73 | 5.9 | 0.9 | Along new surface of gravel |
| 13 | 7/24/2006 | 26.5 | 620632 | 7718374 | 66 | 7.9 | 1.4 | Along bar edge |
| 14 | 7/12/2006 | 26.1 | 621571 | 7717976 | 33 | 7.8 | 4.8 | Small bar near HF channel |
| 15 | 7/12/2006 | 26.2 | 621353 | 7717810 | 33 | 3.7 | 2.3 | Head of bar |
| 16 | 7/12/2006 | 26.1 | 621451 | 7717892 | 33 | 3.7 | 2.8 | Mid-bar |
| 17 | 7/12/2006 | 26.0 | 622021 | 7717955 | 33 | 3.5 | 2.8 | Bar tail |
| 18 | 7/26/2006 | 24.1 | 626700 | 7714233 | 2 16-m | 5.9 | 1.5 | Near HF |
| 19 | 7/19/2006 | 20.8 | 631861 | 7710091 | 33 | 6.1 | 1.1 | Across bar head |
| 20 | 7/19/2006 | 20.5 | 632637 | 7709701 | 33 | 4.1 | 1.1 | Near HF |
| 21 | 7/17/2006 | 20.5 | 632795 | 7709414 | 66 | 6.9 | 1.6 | Along unvegetated gravel at bar tail |
| 22 | 7/19/2006 | 20.3 | 632990 | 7709133 | 100 | 7.2 | 0.7 | Across bar head |
| 23 | 7/19/2006 | 20.0 | 633371 | 7708339 | 66 | 7.6 | 1.3 | Across new gravel exposure |
| 24 | 7/19/2006 | 20.2 | 632836 | 7708680 | 47 | 6.8 | 2.2 | Across bar head |
| 25 | 7/17/2006 | 19.9 | 633478 | 7708129 | 33 | 7.0 | 1.0 | Across point bar |
| 26 | 7/25/2006 | 14.0 | 635900 | 7692993 | 100 | 4.3 | 1.1 | Across interior |
| 27 | 8/9/2006 | 13.8 | 635868 | 7692448 | 100 | 6.8 | 1.1 | Along small finger of gravel |

[1] Northings and Eastings are in NAD83 Oregon North State Plane Projection.

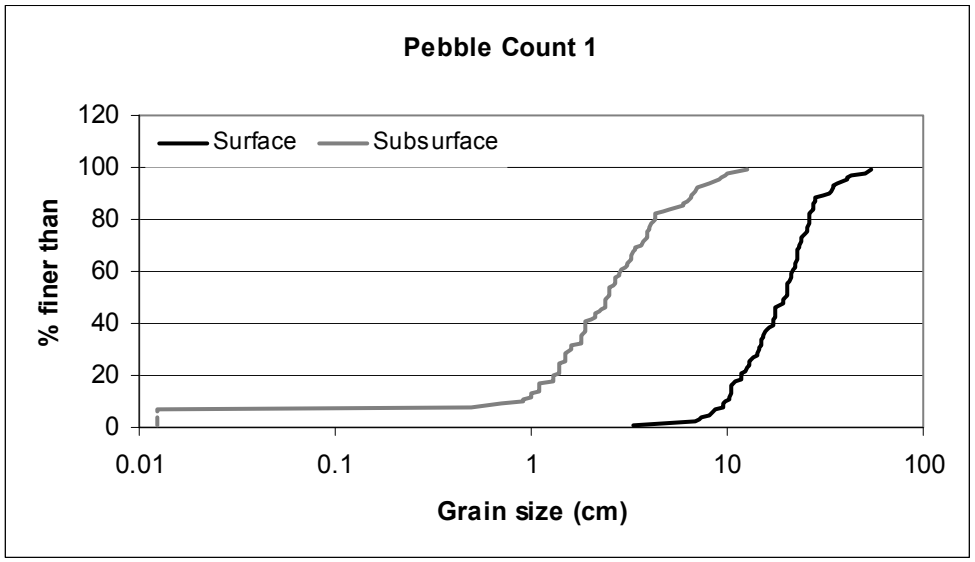
Pebble Count 1
Surface
Subsurface
% finer than
120
100
80
60
40
20
0
0.01
0.1
1
10
100
Grain size (cm)

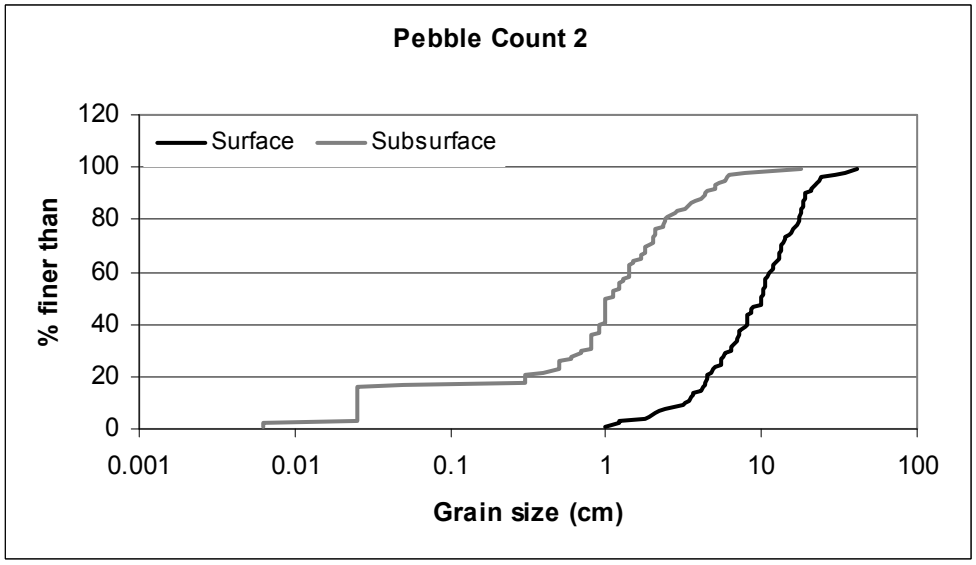
Pebble Count 2
Surface
Subsurface
% finer than
120
100
80
60
40
20
0
0.001
0.01
0.1
1
10
100
Grain size (cm)

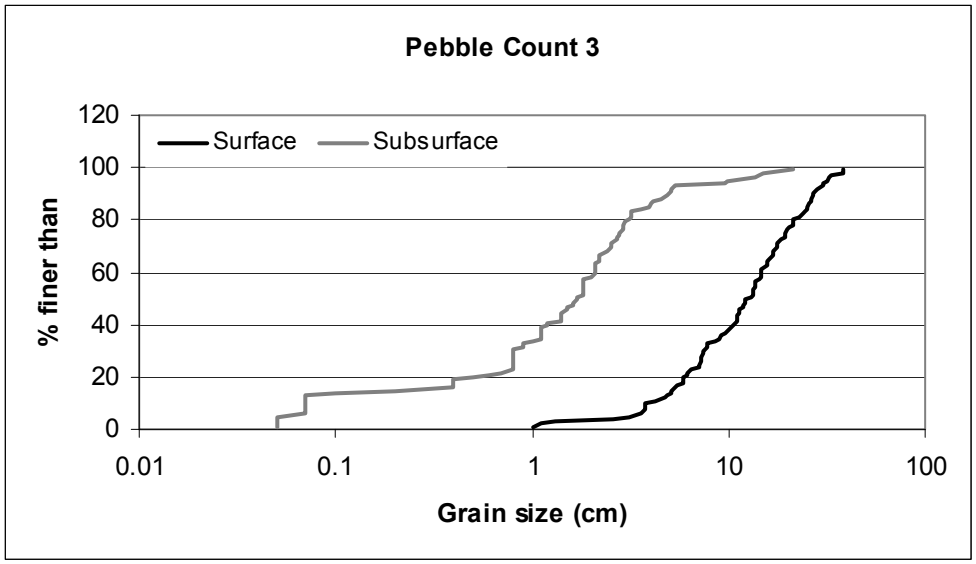
Pebble Count 3
120
100
80
60
40
20
0
% finer than
Surface
Subsurface
0.01
0.1
1
10
100
Grain size (cm)

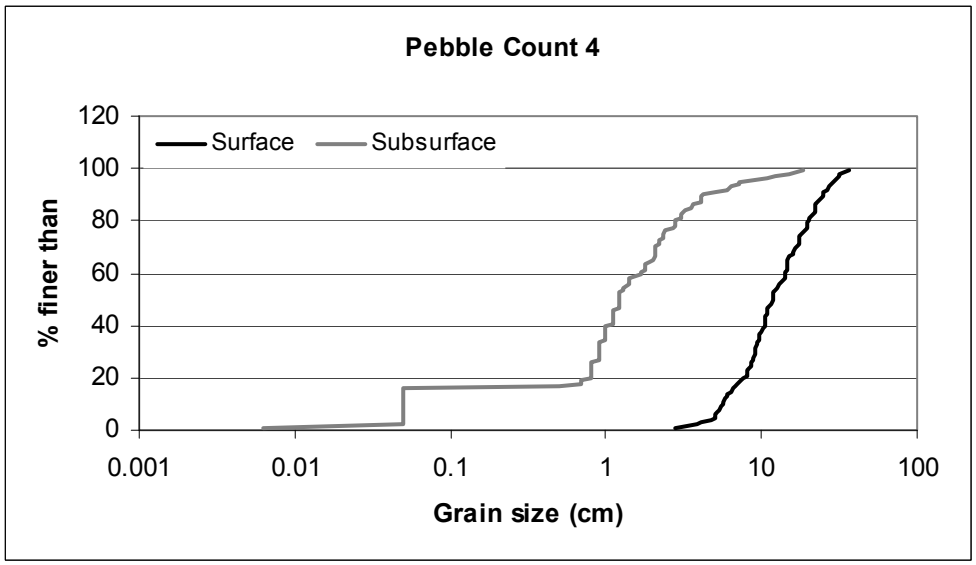
Pebble Count 4
120
100
80
60
40
20
0
% finer than
Surface
Subsurface
0.001
0.01
0.1
1
10
100
Grain size (cm)

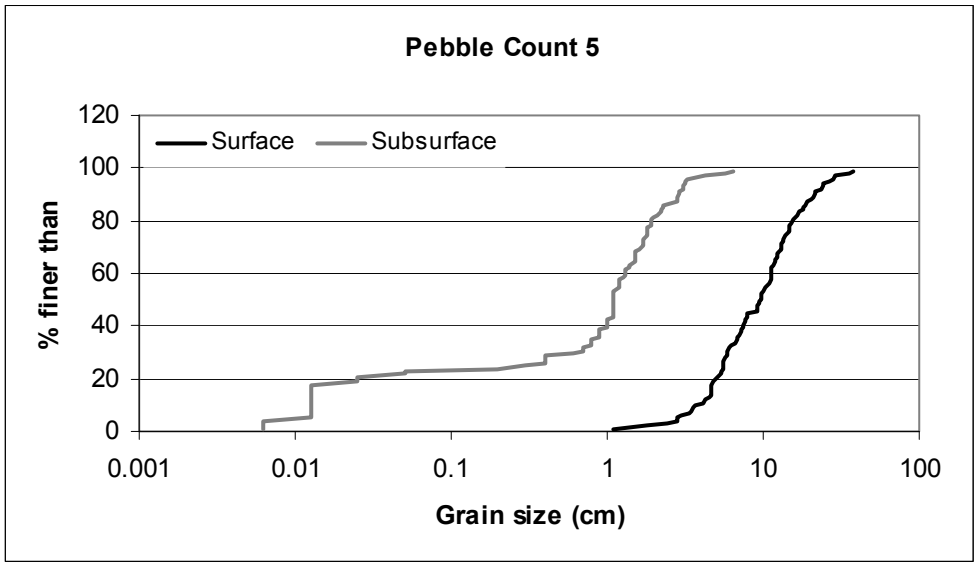
Pebble Count 5
120
100
80
60
40
20
0
% finer than
Surface
Subsurface
0.001
0.01
0.1
1
10
100
Grain size (cm)

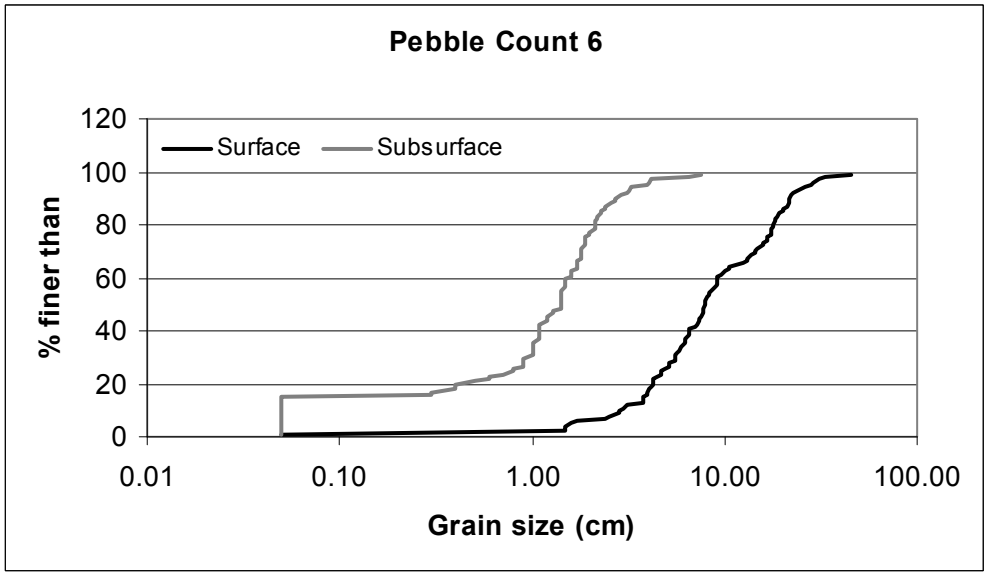
Pebble Count 6
120
100
80
60
40
20
0
% finer than
Surface
Subsurface
0.01
0.10
1.00
10.00
100.00
Grain size (cm)

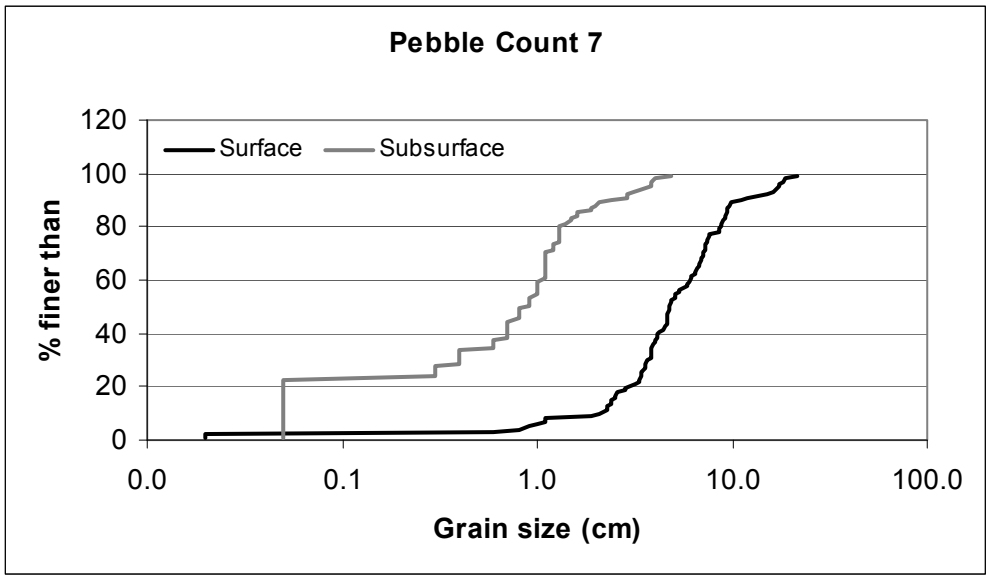
Pebble Count 7
120
100
80
60
40
20
0
Surface
Subsurface
% finer than
0.0
0.1
1.0
10.0
100.0
Grain size (cm)

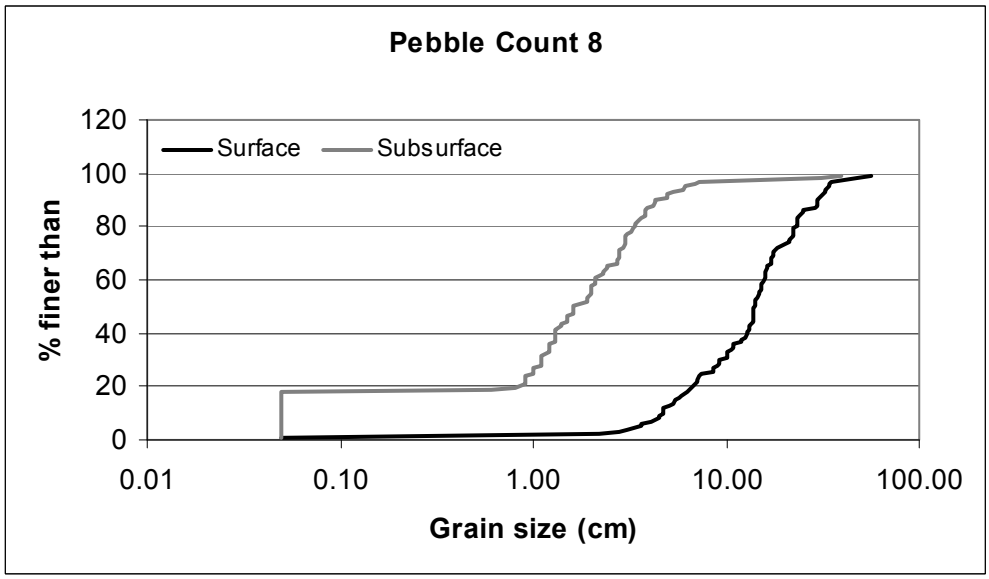
Pebble Count 8
120
100
80
60
40
20
0
Surface
Subsurface
% finer than
0.01
0.10
1.00
10.00
100.00
Grain size (cm)

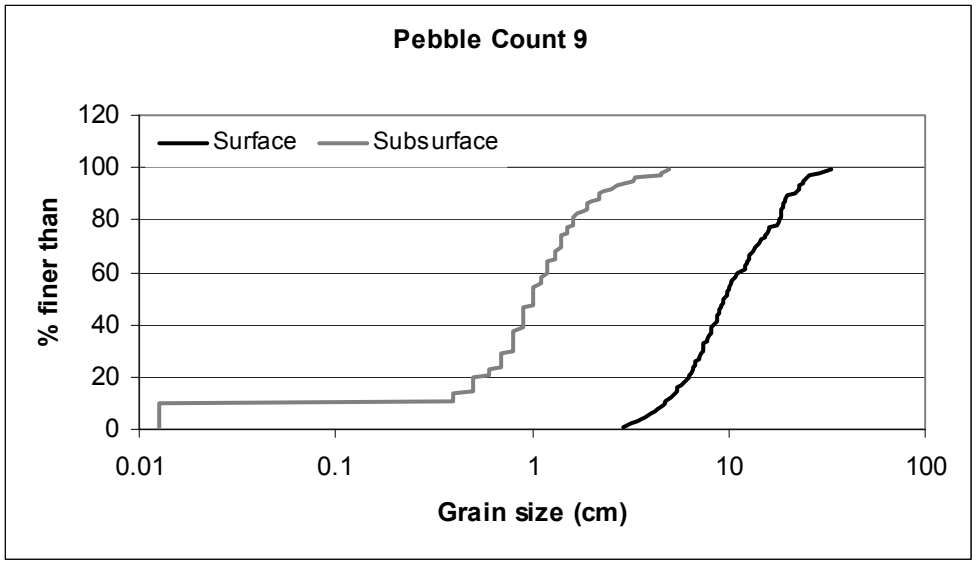
Pebble Count 9
120
100
80
60
40
20
0
% finer than
Surface
Subsurface
0.01
0.1
1
10
100
Grain size (cm)

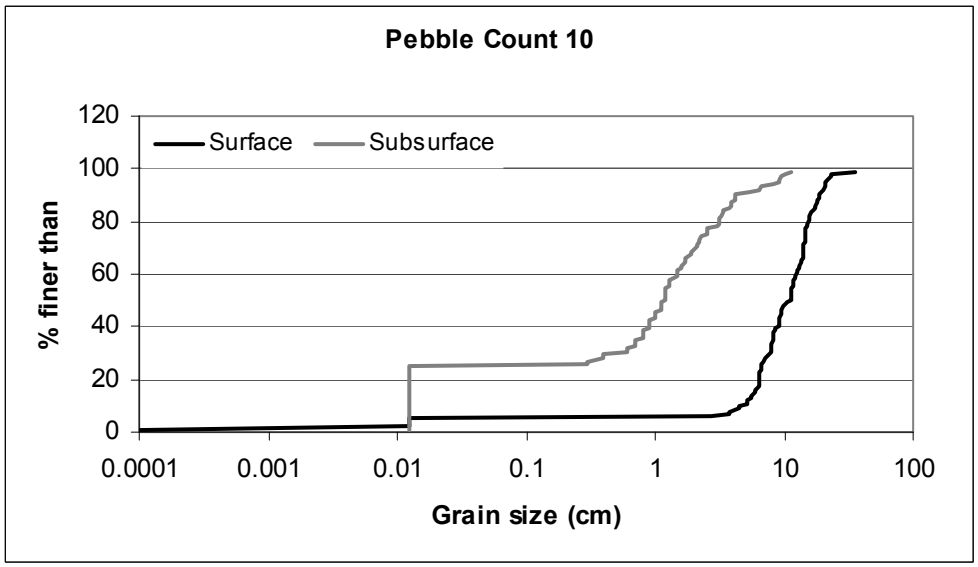
Pebble Count 10
120
100
80
60
40
20
0
% finer than
Surface
Subsurface
0.0001
0.001
0.01
0.1
1
10
100
Grain size (cm)

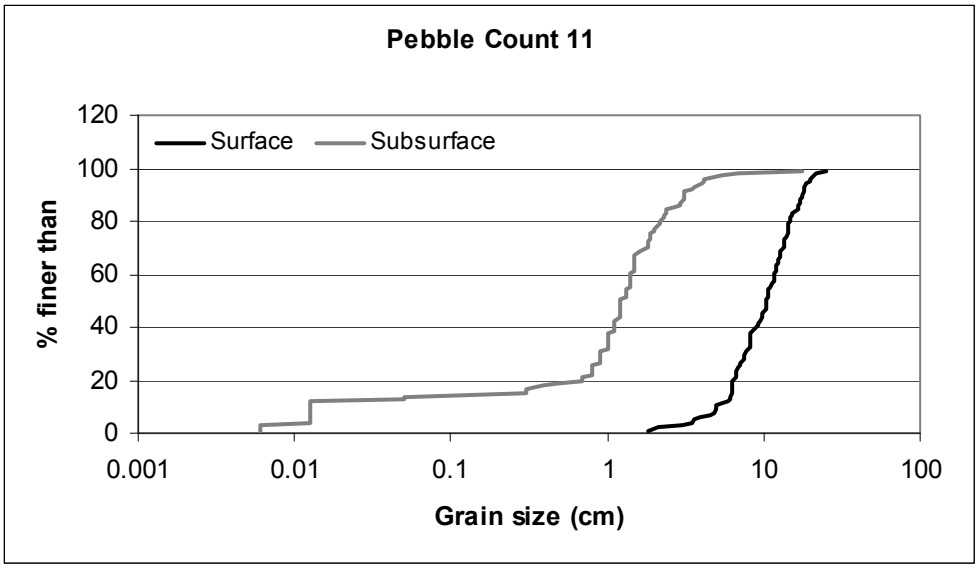
Pebble Count 11
120
100
80
60
40
20
0
% finer than
Surface
Subsurface
0.001
0.01
0.1
1
10
100
Grain size (cm)

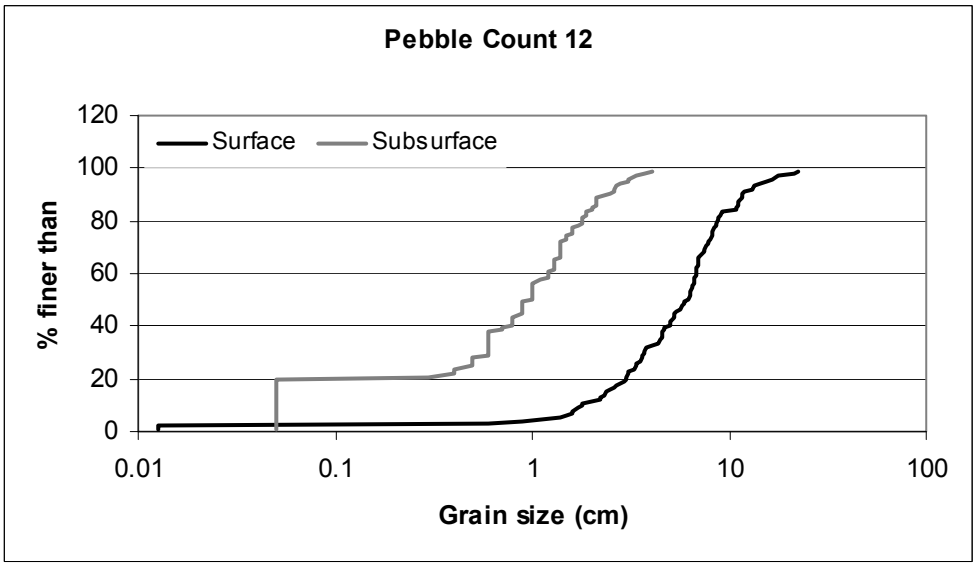
Pebble Count 12
120
100
80
60
40
20
0
% finer than
Surface
Subsurface
0.01
0.1
1
10
100
Grain size (cm)

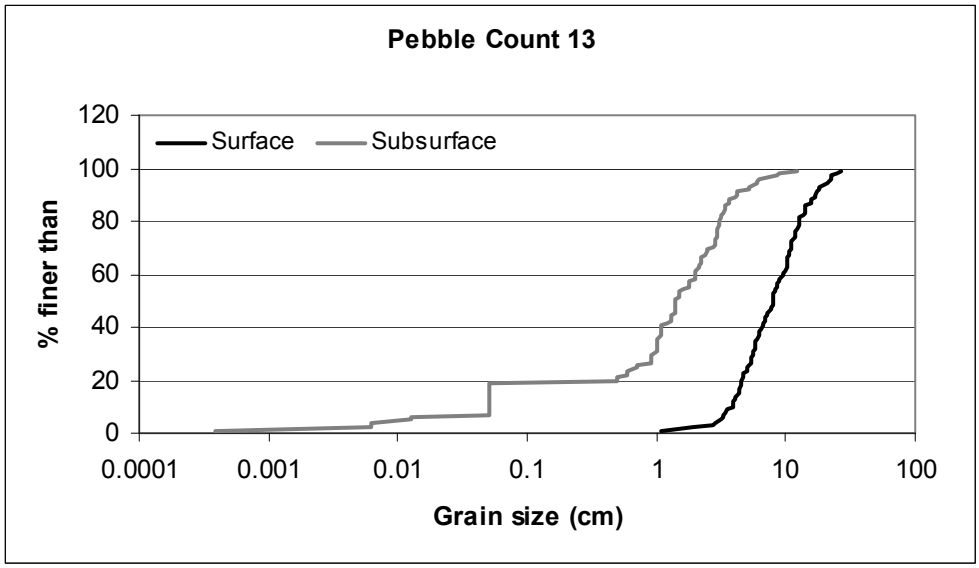
Pebble Count 13
Surface
Subsurface
% finer than
120
100
80
60
40
20
0
0.0001
0.001
0.01
0.1
1
10
100
Grain size (cm)

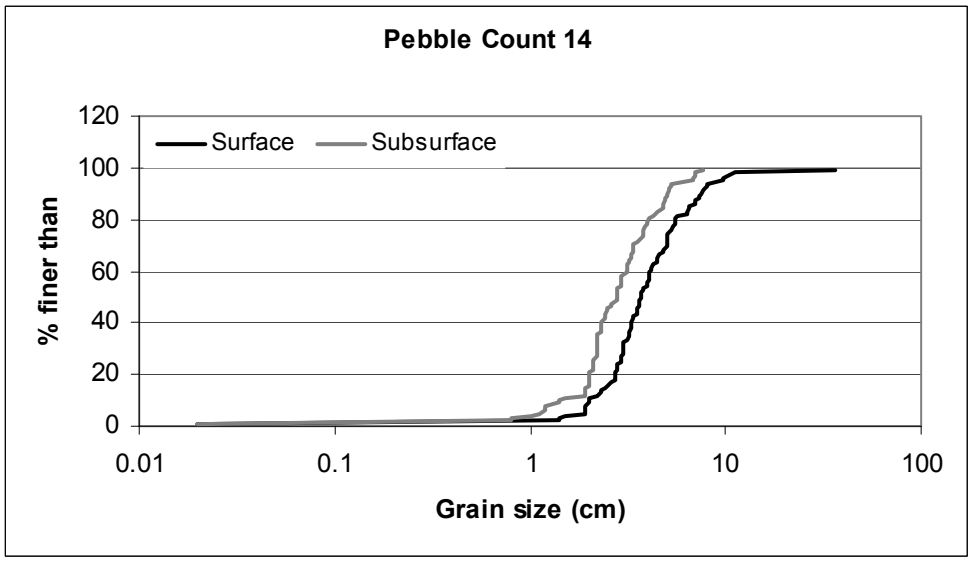
Pebble Count 14
Surface
Subsurface
% finer than
120
100
80
60
40
20
0
0.01
0.1
1
10
100
Grain size (cm)

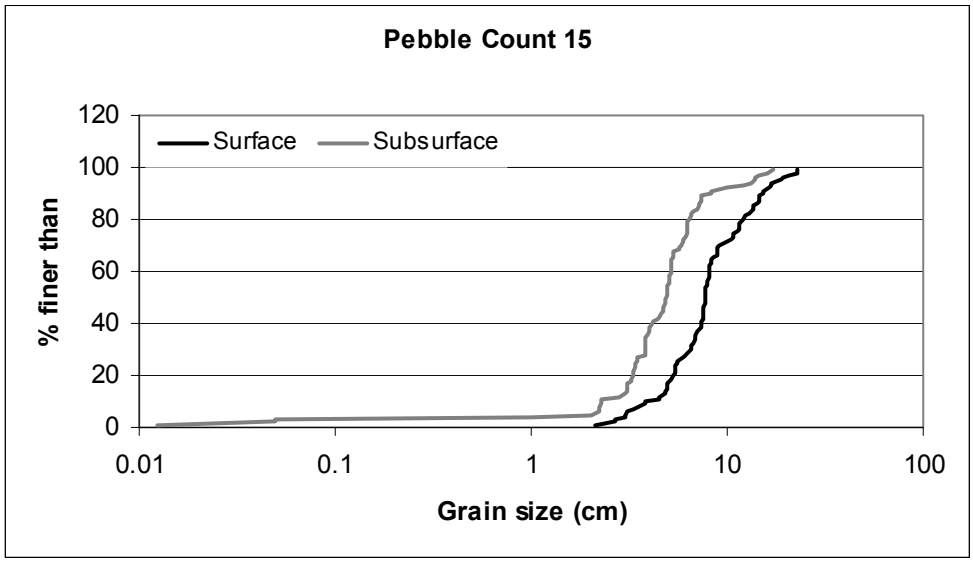
Pebble Count 15
120
100
80
60
40
20
0
% finer than
Surface
Subsurface
0.01
0.1
1
10
100
Grain size (cm)

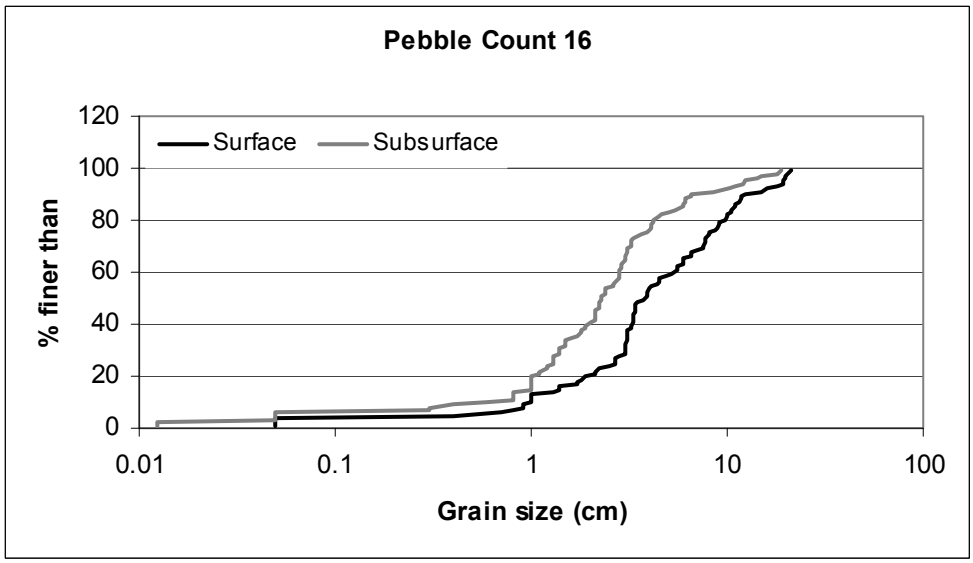
Pebble Count 16
120
100
80
60
40
20
0
% finer than
Surface
Subsurface
0.01
0.1
1
10
100
Grain size (cm)

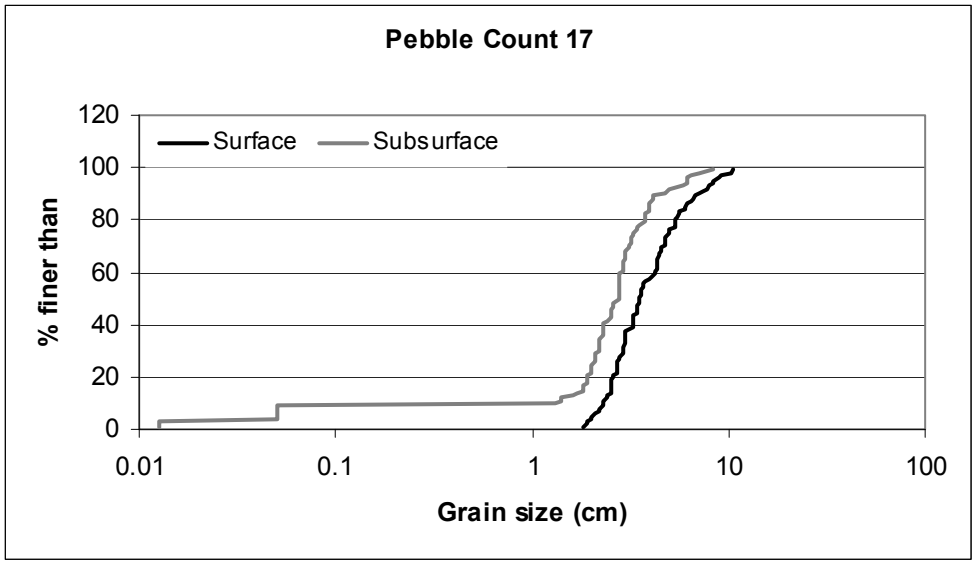
Pebble Count 17
120
100
80
60
40
20
0
% finer than
Surface
Subsurface
0.01
0.1
1
10
100
Grain size (cm)

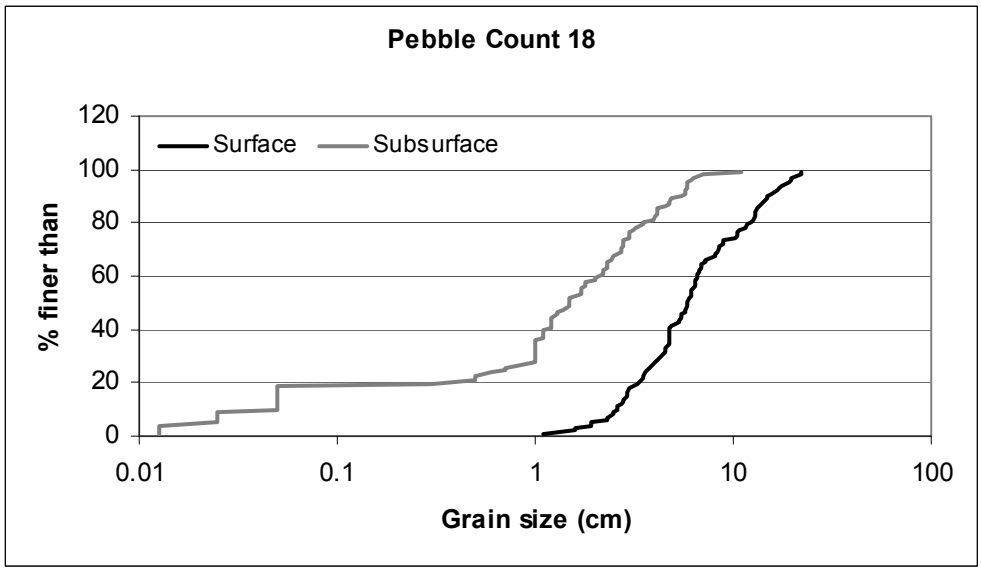
Pebble Count 18
120
100
80
60
40
20
0
% finer than
Surface
Subsurface
0.01
0.1
1
10
100
Grain size (cm)

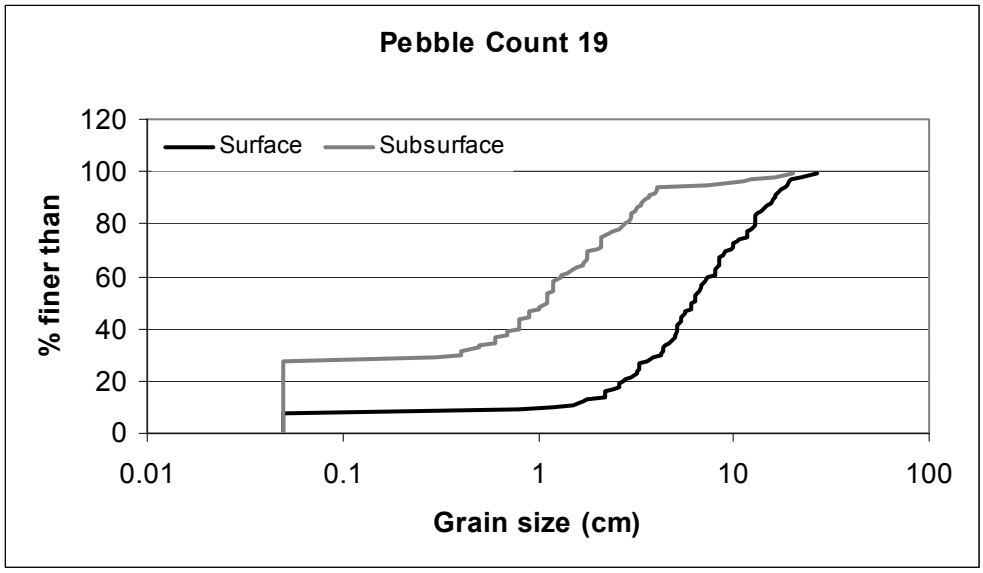
Pebble Count 19
120
100
80
60
40
20
0
Surface
Subsurface
% finer than
0.01
0.1
1
10
100
Grain size (cm)

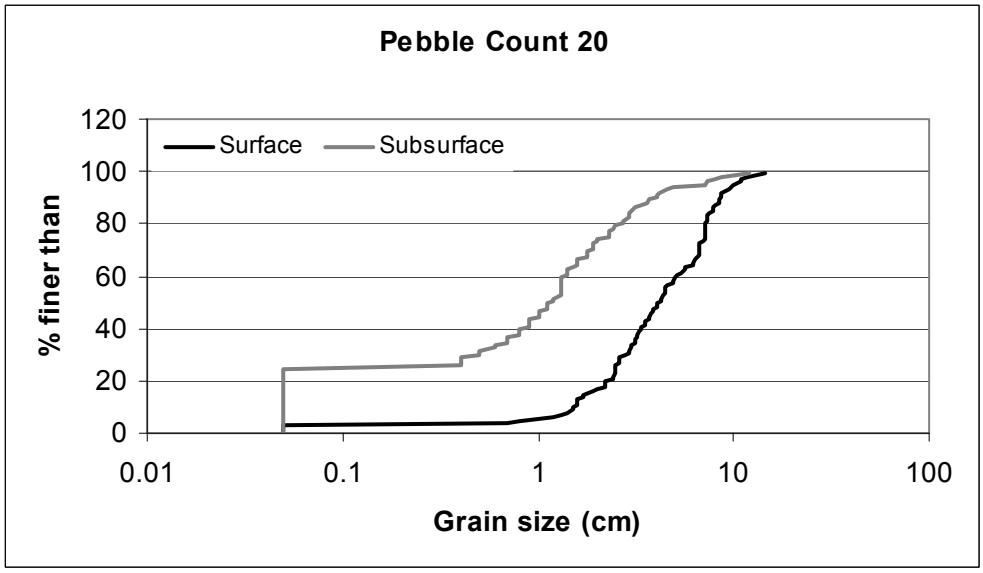
Pebble Count 20
120
100
80
60
40
20
0
Surface
Subsurface
% finer than
0.01
0.1
1
10
100
Grain size (cm)

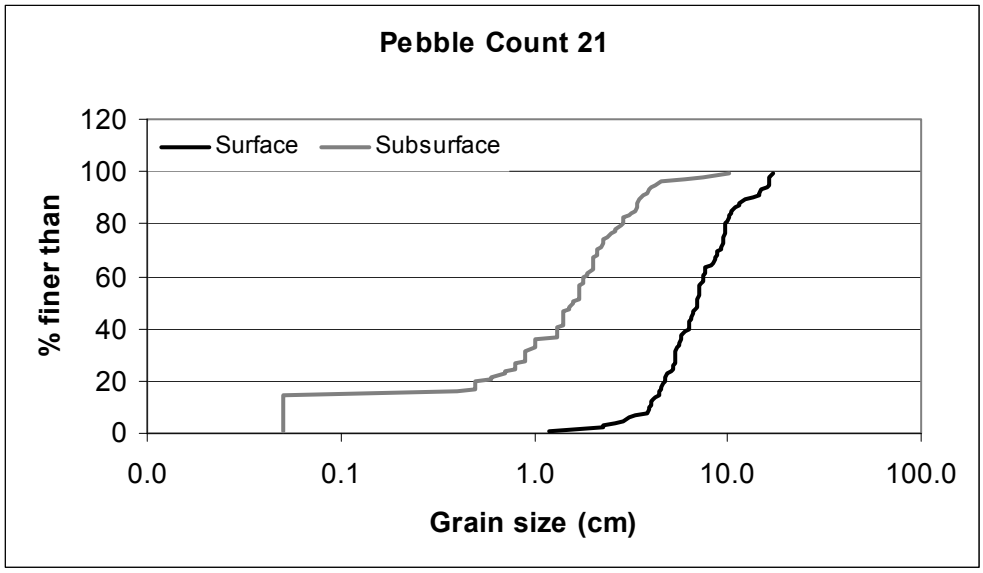
Pebble Count 21
120
100
80
60
40
20
0
Surface
Subsurface
% finer than
0.0
0.1
1.0
10.0
100.0
Grain size (cm)

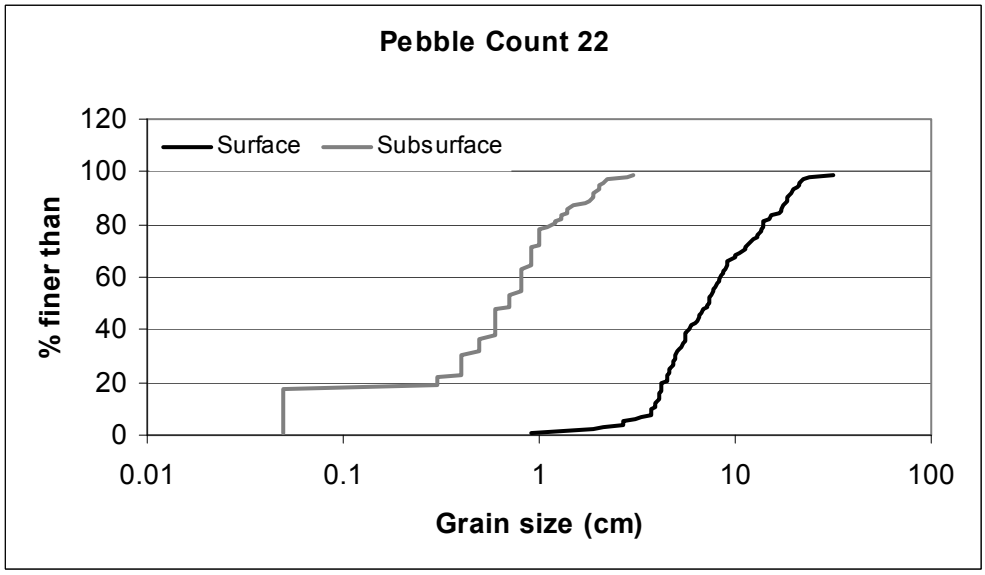
Pebble Count 22
120
100
80
60
40
20
0
Surface
Subsurface
% finer than
0.01
0.1
1
10
100
Grain size (cm)

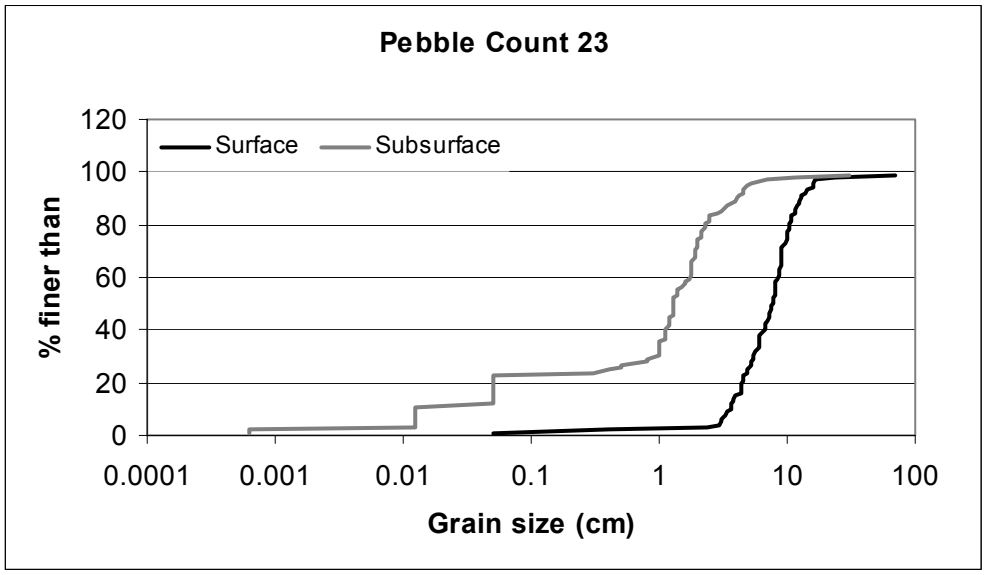
Pebble Count 23
120
100
80
60
40
20
0
% finer than
Surface
Subsurface
0.0001
0.001
0.01
0.1
1
10
100
Grain size (cm)

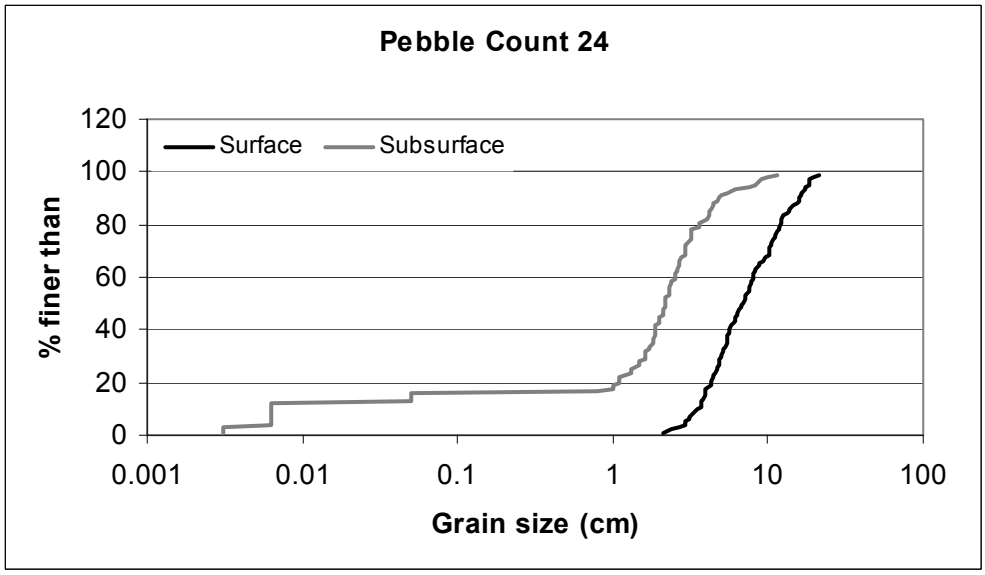
Pebble Count 24
120
100
80
60
40
20
0
% finer than
Surface
Subsurface
0.001
0.01
0.1
1
10
100
Grain size (cm)

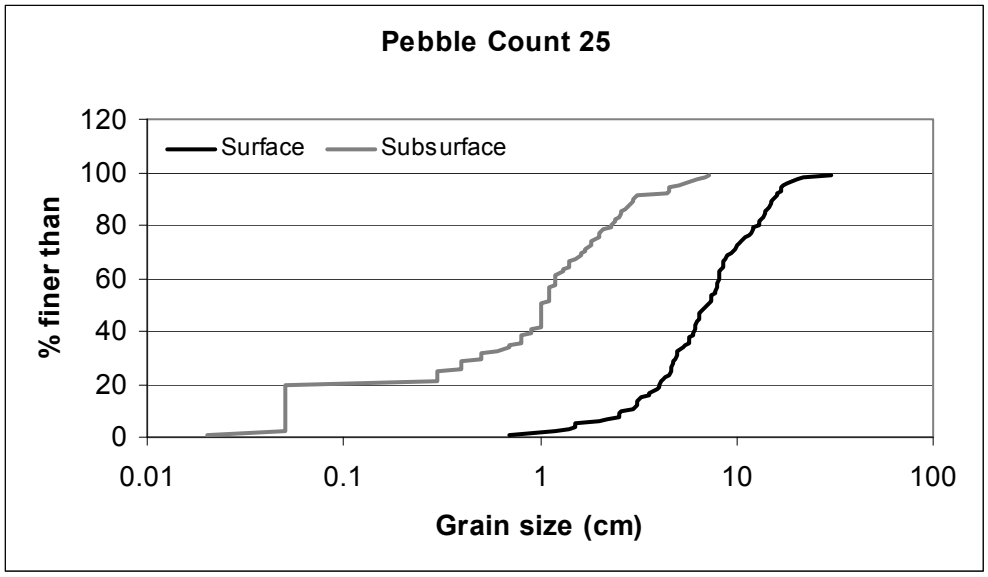
Pebble Count 25
120
100
80
60
40
20
0
Surface
Subsurface
% finer than
0.01
0.1
1
10
100
Grain size (cm)

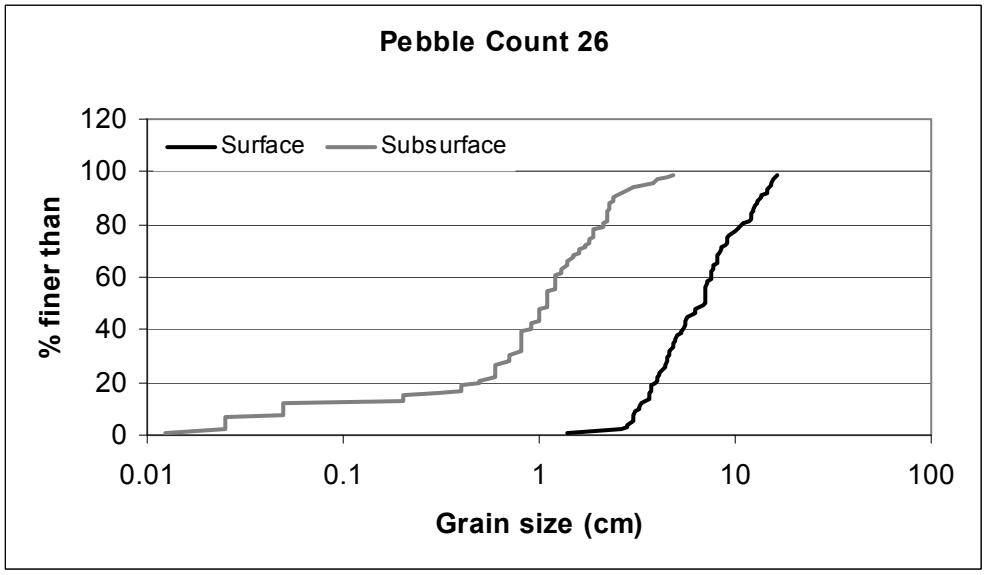
Pebble Count 26
120
100
80
60
40
20
0
Surface
Subsurface
% finer than
0.01
0.1
1
10
100
Grain size (cm)

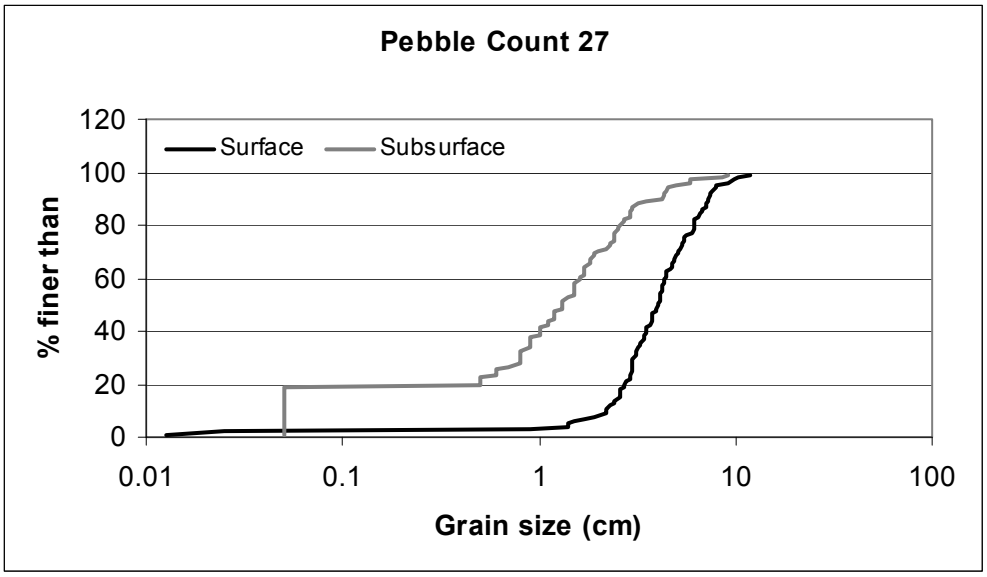
Pebble Count 27
120
100
80
60
40
20
0
% finer than
Surface
Subsurface
0.01
0.1
1
10
100
Grain size (cm)

# APPENDIX C

## LOCATION AND DESCRIPTION OF TEMPERATURE ANOMALIES

## Table C.1: Location and brief description of temperature anomalies

| No. | RKM | Northing (ft)[1] | Easting (ft) | Type of Bar[2] | Field/ TIR | Geomorphic feature | Bar recently reworked? | Conduc tivity (µS/cm) | Ave. ΔT (°C) | Ave. gradient | Ave. Width (m) | Ave. Depth (m) |
|---|---|---|---|---|---|---|---|---|---|---|---|---|
| 1 | 34.6 | 602111.42 | 7721596.65 | MC | Field | Bar Head (Ramp) | N | 55-60 | 0.2 | 0.005 | 5 | 2.5 |
| 2 | 34.6 | 602170.76 | 7721363.09 | MC | Field | BC: Cross Bar | N | 55-60 | 1.4 | 0.015 | 3 | 2 |
| 3 | 34.6 | 602177.07 | 7721298.70 | MC | Field | GW seep | N | 55-60 | 4.8 | 0.015 | 1 | 1.5 |
| 4 | 34.3 | 602906.79 | 7722215.27 | L | Field | GW seep | N | 81.7 | 2.3 | 0.0057 | 1 | 0.05 |
| 5 | 33.5 | 603982.42 | 7722191.28 | L | Both | BC:Back Bar/GW seep | N | - | 0.7 | 0.005 | 15 | 1.5 |
| 6 | 33.1 | 604548.02 | 7720683.87 | MC | Field | BC: Cross Bar | N | - | 2.3 | 0.007 | 3 | 1 |
| 7 | 32.8 | 605196.93 | 7720590.45 | MC | TIR | GW seep | N | - | 3 | -- | Pool | 2 |
| 8 | 32.5 | 605193.15 | 7718937.86 | L | Field | BC: Back Ba/GW seep | N | 80-120s | 2.5 | 0.005 | 81 | 1 |
| 9 | 30.6 | 610165.10 | 77.18132.26 | L | Both | BC: Back Bar/GW seep | N | 55 - | 2.3 | 0.008 | 22 | 1 |
| 10 | 29.7 | 613291.98 | 7717772.59 | L | Field | BC: Back Bar/GW seep | N | 55-60 | 2.1 | 0.01 | 17 | 2 |
| 11 | 29.1 | 614059.56 | 7716988.58 | L | Both | GW seep | N | - | 5.4 | 0.003 | chan edge | -- |
| 12 | 28.4 | 616197.42 | 7716887.59 | L | Both | BC: Back Bar | N | 127 | 4.8 | 0.005 | 1 | 1 |
| 13 | 27.4 | 618168.95 | 7717492.32 | MC | Field | BC: Remnant | N | 70-80 | 0.2 | 0.017 | 1 | 3 |
| 14 | 27.4 | 618325.50 | 7717761.22 | MC | TIR | BC: Cross Bar | N | 50-60s | 1.5 | 0.0029 | 3.7 | 1.5 |
| 15 | 27.2 | 618540.12 | 7717328.19 | MC | Field | Bar Head (Ramp) | N | 50-60s | 1.8 | 0.059 | 0.5 | 0.6 |
| 16 | 26.5 | 620414.91 | 7718201.83 | L | Both | BC: Remnant | Y | 50-120 | 1.1 | 0.007 | 6.7 | 0.2 |
| 17 | 26.5 | 620470.45 | 7718278.84 | L | Both | BC: Back Bar | N | 50-60s | 1.3 | 0.008 | 15 | 0.2 |
| 18 | 26.5 | 620629.53 | 7718336.92 | L | Field | GW seep | N | 80s | 5.1 | 0.007 | 25 | 0.5 |
| 19 | 26.4 | 620683.69 | 7717650.13 | MC | Both | BC: Remnant | Y | 80s | 1 | 0.004 | 3.5 | 0.5 |
| 20 | 26.1 | 621509.86 | 7717982.16 | PB | Both | Bar Head (Ramp) | Y | 50-60 | 2.25 | 0.012 | 22 | 3 |
| 21 | 26.1 | 622222.28 | 7717839.50 | PB | Field | GW seep | N | 50-60 | 5 | 0.007 | 4 | 2-3 |
| 22 | 23.7 | 627363.74 | 7713715.75 | L | Both | BC: Cross Bar | N | 50-60 | 1.5 | 0.02 | 2 | 3 |
| 23 | 23.7 | 627780.23 | 7713957.36 | L | Both | GW seep | N | 70s | 1 | 0.005 | Pool | 1 |
| 24 | 24.2 | 626533.66 | 7714443.42 | MC | Both | BC: Cross-bar | N | 50-60 | 1.1 | 0.007 | 2 | 1 |
| 25 | 24.2 | 626782.37 | 7714245.21 | MC | Both | Bar Head (Ramp) | Y | 50-60 | 2.8 | 0.007 | 2.6 | 1 |
| 26 | 24.2 | 626777.32 | 7714419.43 | MC | Field | BC: Back Bar | N | 50-60 | 0.4 | 0.007 | 27 | 1 |
| 27 | 24.2 | 627079.05 | 7714343.68 | MC | Field | BC: Back Bar | Y | 50-60 | 1.6 | 0.007 | 1 | 1 |
| 28 | 22.4 | 628860.03 | 7713530.39 | MC | TIR | Bar Head (Ramp) | N | - | 1.2 | 0.007 | 66 | 1.5 |
| 29 | 21.2 | 630789.11 | 7710552.19 | L | Field | GW seep | N | 80s | 2.8 | -- | chan edge | -- |
| 30 | 20.6 | 632644.96 | 7708759.47 | L | Both | GW seep | N | 80s | 1 | 0.005 | 2 | 0.1 |

## Table C.1: Location and brief description of temperature anomalies

| No. | RKM | Northing (ft)[1] | Easting (ft) | Type of Bar[2] | Field/ TIR | Geomorphic feature | Bar recently reworked? | Conductivity (µS/cm) | Ave. ΔT (°C) | Ave. gradient | Ave. Width (m) | Ave. Depth (m) |
|---|---|---|---|---|---|---|---|---|---|---|---|---|
| 31 | 20.4 | 632812.87 | 7709376.82 | MC | Field | Bar Head (Ramp) | Y | 50-60s | 1.2 | 0.019 | 1 | 2 |
| 32 | 20.1 | 632929.02 | 7708505.71 | MC | Both | BC: Remnant | Y | 50-60 | 1.9 | 0.015 | 4 | 2 |
| 33 | 20.1 | 633394.87 | 7708307.50 | MC | Both | BC: Remnant | Y | 50-60 | 1.6 | 0.01 | 3.5 | 0.5 |
| 34 | 20.0 | 633799.75 | 7708410.26 | MC | Both | Bar Head (Ramp) | Y | 50-60 | 0.6 | 0.01 | 3 | 1.5 |
| 35 | 19.6 | 633860.35 | 7706996.28 | L | TIR | BC: Back Bar | Y | - | 1.5 | 0.007 | 3 | 0.5 |
| 36 | 19.0 | 633254.36 | 7705173.26 | L | TIR | BC: Back Bar | Y | - | 1.1 | 0.006 | 1 | 1 |
| 37 | 18.8 | 632740.78 | 7704584.94 | L | Both | BC: Back-bar | Y | - | 0.6 | 0.007 | 2.4 | 1 |
| 38 | 17.5 | 631695.45 | 7702119.31 | L | Both | GW seep | N | 100-120 | 1.2 | -- | chan edge | 0.5 |
| 39 | 17.5 | 632220.64 | 7700837.89 | L | Field | GW seep | N | 226 | 6.3 | 0.005 | 0.05 | 0.01 |
| 40 | 16.7 | 632505.83 | 7698528.81 | L | Field | Bar Head (Ramp) | N | - | 1.9 | 0.013 | 35 | 0.5 |
| 41 | 15.0 | 634024.60 | 7698883.91 | MC | TIR | Bar Head (Ramp) | Y | - | 1 | 0.012 | 29 | 2.5 |
| 42 | 14.6 | 635867.83 | 7694699.70 | MC | TIR | Bar Head (Ramp) | Y | - | 1.6 | 0.01 | 4 | 1.5 |
| 43 | 13.8 | 635261.83 | 7692058.58 | PB | TIR | BC: Remnant | Y | - | 0.9 | 0.01 | 2.5 | 2.5 |
| 44 | 13.5 | 635525.69 | 7690794.84 | MC | Field | BC: Cross Bar? | N | - | 1 | 0.007 | 4 | 1 |
| 45 | 13.2 | 635846.36 | 7690601.68 | MC | TIR | Bar Head (Ramp) | Y | - | 1.1 | 0.007 | 20 | 1 |
| 46 | 27.2 | 619013.55 | 7717458.23 | MC | TIR | Bar Head (Ramp) | Y | 50-60s | 1.1 | 0.004 | 7 | 0.5 |
| 47 | 27.2 | 618704.24 | 7717763.75 | L | TIR | GW seep | Y | - | 1.8 | 0.007 | 3 | 0.5 |
| 48 | 26.4 | 620820.82 | 7718413.50 | MC | TIR | Bar Head (Ramp) | Y | - | 1.1 | 0.01 | 3 | 0.75 |
| 49 | 14.8 | 635734.06 | 7695136.91 | MC | TIR | Bar Head (Ramp) | Y | 50-60s | 1.4 | 0.01 | 2 | 2.5 |
| 50 | 24.1 | 626799.66 | 7713497.57 | L | TIR | BC: BBC?/Bar Head | Y | - | 1.8 | 0.007 | 8 | 0.5 |
| 51 | 24.1 | 626818.60 | 7713455.90 | L | TIR | Bar Head (Ramp) | Y | - | 0.7 | 0.007 | 3.6 | 0.5 |
| 52 | 24.1 | 626764.31 | 7713815.21 | L | TIR | Bar Head (Ramp) | Y | - | 0.8 | 0.007 | 1 | 0.5 |

[1] Northings and Eastings are in NAD83 Oregon North State Plane Projection.
[2] MC = mid-channel; L = lateral; PB = point bar

# APPENDIX D

# TIR METHODOLOGY AND REPORT

# Airborne Thermal Infrared Remote Sensing
Clackamas River, OR

*Submitted to:*

Barbara Burkholder
Water Resources Graduate Program
Oregon State University
Wilkinson Hall 213
Corvallis OR 9733

*Submitted by:*

**Watershed Sciences, Inc.**
111 NW 2nd Street, Unit 1
Corvallis, OR 97330

Survey Date: August 12, 2006
Report Date: October 15, 2006

# REPORT FOR THERMAL INFRARED REMOTE SENSING CLACKAMAS RIVER, OR

## Table of Contents

# Background

In 2006, researchers at the Water Resources Graduate Program at Oregon State University contracted with Watershed Sciences, Inc. to acquire thermal infrared (TIR) and true color imagery of the Clackamas River, OR from the River Mill Dam near the town of Estacada, OR to Carver, OR (~15 river miles). The objective of the survey was to map surface temperature patterns during both the minimum and maximum of the diurnal temperatures cycles in the river. Consequently, two flights were conducted. The first was conducted just prior to dawn on August 12th in order to capture daily minimum water temperatures. A second flight was also conducted on August 12th during the mid-afternoon in order to capture heat-of-the-day conditions.

Airborne thermal infrared (TIR) remote sensing has proven an effective method for mapping spatial temperature patterns in rivers and streams. These data are used to establish baseline conditions and direct future ground level monitoring. The TIR imagery illustrates the location and thermal influence of point sources, tributaries, and surface springs. This report details the work performed, including methodology and quantitative assessments of data quality. The images contained in this report are not meant to be comprehensive, but provide examples of image scenes and interpretations.

# Survey Extent

The TIR data were acquired on August 12, 2006 and consisted of an early morning flight (5:56–6:38) and a mid-afternoon flight (14:26–15:08). Both flights were conducted over the same river extent starting at the River Mill Dam (mile 23.0) and proceeding downstream to the Carver Bridge (mile 8.0). If the river split into multiple channels and the channels were outside of the sensor field of view, then a survey was conducted along each channel resulting in multiple flight lines over some sections of the river (see Figure 1). The map in Figure 1 also shows the location of temperature data loggers deployed by Watershed Sciences prior to the flight and used to calibrate the TIR images.

# Methods

## *Data Collection*

Instrumentation: Images were collected with a Space Instruments FireMapper 2.0 sensor (8-12μm) mounted on the underside of a Bell Jet Ranger Helicopter (Figure 2). The TIR sensor was co-mounted with a high-resolution true color digital camera (*Nikon D2X w/ 24mm lens, 6.9 mega-pixels*). Both cameras were positioned to look vertically down from the aircraft (nadir).

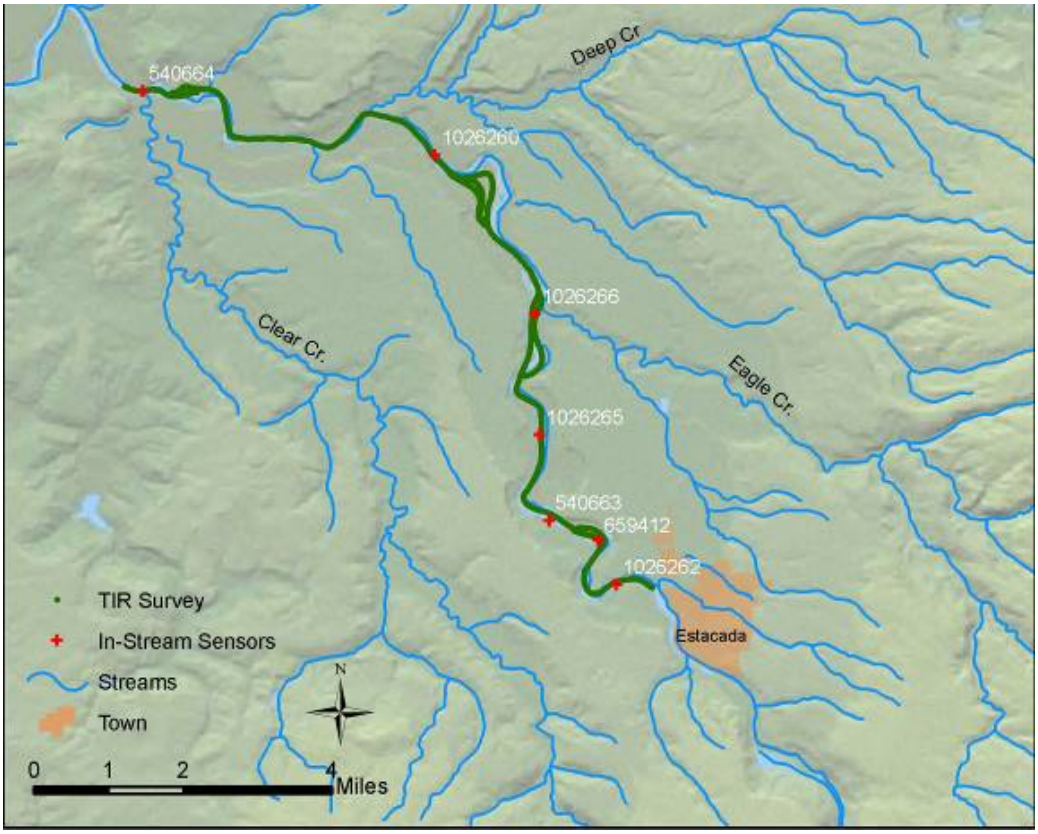


Figure 1 – The extent of the TIR survey conducted on the Clackamas River, OR on August 12, 2006. In-stream sensors used to calibrate the TIR images are shown on the map and labeled by serial number.

The TIR sensor has a horizontal field of view (H-FOV) of 44$^{o}$ and a pixel array of 320 x 240 pixels. The Firemapper 2.0 is a calibrated radiometer with internal non-uniformity correction and drift compensation. Thermal infrared images were recorded directly from the sensor to an on-board computer as raw counts, which were then converted to radiant temperatures. The individual images were referenced with time, position, and heading information provided by a global positioning system (GPS). General specifications of the sensor are listed in Table 1.


Figure 2 – Bell Jet Ranger equipped with a thermal infrared radiometer and high resolution digital camera. The sensors are contained in a composite fiber enclosure attached to the

underside of the helicopter and flown longitudinally along the stream channel.

Image Characteristics: The aircraft was flown longitudinally along the stream corridor in order with the river in the center of the display. The objective was for the stream to occupy 30-60% of the image. The TIR sensor is set to acquire images at its maximum rate (*~1 image/2 seconds*) resulting in considerable vertical overlap between images. The airplane maintained an average flight altitude of 1,200ft (366 m) above ground level (AGL) resulting in a planned image ground footprint width of 977 ft (298 m) and a native pixel resolution of 3.1 ft (0.9 meters).

*Table 1. Summary of Thermal Image Acquisition Parameters.*

| | |
|---|---|
| Date: | August 12, 2006 |
| Acquisition Time: | 5:56 – 6:38 (AM Flight) |
| | 14:26 – 15:08 (PM Flight) |
| Flight Above Ground Level (AGL): | 366 m (1200 ft) |
| Sensor: | Space Instruments |
| | Firemapper 2.0 |
| Wavelength: | 8-12μm |
| Temperature Resolution: | 0.01°C |
| Noise Equivalent Temperature Differences (NETD) | 0.07°C |
| Encoding Level: | 16 bit |
| Horizontal Field-of-View: | 44.3° |
| Image Footprint Width: | 298 m (977 ft) |
| Pixel Resolution: | 0.9 m (3.1 ft) |

Ground Control: Watershed Sciences deployed in-stream data loggers prior to the flight in order to calibrate and verify the accuracy of the TIR data. The data loggers were distributed at public access points along the survey extent. The sensors were placed on the bottom of the river in locations with good vertical mixing.

## *Data Processing*

Calibration: Calibration of the sensor is performed in the lab using an extended area black body to relate the response characteristics of the sensor to emitted radiance. The raw TIR images collected during the survey contain digital numbers that were converted to radiance (*$W/m^2$*sr*micron*) values based on the pre-season calibration.

The radiance values were adjusted based on a comparison of the measured radiance to the calculated radiance at each ground truth location. This adjustment was performed to correct for path length attenuation and the emissivity of natural water. The in-stream data were assessed at the time the image was acquired, with radiant values representing the median of ten points sampled from the image at the data logger location. The radiance values were then converted to surface temperatures using Planck's Black Body equation.

Interpretation and Sampling: Once calibrated, the images were integrated into a GIS in which an analyst interpreted and sampled stream temperatures. Sampling consisted of querying radiant temperatures (pixel values) from the center of the stream channel and saving the median value of a ten-point sample to a GIS database file. The temperatures of detectable surface inflows (i.e. surface springs, tributaries) were also sampled at their mouths. During sampling, the analyst provided interpretations of the spatial variations in surface temperatures observed in the images.

Geo-referencing: The images are tagged with a GPS position and heading at the time they are acquired. Since the TIR camera is maintained at vertical down-look angles, the geographic coordinates provide an accurate index to the location of the image scene. Due to the relatively small footprint of the imagery and independently stabilized mount, image pixels are not individually registered to real world coordinates. The image index is saved as an ESRI point shapefile containing the image name registered to an X and Y position (Oregon Lambert Projection) of sensor location at time of capture. In order to provide further spatial reference, the TIR images were assigned a river mile based on a routed stream layer (Figure 3).


*Figure 3 –Each point on the map represents a thermal image location. The inset box shows the information recorded with each image point during acquisition.*

Temperature Profiles: The median temperatures for each sampled image were plotted versus the corresponding river mile to develop a longitudinal temperature profile. The profile illustrates how stream temperatures vary spatially along the stream gradient. The location and median temperature of all sampled surface water inflows (e.g. tributaries, surface springs, etc.) are included on the plot to illustrate how these inflows influence the main stem temperature patterns. Radiant temperatures were only sampled along what appeared to be the main flow channel in the river.

Geo-Rectification: The true color images were geo-rectified to real world coordinates using panchromatic ortho-photos (*2000 available on the internet*) as the reference layer. The true color digital images were initially oriented using the position and directional information collected on the aircraft. Individual frames were then geo-rectified by finding a minimum of six common ground control points (GCP's) between the true color images and existing ortho-photos. The images were then warped using a 1$^{st}$ order polynomial transformation. TIR images were geo-rectified

using the same general methodology with the true color images used as the control layer at an average of twelve ground control points. Due to the low relief along the river bottom, the photos were not corrected for terrain displacement.

## *Thermal Image Characteristics*

Surface Temperatures: Thermal infrared sensors measure TIR energy emitted at the water's surface. Since water is essentially opaque to TIR wavelengths, the sensor is only measuring water surface temperature. Thermal infrared data accurately represents bulk water temperatures where the water column is thoroughly mixed; however, thermal stratification can form in reaches that have little or no mixing. Thermal stratification in a free flowing river is inherently unstable due to variations in channel shape, bed composition, and in-stream objects (i.e. rocks, trees, debris, etc.) that cause turbulent flow and can usually be detected in the imagery.

Expected Accuracy: Thermal infrared radiation received at the sensor is a combination of energy emitted from the water's surface, reflected from the water's surface, and absorbed and re-radiated by the intervening atmosphere. Water is a good emitter of TIR radiation and has relatively low reflectivity (~ 4 to 6%). However, variable water surface conditions (i.e. riffle versus pool), slight changes in viewing aspect, and variable background temperatures (i.e. sky versus trees) can result in differences in the calculated radiant temperatures within the same image or between consecutive images. The apparent temperature variability is generally less than 0.5$^{o}$C (Torgersen et al. 2001[1]). However, the occurrence of reflections as an artifact (or noise) in the TIR images is a consideration during image interpretation and analysis. In general, apparent stream temperature changes of < 0.5$^{o}$C are not considered significant unless associated with a surface inflow (e.g. tributary).

Differential Heating: In stream segments with flat surface conditions (i.e. pools) and relatively low mixing rates, observed variations in spatial temperature patterns can be the result of differences in the instantaneous heating rate at the water's surface. In the TIR images, indicators of differential surface heating include seemingly cooler radiant temperatures in shaded areas compared to surfaces exposed to direct sunlight.

Feature Size and Resolution: A small stream width logically translates to fewer pixels "in" the stream and greater integration with non-water features such as rocks and vegetation. Consequently, a narrow channel (relative to the pixel size) can result in higher inaccuracies in the measured radiant temperatures. This is a consideration when sampling the radiant temperatures at tributary mouths and surface springs.

---

[1] Torgersen, C.E., R. Faux, B.A. McIntosh, N. Poage, and D.J. Norton. 2001. Airborne thermal remote sensing for water temperature assessment in rivers and streams. *Remote Sensing of Environment* 76(3): 386-398.

Temperatures and Color Maps: The TIR images collected during this survey consist of a single band. As a result, visual representation of the imagery *(in a report or GIS environment*) requires the application of a color map or legend to the pixel values. The selection of a color map should highlight features most relevant to the analysis (i.e. *spatial variability of stream temperatures*). For example, a continuous, gradient style color map that incorporates all temperatures in the image frame will provide a smoother transition in colors throughout the entire image, but will not highlight temperature differences in the stream. Conversely, a color map that focuses too narrowly cannot be applied to the entire river and will "washout" terrestrial and vegetation features.

Image Uniformity: The TIR sensor used for this study uses a focal plane array of detectors to sample incoming radiation. A challenge when using this technology is to achieve uniformity across the detector array. This sensor has an automatic correction scheme which nearly eliminates non-uniformity across the image frame.

# Results

## Weather Conditions

Weather conditions were considered good for the survey. Table 2 summarizes the weather conditions recorded at the Troutdale, OR Airport during the time frame of the survey.

| Time PDT | Temp °F | Temp °C | Humidity % | Wind Direction | Wind Speed MPH | Sky Conditions |
|---|---|---|---|---|---|---|
| 4:37 AM | 51.8 | 11.0 | 82 | Calm | Calm | Mostly Cloudy |
| 4:53 AM | 51.1 | 10.6 | 86 | Calm | Calm | Scat. Clouds |
| 5:53 AM | 50.0 | 10.0 | 89 | Calm | Calm | Mostly Cloudy |
| 6:53 AM | 51.1 | 10.6 | 86 | Calm | Calm | Mostly Cloudy |
| 7:04 AM | 51.8 | 11.0 | 82 | Calm | Calm | Overcast |
| 7:53 AM | 54.0 | 12.2 | 83 | Calm | Calm | Overcast |
| 8:53 AM | 55.0 | 12.8 | 80 | Calm | Calm | Overcast |
| 9:53 AM | 57.9 | 14.4 | 72 | Variable | 3.5 | Overcast |
| 10:53 AM | 60.1 | 15.6 | 64 | Variable | 3.5 | Overcast |
| 11:53 AM | 63.0 | 17.2 | 60 | Variable | 3.5 | Scat. Clouds |
| 12:53 PM | 66.0 | 18.9 | 56 | Variable | 3.5 | Clear |
| 1:53 PM | 71.1 | 21.7 | 47 | NW | 4.6 | Clear |
| 2:53 PM | 73.9 | 23.3 | 43 | Variable | 4.6 | Clear |
| 3:53 PM | 77.0 | 25.0 | 42 | Variable | 5.8 | Clear |
| 4:53 PM | 79.0 | 26.1 | 39 | West | 8.1 | Clear |
| 5:53 PM | 80.1 | 26.7 | 38 | Variable | 5.8 | Clear |
| 6:53 PM | 79.0 | 26.1 | 38 | Variable | 6.9 | Clear |

Table 2. Weather conditions observed at the Troutdale Airport on August 12, 2006.

## *Thermal Accuracy*

Table 3 provides a comparison between the kinetic temperatures recorded by the in-stream data loggers and the radiant temperatures derived from the TIR images for both the morning (AM) and afternoon (PM) flights on the Clackamas River. Since the in-stream data were used to compute an adjustment to the radiant temperatures, the table illustrates the range of differences after the images were calibrated. The correction was computed as an average offset from the raw radiant values for all sensor locations. Since the in-stream data are used in the radiant temperature calibration, they should not be considered an independent check of radiant temperatures.

The range of differences between the radiant temperatures and kinetic temperatures were generally within target values (±0.5$^{o}$C).

Table 3 – Comparison of radiant temperatures derived from the TIR images and kinetic temperatures from the in-stream monitors.

| Serial | Image | Local | Kinetic T© | Radiant T© | Difference T© |
|---|---|---|---|---|---|
| **Morning Flight** | | | | | |
| 1026262 | t01046 | 5:57 | 17.1 | 17.3 | -0.2 |
| 659412 | t02022 | 6:02 | 17.0 | 16.9 | 0.1 |
| 540663 | t03018 | 6:08 | 16.7 | 17.1 | -0.4 |
| 1026265 | t03067 | 6:12 | 16.4 | 16.5 | -0.1 |
| 1026266 | t04043 | 6:19 | 16.0 | 16.1 | -0.1 |
| 1026260 | t05006 | 6:29 | 16.2 | 16.5 | -0.4 |
| 540664 | t05271 | 6:38 | 16.4 | 16.2 | 0.2 |
| **Afternoon Flight** | | | | | |
| 1026262 | t06161 | 14:29 | 17.8 | 17.5 | 0.3 |
| 659412 | t06008 | 14:34 | 18.6 | 18.8 | -0.2 |
| 540663 | t07045 | 14:35 | 18.8 | 19.3 | -0.5 |
| 1026265 | t08023 | 14:40 | 19.7 | 20.0 | -0.3 |
| 1026266 | t08218 | 14:46 | 21.2 | 21.0 | 0.1 |
| 1026260 | t09008 | 14:59 | 19.9 | 20.4 | -0.5 |
| 540664 | t09297 | 15:08 | 19.1 | 19.0 | 0.1 |

## *Longitudinal Profiles*

Median sampled temperatures were plotted versus river mile for the Clackamas River from River Mill Dam to the Carver Bridge for both the AM and PM flights (Figures 4 and 5). Tributaries and other sampled surface inflows (i.e. springs/seeps, side channels, off channel) are plotted on the profiles. The profiles were plotted over the same temperature ranges to more easily allow cross comparison.

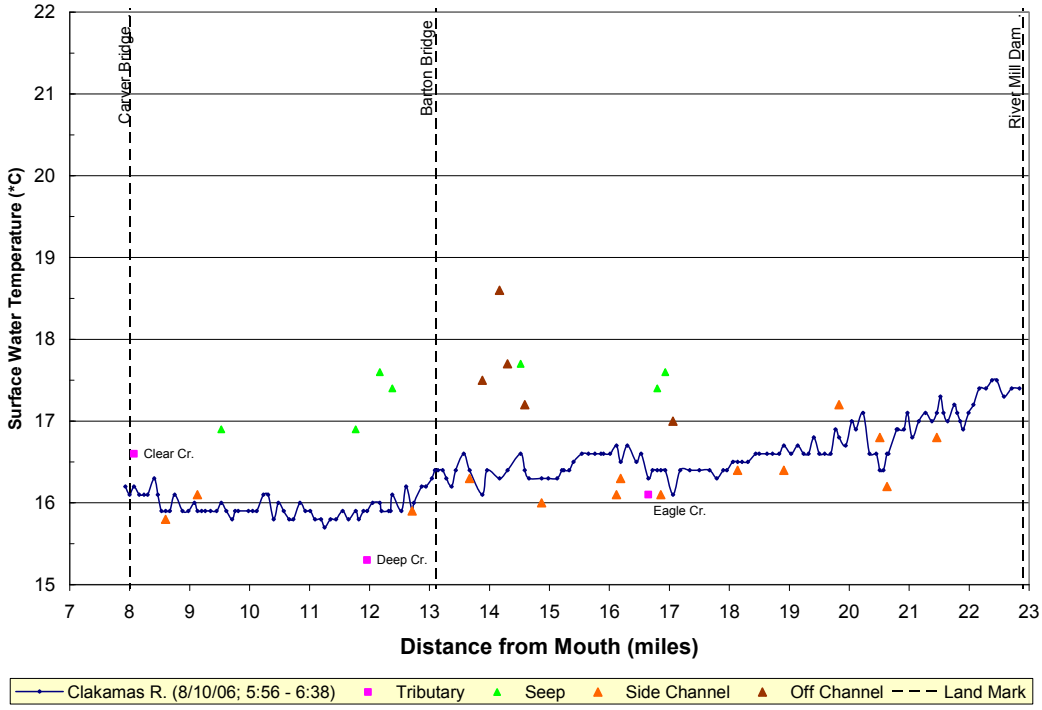


Figure 4 - Median sampled temperatures plotted versus river mile for the Clackamas River during the early morning of August 12, 2006.

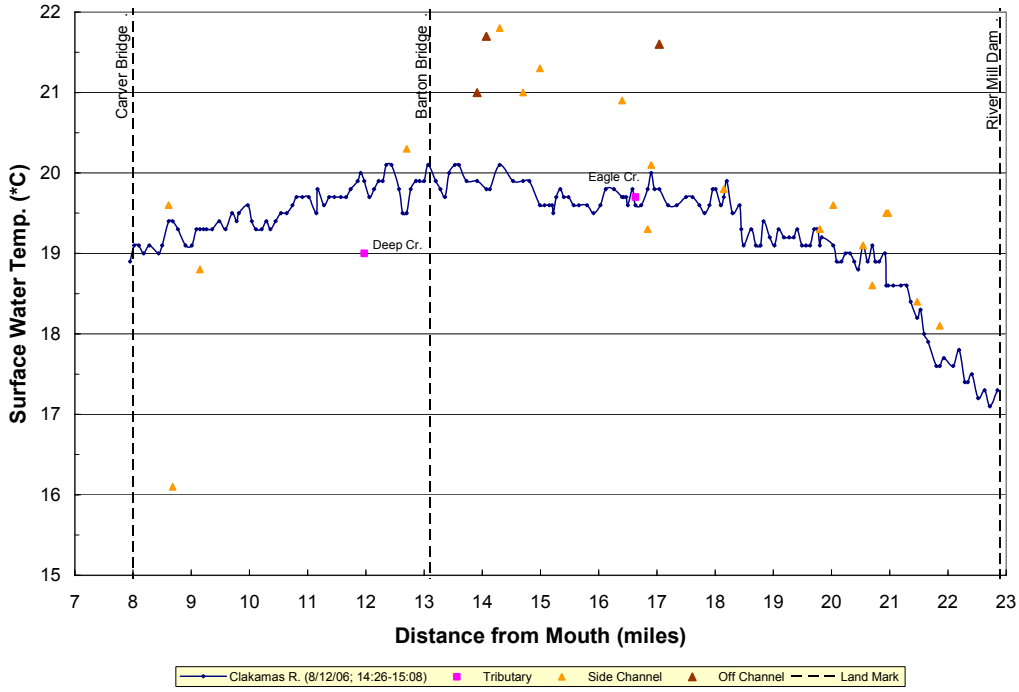


Figure 5 - Median sampled temperatures plotted versus river mile for the Clackamas River during the mid-afternoon on August 12, 2006.

# Observation and Analysis

## Morning Flight

Radiant water temperatures below River Mill Dam were ~17.4°C at the time of the TIR survey with water temperatures in the main channel getting progressively cooler moving downstream. Over the full 15-mile survey water temperatures ranged from ~17.5°C to a local minimum of 15.7°C (mile 11.3). While the range of sampled temperatures (1.8°C) was relatively small, inspection of the profile shows some apparent spatial trends along the river gradient.

Between river miles 21.0 and 20.6, stream temperatures exhibited a decrease of ~0.7°C before increasing again in the downstream direction. While the magnitude of this decrease is close to the expected frame-to-frame variability (i.e. 0.5°C), this was a notably larger change than observed at other locations along the profile and may warrant further investigation. Radiant water temperatures appeared relatively constant (~16.4°C ±0.3°C) between river mile 19.7 and 13.0 (*near Barton Bridge*). Downstream of Barton Bridge, bulk water temperatures again decreased before leveling off at ~15.8°C.

As mentioned previously, radiant water temperatures were sampled along the main channel as determined based on size (***i.e. channel width***) and apparent flow. Secondary channels were classified as side channels and fourteen were sampled during the early morning flight. The side channels were sampled at the point where they rejoined the main channel. Most of the side channels had water temperatures consistent with water temperatures in the main stem.

Off-Channel features were identified as standing water or ponds that had surface connectivity to the main channel. During the morning flight, five off-channel features were identified and each had warmer radiant temperatures than the main channel. A number of "seeps" were also detected during the morning flight. These features were detected as areas of surface water that had significantly (i.e. >= 0.5°C) different radiant temperatures then the main stem and appeared (*through interpretation of the imagery*) as an area of potential upwelling. The measured radiant temperatures were between 16.9°C and 17.7°C. Examples of both off-channel features and seeps are contained in the Sample Images section of this report.

## Afternoon Flight

During the afternoon flights, radiant water temperatures were ~17.4°C and increased steadily downstream of the River Mill Dam (mile 23.0) reaching ~19.6°C at river mile 18.2. Surface water temperatures appeared to increase slightly (19.6°C to 20.1°C) before exhibiting a steady decrease of ~1.0°C between the Barton Bridge (mile 13.0) and the Carver Bridge (mile 8.0).
As with the morning flight, all detected surface water inflows were sampled where they entered the main channel. A total of nineteen side channels were sampled during

analysis of the afternoon imagery. Of these, seven side channels had radiant temperatures that were significantly different than the main channel. Three off-channel features were sampled and each had warmer surface temperatures than the main channel.

There we no "seeps" detected during the afternoon flight. Inspection of the TIR imagery showed that there was often little thermal contrast between terrain features and the surface water temperatures. This decreased contrast often made it difficult to detect small features with similar apparent temperatures (i.e. the stream bank and a small seep). Consequently, the seeps were detectable in the morning flight because of the cold back ground temperatures during the morning hours. The lack of detected seeps during the afternoon flight was probably due to the decreased contrast between the land and the water and not due to the absence of the seep.

## Comparison AM versus PM

A comparison of longitudinal temperature profiles from the afternoon and morning flight provides additional information on the processes driving spatial temperature patterns in the Clackamas River (Figure 6).

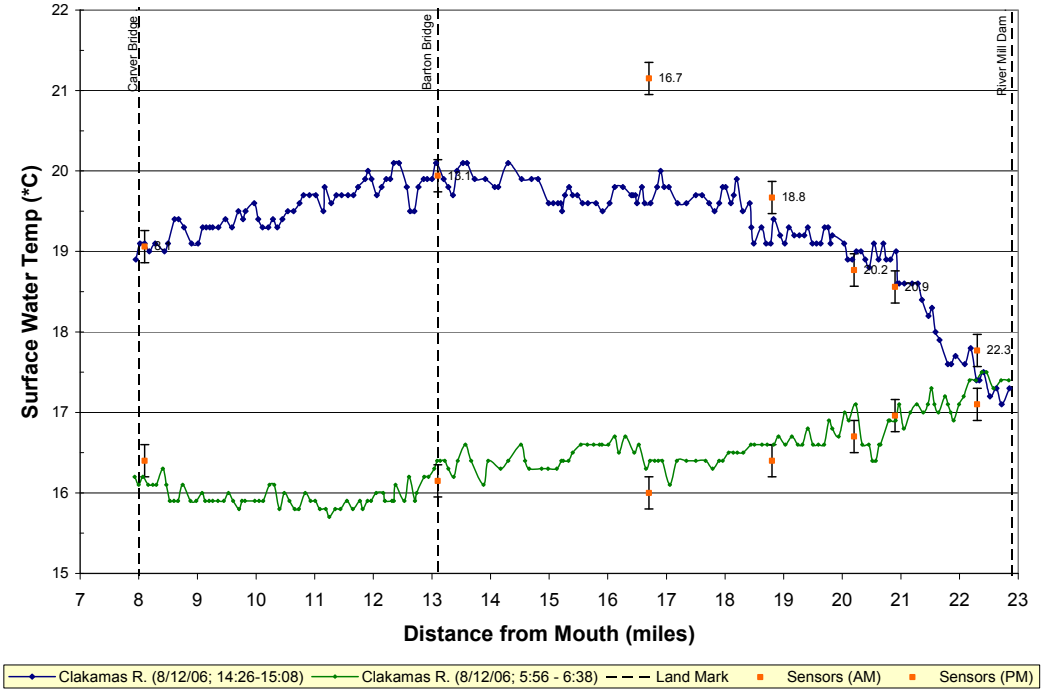


Figure 6 – Comparison of the longitudinal temperature profiles for the morning and afternoon flights on the Clackamas River. The plot also shows the location and recorded temperatures from the in-stream data loggers. The in-streams sensor temperatures at the time of the overflight are shown on the profiles. Note that the sensor at river mile 16.7 was not located within the main flow and therefore not representative of the bulk water temperatures during the afternoon flight.

While temperatures at the outlet of the dam were very similar between the morning and afternoon flights, the downstream spatial temperature patterns were almost mirror images. Both profiles show consistent temperature patterns over similar reaches. For example, both patterns showed a decrease in longitudinal heating (PM) or cooling (AM) between river miles 18 and 19. The warming (PM) (or cooling (AM)) continued at a lower rate in both profiles until approximately Barton Bridge (mile 13). In both profiles, the reach between Barton and Carver Bridges showed a distinct change in the downstream temperature pattern.

Over the surveyed reach, the Clackamas River was characterized by multiple channels, large gravel bars, and a number of off-channel ponds. This channel complexity combined with the observed spatial temperature patterns and evidence of "seeps" in the TIR imagery, suggests that hyporheic flow paths may have a regulating influence on in-stream temperature patterns. This is particularly true in the reach between Barton and Carver Bridges, which showed downstream cooling during heat-of the day conditions and almost constant temperatures in the early morning profile.

## Follow-On

This report provides some hypotheses on the processes influencing spatial temperature patterns at this scale based on analysis of the TIR imagery. These hypotheses and observations are considered to be a starting point for more rigorous spatial analysis and fieldwork. Follow-on analysis may include:

- Since the seeps detected in the imagery are small, they should be considered detection of a process within a given reach and provide information on the type of channel and geomorphoric conditions under which that process occurs in the Clackamas River. Follow on analysis may look at the significance of these seeps to temperatures at different spatial scale and localize thermal habitat for cold water fish.

- The TIR imagery and derived data sets provide a spatial context for analysis of seasonal temperature data from in-stream data loggers and for future deployment and distribution of in-stream monitoring stations.

- The rectified true color images provide a good data source evaluation of other physical habitat characteristics within the stream. These images may provide information at a spatial resolution and temporal significance that are not available from other sources.

# Sample Images

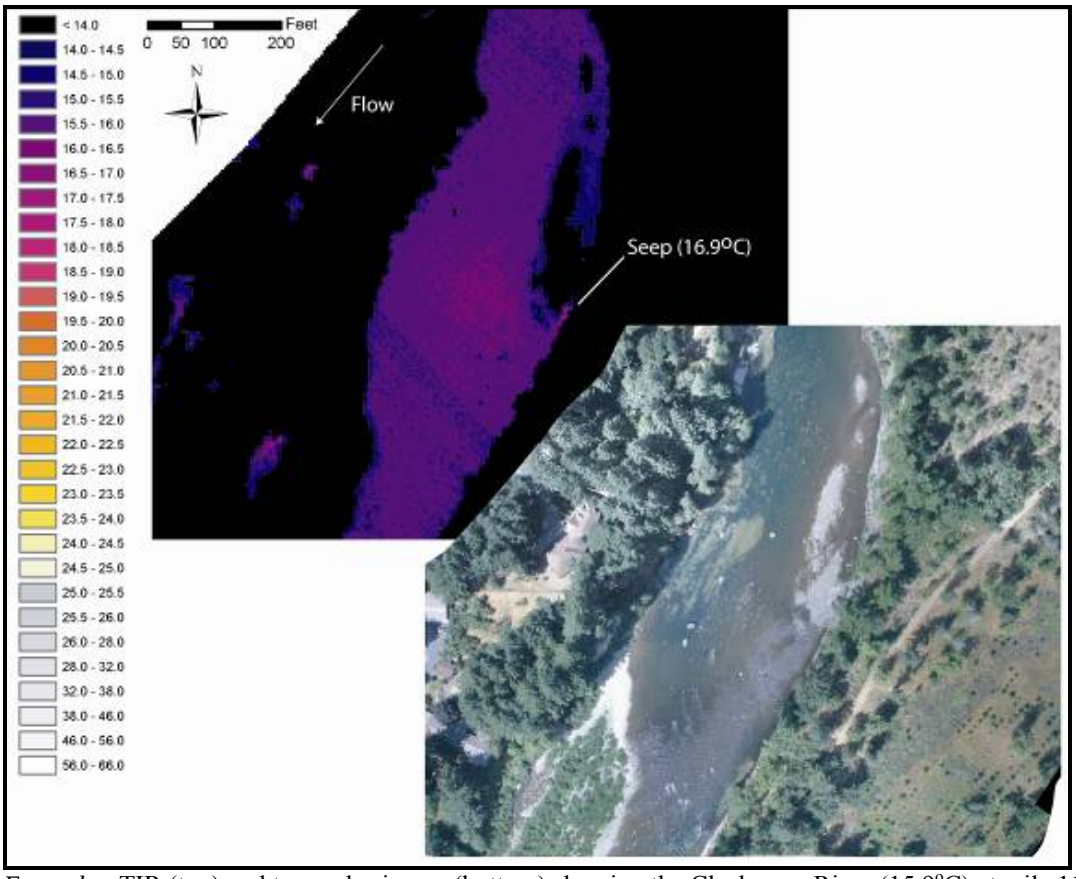


*Example:* TIR (top) and true color image (bottom) showing the Clackamas River (15.9°C) at mile 11.8. The image pair shows an example the detection of apparent seep at the downstream end of the gravel bar along the left bank. The seeps were detectable in the early morning flight due to the large thermal contrast been the cold bank and terrain features and the water surface. The illustrated TIR image is from the geo-rectified mosaic and illustrates some of the slight uniformity and frame-to-frame differences in the thermal imagery.

The color map used to display the images exaggerates these differences. These artifacts can reduced in the mosaic by using smoothing or averaging options available in most mosaicing programs. However, averaging can also result in the loss of small features such as the seeps due to small differences in pixel registration between frames.

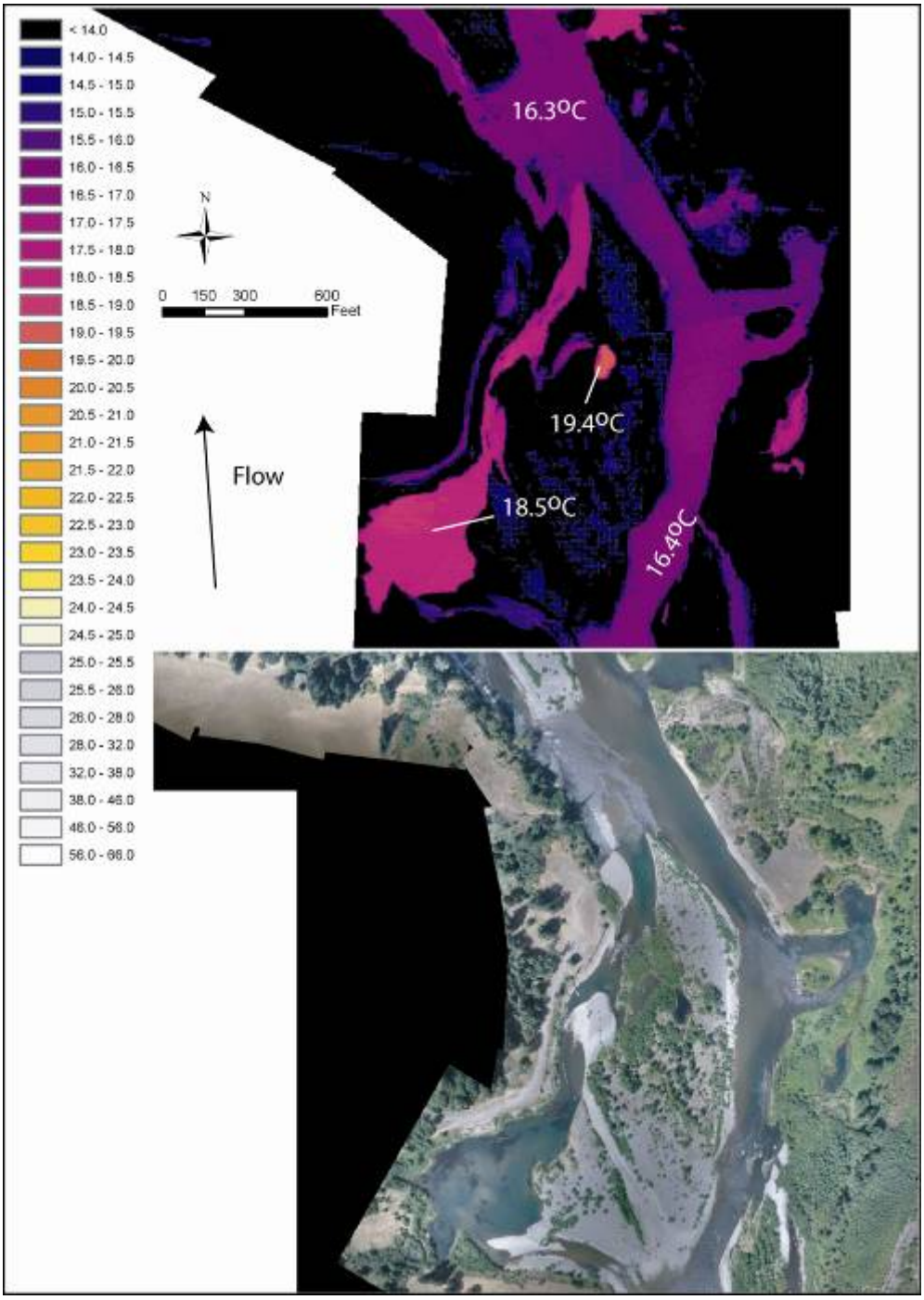


*Example*: The TIR image (top) and true color image (bottom) shows the Clackamas River between miles 14.0 and 15.0. While bulk temperatures in the main channel are relatively constant, the side-channels and off-channel ponds show considerable variability in the surface temperatures. A number of seeps are also visible along the islands and gravel bars.

# Deliverables

The TIR imagery is provided in two forms: 1) individual un-rectified frames and 2) a continuous geo-rectified mosaic. The mosaic allows for easy viewing of the continuum of temperatures along the stream gradient, but also shows edge match differences and geometric transformation effects. The un-rectified frames are useful for viewing images at their native resolutions. The native resolution is often better for detecting smaller thermal features. A GIS point layer is included which provides an index of image locations, the results of temperature sampling, and interpretations made during the analysis.

Deliverables are provided on DVD:

| Geo-Corrected Imagery is stored as: **Oregon Lambert, NAD83, Units = Int. Feet.** |
|---|

- Unrectified – contains un-rectified single frame images.
  - Clackamas AM – calibrated, but un-rectified TIR image frames from the morning flight in ESRI GRID Format. These images retain the native resolution of the sensor. GRID cell value = radiant temp. ($^{o}$C) * 10.
  - Clackamas PM – calibrated, but un-rectified TIR image frames from the morning flight in ESRI GRID Format. These images retain the native resolution of the sensor. GRID cell value = radiant temp. ($^{o}$C) * 10.
  - TrueColor – un-rectified true color images (jpg).
  - Indices – ESRI shapefile (points) showing image locations for both TIR and true color image files.
- Rectified – contains geo-rectified images.
  - Clackamas AM – calibrated, but un-rectified TIR image frames from the morning flight in ESRI GRID Format. These images retain the native resolution of the sensor. GRID cell value = radiant temp. ($^{o}$C) * 10.
  - Clackamas PM – calibrated and rectified TIR image frames from the morning flight in ESRI GRID Format. These images retain the native resolution of the sensor. GRID cell value = radiant temp. ($^{o}$C) * 10.
  - Mosaics – Geo-rectified images mosaics for both the true color and thermal IR images in geo-tiff format.
- Report – Copy of this report.
- Longitudinal Profile – Excel File containing the longitudinal temperature profiles.
- Project – ArcGIS project illustrating the mosaic and the photo_index for the rectified images.

# Contact Information

Russell Faux
Watershed Sciences, Inc.
111 NW 2nd Street, Unit 1
Corvallis, OR 97330

# APPENDIX E

## TOTAL STATION SURVEY DATA FOR FELDHEIMER, EAGLE CREEK AND BARTON BARS

## Table E.1: 2006 Total station survey data for Feldheimer bar (RKM 30)

| Point # | Date | Northing (ft) | Easting (ft) | Elevation (ft) | Description |
|---|---|---|---|---|---|
| 7000 | 07/30/2006 | 612319.688 | 7718189.536 | 228.134 | WATER EDGE |
| 7001 | 07/30/2006 | 612343.963 | 7718192.33 | 228.089 | WATER EDGE |
| 7002 | 07/30/2006 | 612368.502 | 7718201.301 | 228.024 | WATER EDGE |
| 7003 | 07/30/2006 | 612396.02 | 7718212.234 | 227.979 | WATER EDGE |
| 7004 | 07/30/2006 | 612422.982 | 7718219.838 | 227.885 | WATER EDGE |
| 7005 | 07/30/2006 | 612442.807 | 7718232.944 | 227.728 | WATER EDGE |
| 7006 | 07/30/2006 | 612473.584 | 7718246.25 | 227.581 | WATER EDGE |
| 7007 | 07/30/2006 | 612505.584 | 7718255.408 | 227.522 | WATER EDGE |
| 7008 | 07/30/2006 | 612529.436 | 7718272.684 | 227.123 | WATER EDGE |
| 7009 | 07/30/2006 | 612567.724 | 7718276.008 | 226.824 | WATER EDGE |
| 7010 | 07/30/2006 | 612608.622 | 7718270.963 | 226.79 | WATER EDGE |
| 7011 | 07/30/2006 | 612642.935 | 7718268.498 | 226.796 | WATER EDGE |
| 7012 | 07/30/2006 | 612676.212 | 7718262.128 | 226.736 | WATER EDGE |
| 7013 | 07/30/2006 | 612711.903 | 7718259.837 | 226.703 | WATER EDGE |
| 7014 | 07/30/2006 | 612747.745 | 7718254.769 | 226.8 | WATER EDGE |
| 7015 | 07/30/2006 | 612780.982 | 7718249.011 | 226.736 | WATER EDGE |
| 7016 | 07/30/2006 | 612832.505 | 7718243.281 | 226.749 | WATER EDGE |
| 7017 | 07/30/2006 | 612876.603 | 7718229.77 | 226.809 | WATER EDGE |
| 7018 | 07/30/2006 | 612924.865 | 7718213.648 | 226.753 | WATER EDGE |
| 7019 | 07/30/2006 | 612966.817 | 7718201.27 | 226.713 | WATER EDGE |
| 7020 | 07/30/2006 | 613006.845 | 7718181.591 | 226.75 | WATER EDGE |
| 7021 | 07/30/2006 | 613037.406 | 7718162.535 | 226.751 | WATER EDGE |
| 7022 | 07/30/2006 | 613080.578 | 7718141.542 | 226.744 | WATER EDGE |
| 7023 | 07/30/2006 | 613102.404 | 7718130.631 | 226.665 | WATER EDGE |
| 7024 | 07/30/2006 | 613105.608 | 7718116.916 | 226.697 | WATER EDGE |
| 7025 | 07/30/2006 | 613091.242 | 7718115.062 | 226.654 | WATER EDGE |
| 7500 | 07/30/2006 | 612299.443 | 7718129.723 | 228.795 | TOPO_PT |
| 7501 | 07/30/2006 | 612305.727 | 7718142.345 | 227.955 | TOPO_PT |
| 7502 | 07/30/2006 | 612313.462 | 7718153.869 | 228.446 | TOPO_PT |
| 7503 | 07/30/2006 | 612334.105 | 7718148.962 | 228.25 | TOPO_PT |
| 7504 | 07/30/2006 | 612334.205 | 7718136.255 | 228.095 | TOPO_PT |
| 7505 | 07/30/2006 | 612334.386 | 7718121.403 | 228.257 | TOPO_PT |
| 7506 | 07/30/2006 | 612349.578 | 7718114.418 | 228.418 | TOPO_PT |
| 7507 | 07/30/2006 | 612349.471 | 7718124.92 | 227.766 | TOPO_PT |
| 7508 | 07/30/2006 | 612349.116 | 7718136.176 | 228.697 | TOPO_PT |
| 7509 | 07/30/2006 | 612361.61 | 7718157.719 | 228.786 | TOPO_PT |
| 7510 | 07/30/2006 | 612384.396 | 7718096.783 | 230.735 | TOPO_PT |
| 7511 | 07/30/2006 | 612393.169 | 7718121.981 | 227.58 | TOPO_PT |
| 7512 | 07/30/2006 | 612403.217 | 7718148.36 | 228.439 | TOPO_PT |
| 7513 | 07/30/2006 | 612412.542 | 7718166.654 | 230.423 | TOPO_PT |
| 7514 | 07/30/2006 | 612442.015 | 7718115.331 | 227.262 | TOPO_PT |
| 7515 | 07/30/2006 | 612430.593 | 7718093.631 | 231.02 | TOPO_PT |
| 7516 | 07/30/2006 | 612434.57 | 7718103.423 | 227.426 | TOE |
| 7517 | 07/30/2006 | 612439.386 | 7718137.672 | 228.677 | TOPO_PT |
| 7518 | 07/30/2006 | 612447.42 | 7718163.341 | 229.876 | TOPO_PT |
| 7519 | 07/30/2006 | 612471.356 | 7718105.097 | 227.365 | PETER_TR_ROCK |
| 7520 | 07/30/2006 | 612473.872 | 7718115.967 | 227.858 | TOE |
| 7521 | 07/30/2006 | 612489.666 | 7718072.738 | 231.069 | TOPO_PT |
| 7522 | 07/30/2006 | 612507.952 | 7718101.951 | 227.727 | TOPO_PT |
| 7523 | 07/30/2006 | 612509.03 | 7718124.497 | 228.845 | TOPO_PT |
| 7524 | 07/30/2006 | 612542.392 | 7718081.851 | 226.445 | TOE |
| 7525 | 07/30/2006 | 612541.8 | 7718061.65 | 226.925 | TOPO_PT |
| 7526 | 07/30/2006 | 612539.198 | 7718089.719 | 228.334 | TOPO_PT |
| 7527 | 07/30/2006 | 612538.977 | 7718046.934 | 231.894 | TOPO_PT |

## Table E.1: 2006 Total station survey data for Feldheimer bar (RKM 30)

| Point # | Date | Northing (ft) | Easting (ft) | Elevation (ft) | Description |
|---|---|---|---|---|---|
| 7528 | 07/30/2006 | 612551.657 | 7718070.806 | 225.803 | TOPO_PT |
| 7529 | 07/30/2006 | 612556.243 | 7718077.339 | 226.181 | TOE |
| 7530 | 07/30/2006 | 612558.678 | 7718085.754 | 229.574 | TOPO_PT |
| 7531 | 07/30/2006 | 612553.622 | 7718070.989 | 225.545 | POOL |
| 7532 | 07/30/2006 | 612553.306 | 7718069.697 | 225.579 | POOL |
| 7533 | 07/30/2006 | 612552.72 | 7718070.384 | 225.533 | POOL |
| 7534 | 07/30/2006 | 612572.439 | 7718062.414 | 225.475 | POOL |
| 7535 | 07/30/2006 | 612572.135 | 7718062.01 | 225.549 | POOL |
| 7536 | 07/30/2006 | 612572.083 | 7718062.025 | 225.551 | POOL |
| 7537 | 07/30/2006 | 612572.036 | 7718062.444 | 225.5 | POOL |
| 7538 | 07/30/2006 | 612598.99 | 7718060.497 | 225.461 | POOL |
| 7539 | 07/30/2006 | 612599.665 | 7718061.293 | 225.351 | POOL |
| 7540 | 07/30/2006 | 612598.914 | 7718061.152 | 225.401 | POOL |
| 7541 | 07/30/2006 | 612612 | 7718051.04 | 225.212 | POOL |
| 7542 | 07/30/2006 | 612611.206 | 7718049.862 | 225.305 | POOL |
| 7543 | 07/30/2006 | 612610.867 | 7718050.877 | 225.179 | POOL |
| 7544 | 07/30/2006 | 612623.372 | 7718056.97 | 225.612 | TOE |
| 7545 | 07/30/2006 | 612619.701 | 7718050.88 | 225.227 | TOPO_PT |
| 7546 | 07/30/2006 | 612620.887 | 7718052.364 | 225.242 | POOL |
| 7547 | 07/30/2006 | 612625.201 | 7718053.619 | 225.218 | POOL |
| 7548 | 07/30/2006 | 612629.157 | 7718052.134 | 225.241 | POOL |
| 7549 | 07/30/2006 | 612629.008 | 7718048.932 | 225.243 | POOL |
| 7550 | 07/30/2006 | 612626.78 | 7718048.695 | 225.235 | POOL |
| 7551 | 07/30/2006 | 612624.233 | 7718048.007 | 225.255 | POOL |
| 7552 | 07/30/2006 | 612623.345 | 7718045.157 | 225.243 | POOL |
| 7553 | 07/30/2006 | 612619.04 | 7718047.253 | 225.209 | POOL |
| 7554 | 07/30/2006 | 612630.227 | 7718041.102 | 225.141 | POOL |
| 7555 | 07/30/2006 | 612638.827 | 7718036.882 | 225.18 | POOL |
| 7556 | 07/30/2006 | 612643.343 | 7718035.384 | 225.184 | POOL |
| 7557 | 07/30/2006 | 612649.755 | 7718036.195 | 225.165 | POOL |
| 7558 | 07/30/2006 | 612653.408 | 7718040.218 | 225.155 | POOL |
| 7559 | 07/30/2006 | 612651.304 | 7718041.304 | 225.12 | POOL |
| 7560 | 07/30/2006 | 612640.19 | 7718044.625 | 225.137 | POOL |
| 7561 | 07/30/2006 | 612615.509 | 7718039.791 | 225.981 | TOPO_PT |
| 7562 | 07/30/2006 | 612660.1 | 7718036.548 | 225.104 | POOL |
| 7563 | 07/30/2006 | 612662.336 | 7718031.769 | 225.108 | POOL |
| 7564 | 07/30/2006 | 612625.987 | 7718060.823 | 227.114 | TOPO_PT |
| 7565 | 07/30/2006 | 612631.454 | 7718065.433 | 230.091 | TOPO_PT |
| 7566 | 07/30/2006 | 612670.626 | 7718032.25 | 224.995 | POOL |
| 7567 | 07/30/2006 | 612673.515 | 7718027.815 | 225.081 | POOL |
| 7568 | 07/30/2006 | 612678.131 | 7718020.554 | 225.041 | POOL |
| 7569 | 07/30/2006 | 612678.167 | 7718020.386 | 225.031 | POOL |
| 7570 | 07/30/2006 | 612683.077 | 7718018.922 | 225.063 | POOL |
| 7571 | 07/30/2006 | 612690.234 | 7718023.908 | 225.035 | POOL |
| 7572 | 07/30/2006 | 612686.817 | 7718012.111 | 225.007 | POOL |
| 7573 | 07/30/2006 | 612701.016 | 7718022.747 | 225.039 | POOL |
| 7574 | 07/30/2006 | 612702.839 | 7718006.506 | 225.078 | POOL |
| 7575 | 07/30/2006 | 612709.793 | 7718003.337 | 225.087 | POOL |
| 7576 | 07/30/2006 | 612720.976 | 7717999.608 | 225.046 | POOL |
| 7577 | 07/30/2006 | 612726.315 | 7718009.184 | 225.008 | POOL |
| 7578 | 07/30/2006 | 612719.647 | 7718014.044 | 225.087 | POOL |
| 7579 | 07/30/2006 | 612708.68 | 7718015.841 | 225.104 | POOL |
| 7580 | 07/30/2006 | 612704.19 | 7718021.001 | 225.146 | POOL |
| 7581 | 07/30/2006 | 612710.935 | 7718020.592 | 225.304 | TOE |
| 7582 | 07/30/2006 | 612712.951 | 7718028.409 | 229.281 | TOPO_PT |

## Table E.1: 2006 Total station survey data for Feldheimer bar (RKM 30)

| Point # | Date | Northing (ft) | Easting (ft) | Elevation (ft) | Description |
|---|---|---|---|---|---|
| 7583 | 07/30/2006 | 612686.093 | 7717995.331 | 231.017 | TOPO_PT |
| 7584 | 07/30/2006 | 612703.384 | 7718013.253 | 224.69 | TOPO_PT |
| 7585 | 07/30/2006 | 612716.046 | 7718008.216 | 224.701 | TOPO_PT |
| 7586 | 07/30/2006 | 612730.09 | 7717988.615 | 225.997 | TOE |
| 7587 | 07/30/2006 | 612725.598 | 7717980.855 | 231.315 | TOPO_PT |
| 7588 | 07/30/2006 | 612731.101 | 7717993.828 | 225.01 | POOL |
| 7589 | 07/30/2006 | 612733.64 | 7717998.189 | 224.789 | POOL |
| 7590 | 07/30/2006 | 612734.115 | 7718000.305 | 224.903 | POOL |
| 7591 | 07/30/2006 | 612743.828 | 7717998.081 | 225.011 | POOL |
| 7592 | 07/30/2006 | 612750.13 | 7717997.431 | 224.91 | POOL |
| 7593 | 07/30/2006 | 612761.556 | 7717994.133 | 224.931 | POOL |
| 7594 | 07/30/2006 | 612766.227 | 7717985.757 | 224.982 | POOL |
| 7595 | 07/30/2006 | 612756.631 | 7717985.66 | 224.954 | POOL |
| 7596 | 07/30/2006 | 612748.265 | 7717988.773 | 224.933 | POOL |
| 7597 | 07/30/2006 | 612742.591 | 7717991.274 | 224.928 | POOL |
| 7598 | 07/30/2006 | 612751.958 | 7717992.751 | 224.552 | TOPO_PT |
| 7599 | 07/30/2006 | 612747.069 | 7717992.98 | 224.791 | TOPO_PT |
| 7600 | 07/30/2006 | 612749.445 | 7718000.939 | 225.02 | TOPO_PT |
| 7601 | 07/30/2006 | 612760.434 | 7717999.308 | 225.241 | TOPO_PT |
| 7602 | 07/30/2006 | 612741.896 | 7718011.996 | 226.176 | TOPO_PT |
| 7603 | 07/30/2006 | 612743.805 | 7718019.121 | 229.128 | TOPO_PT |
| 7604 | 07/30/2006 | 612771.334 | 7717994.486 | 225.123 | TOPO_PT |
| 7605 | 07/30/2006 | 612768.587 | 7717988.52 | 224.94 | POOL |
| 7606 | 07/30/2006 | 612765.77 | 7717980.023 | 225.039 | TOPO_PT |
| 7607 | 07/30/2006 | 612772.388 | 7718007.641 | 229.35 | TOP |
| 7608 | 07/30/2006 | 612771.392 | 7718003.668 | 226.643 | TOE |
| 7609 | 07/30/2006 | 612827.053 | 7717973.39 | 225.311 | TOPO_PT |
| 7610 | 07/30/2006 | 612761.999 | 7717977.318 | 225.56 | TOE |
| 7611 | 07/30/2006 | 612823.768 | 7717966.475 | 224.752 | TOPO_PT |
| 7612 | 07/30/2006 | 612760.148 | 7717967.404 | 230.053 | TOPO_PT |
| 7613 | 07/30/2006 | 612820.793 | 7717958.444 | 224.923 | TOPO_PT |
| 7614 | 07/30/2006 | 612820.876 | 7717958.22 | 224.889 | TOPO_PT |
| 7615 | 07/30/2006 | 612814.802 | 7717951.874 | 228.342 | TOPO_PT |
| 7616 | 07/30/2006 | 612829.489 | 7717978.935 | 225.266 | TOE |
| 7617 | 07/30/2006 | 612878.24 | 7717942.868 | 224.159 | POOL |
| 7618 | 07/30/2006 | 612880.811 | 7717936.153 | 224.124 | POOL |
| 7619 | 07/30/2006 | 612833.689 | 7717984.487 | 228.119 | TOP |
| 7620 | 07/30/2006 | 612882.871 | 7717945.217 | 224.055 | POOL |
| 7621 | 07/30/2006 | 612891.187 | 7717943.108 | 224.123 | POOL |
| 7622 | 07/30/2006 | 612897.866 | 7717932.319 | 224.105 | POOL |
| 7623 | 07/30/2006 | 612894.758 | 7717924.495 | 224.778 | TOE |
| 7624 | 07/30/2006 | 612897.615 | 7717930.342 | 224.415 | TOPO_PT |
| 7625 | 07/30/2006 | 612885.802 | 7717910.908 | 230.264 | TOPO_PT |
| 7626 | 07/30/2006 | 612908.918 | 7717947.311 | 224.559 | TOE |
| 7627 | 07/30/2006 | 612919.141 | 7717927.066 | 223.973 | POOL |
| 7628 | 07/30/2006 | 612927.44 | 7717924.612 | 224.067 | POOL |
| 7629 | 07/30/2006 | 612931.42 | 7717921.671 | 224.009 | POOL |
| 7630 | 07/30/2006 | 612925.691 | 7717919.417 | 224.02 | POOL |
| 7631 | 07/30/2006 | 612919.042 | 7717921.731 | 223.952 | POOL |
| 7632 | 07/30/2006 | 612938.795 | 7717883.335 | 231.46 | TOP |
| 7633 | 07/30/2006 | 612944.852 | 7717897.689 | 224.542 | TOE |
| 7634 | 07/30/2006 | 612950.189 | 7717907.445 | 223.956 | POOL |
| 7635 | 07/30/2006 | 612955.718 | 7717908.485 | 223.928 | POOL |
| 7636 | 07/30/2006 | 612959.417 | 7717915.267 | 223.924 | POOL |
| 7637 | 07/30/2006 | 612953.696 | 7717911.598 | 223.972 | POOL |

## Table E.1: 2006 Total station survey data for Feldheimer bar (RKM 30)

| Point # | Date | Northing (ft) | Easting (ft) | Elevation (ft) | Description |
|---|---|---|---|---|---|
| 7638 | 07/30/2006 | 612950.055 | 7717914.086 | 223.943 | POOL |
| 7639 | 07/30/2006 | 612956.925 | 7717921.924 | 224.11 | TOPO_PT |
| 7640 | 07/30/2006 | 612960.757 | 7717930.606 | 224.56 | TOPO_PT |
| 7641 | 07/30/2006 | 612969.086 | 7717914.134 | 223.838 | POOL 1 |
| 7642 | 07/30/2006 | 612962.198 | 7717944.155 | 227.939 | TOPO_PT |
| 7643 | 07/30/2006 | 612961.448 | 7717898.287 | 223.852 | POOL 1 |
| 7644 | 07/30/2006 | 612976.347 | 7717885.927 | 223.839 | POOL 1 |
| 7645 | 07/30/2006 | 612988.813 | 7717881.542 | 223.834 | POOL 1 |
| 7646 | 07/30/2006 | 613002.926 | 7717873.673 | 223.8 | POOL 1 |
| 7647 | 07/30/2006 | 613017.088 | 7717866.883 | 223.844 | POOL 1 |
| 7648 | 07/30/2006 | 613036.34 | 7717861.964 | 223.921 | POOL 1 |
| 7649 | 07/30/2006 | 613051.131 | 7717856.715 | 223.906 | POOL 1 |
| 7650 | 07/30/2006 | 613064.224 | 7717853.77 | 223.926 | POOL 1 |
| 7651 | 07/30/2006 | 613070.679 | 7717867.707 | 223.822 | POOL 1 |
| 7652 | 07/30/2006 | 613050.993 | 7717879.864 | 223.895 | POOL 1 |
| 7653 | 07/30/2006 | 613035.656 | 7717894.211 | 223.831 | POOL 1 |
| 7654 | 07/30/2006 | 613011.21 | 7717911.632 | 223.845 | POOL 1 |
| 7655 | 07/30/2006 | 612987.936 | 7717921.759 | 223.936 | POOL 1 |
| 7656 | 07/30/2006 | 612973.345 | 7717918.262 | 223.952 | POOL 1 |
| 7657 | 07/30/2006 | 612967.472 | 7717912.15 | 223.908 | POOL 1 |
| 7658 | 07/30/2006 | 613020.37 | 7717922.225 | 226.608 | TOP |
| 7659 | 07/30/2006 | 613038.519 | 7717897.84 | 224.609 | TOPO_PT |
| 7660 | 07/30/2006 | 613045.38 | 7717905.056 | 225.041 | TOPO_PT |
| 7661 | 07/30/2006 | 613061.992 | 7717895.352 | 224.106 | TOPO_PT |
| 7662 | 07/30/2006 | 613059.862 | 7717881.688 | 224.707 | TOPO_PT |
| 7663 | 07/30/2006 | 613072.168 | 7717872.042 | 224.153 | TOPO_PT |
| 7664 | 07/30/2006 | 613077.847 | 7717877.331 | 224.943 | TOPO_PT |
| 7665 | 07/30/2006 | 613085.158 | 7717882.447 | 223.941 | TOPO_PT |
| 7666 | 07/30/2006 | 613013.494 | 7717859.013 | 227.246 | TOP |
| 7667 | 07/30/2006 | 613083.444 | 7717820.316 | 229.416 | TOP |
| 7668 | 07/30/2006 | 613086.705 | 7717833.222 | 227.183 | TOP |
| 7669 | 07/30/2006 | 613092.961 | 7717843.318 | 224.133 | TOE |
| 7670 | 07/30/2006 | 613095.217 | 7717850.208 | 224.02 | TOPO_PT |
| 7671 | 07/30/2006 | 613097.727 | 7717857.387 | 223.374 | POOL |
| 7672 | 07/30/2006 | 613101.882 | 7717862.261 | 223.336 | POOL |
| 7673 | 07/30/2006 | 613093.965 | 7717866.999 | 223.414 | POOL |
| 7674 | 07/30/2006 | 613075.378 | 7717897.691 | 223.223 | POOL 2 |
| 7675 | 07/30/2006 | 613080.548 | 7717893.617 | 223.258 | POOL 2 |
| 7676 | 07/30/2006 | 613086.751 | 7717893.209 | 223.134 | POOL 2 |
| 7677 | 07/30/2006 | 613096.848 | 7717879.013 | 223.276 | POOL 2 |
| 7678 | 07/30/2006 | 613107.413 | 7717864.762 | 223.238 | POOL 2 |
| 7679 | 07/30/2006 | 613116.186 | 7717844.289 | 223.25 | POOL 2 |
| 7680 | 07/30/2006 | 613124.352 | 7717832.813 | 223.205 | POOL 2 |
| 7681 | 07/30/2006 | 613143.547 | 7717818.125 | 223.143 | POOL 2 |
| 7682 | 07/30/2006 | 613157.933 | 7717820.193 | 223.306 | POOL 2 |
| 7683 | 07/30/2006 | 613163.555 | 7717822.515 | 223.265 | POOL 2 |
| 7684 | 07/30/2006 | 613150.032 | 7717834.856 | 223.244 | POOL 2 |
| 7685 | 07/30/2006 | 613153.067 | 7717842.492 | 223.261 | POOL 2 |
| 7686 | 07/30/2006 | 613172.804 | 7717834.425 | 223.271 | POOL 2 |
| 7687 | 07/30/2006 | 613185.93 | 7717825.005 | 223.239 | POOL 2 |
| 7688 | 07/30/2006 | 613171.298 | 7717844.546 | 223.31 | POOL 2 |
| 7689 | 07/30/2006 | 613152.259 | 7717855.068 | 223.284 | POOL 2 |
| 7690 | 07/30/2006 | 613136.568 | 7717866.328 | 223.228 | POOL 2 |
| 7691 | 07/30/2006 | 613118.559 | 7717875.636 | 223.179 | POOL 2 |
| 7692 | 07/30/2006 | 613110.806 | 7717881.459 | 223.283 | POOL 2 |

## Table E.1: 2006 Total station survey data for Feldheimer bar (RKM 30)

| Point # | Date | Northing (ft) | Easting (ft) | Elevation (ft) | Description |
|---|---|---|---|---|---|
| 7693 | 07/30/2006 | 613125.009 | 7717890.475 | 228.724 | TOP |
| 7694 | 07/30/2006 | 613153.888 | 7717837.03 | 223.449 | TOPO_PT |
| 7695 | 07/30/2006 | 613167.015 | 7717858.936 | 226.211 | TOP |
| 7696 | 07/30/2006 | 613186.402 | 7717820.665 | 223.302 | TOPO_PT |
| 7697 | 07/30/2006 | 613180.886 | 7717806.541 | 223.497 | TOPO_PT |
| 7698 | 07/30/2006 | 613142.766 | 7717807.118 | 227.027 | TOP |
| 7699 | 07/30/2006 | 613232.79 | 7717802.708 | 223.927 | TOPO_PT |
| 7700 | 07/30/2006 | 613219.867 | 7717787.723 | 223.561 | TOPO_PT |
| 7701 | 07/30/2006 | 613207.872 | 7717775.9 | 224.487 | TOPO_PT |
| 7702 | 07/30/2006 | 613241.865 | 7717816.796 | 225.793 | TOP |
| 7703 | 07/30/2006 | 613241.51 | 7717814.889 | 224.087 | TOE |
| 7704 | 07/30/2006 | 613250.419 | 7717795.705 | 223.147 | TOPO_PT |
| 7705 | 07/30/2006 | 613239.242 | 7717778.619 | 223.949 | TOPO_PT |
| 7706 | 07/30/2006 | 613224.156 | 7717768.464 | 224.696 | TOPO_PT |
| 7707 | 07/30/2006 | 613205.158 | 7717755.034 | 228.494 | TOP |
| 7708 | 07/30/2006 | 613270.197 | 7717784.641 | 221.321 | POOL |
| 7709 | 07/30/2006 | 613274.791 | 7717781.35 | 220.895 | POOL |
| 7710 | 07/30/2006 | 613283.225 | 7717778.615 | 220.566 | POOL |
| 7711 | 07/30/2006 | 613274.421 | 7717778.206 | 220.865 | POOL |
| 7712 | 07/30/2006 | 613272.122 | 7717776.352 | 221.155 | POOL |
| 7713 | 07/30/2006 | 613270.722 | 7717773.87 | 221.899 | TOPO_PT |
| 7714 | 07/30/2006 | 613261.763 | 7717767.287 | 223.251 | TOPO_PT |
| 7715 | 07/30/2006 | 613276.259 | 7717768.468 | 222.219 | TOPO_PT |
| 7716 | 07/30/2006 | 613285.578 | 7717766.55 | 221.112 | TOPO_PT |
| 7717 | 07/30/2006 | 613285.467 | 7717779.506 | 220.611 | WATER_E |
| 7719 | 07/30/2006 | 613263.136 | 7717798.582 | 224.196 | TOP |
| 7720 | 07/30/2006 | 613258.297 | 7717755.356 | 224.583 | TOP |

Note: Northings and Eastings are in NAD83 Oregon North State Plane Projection. Elevations are relative to the NAVD88 vertical datum.

## Table E.2: 2006 Total station survey data for Eagle Creek bar (RKM 26)

| Point # | Date | Northing (ft) | Easting (ft) | Elevation (ft) | Description |
|---|---|---|---|---|---|
| 0002 | 07/31/2006 | 623193.315 | 7717187.880 | 178.42 | GW WELL 1 |
| 0003 | 07/31/2006 | 623813.82 | 7716717.63 | 174.76 | DS WATER EDGE |
| 0001 | 07/31/2006 | 620628.2 | 7717437.82 | 198.48 | US WATER EDGE |
| 5000 | 07/31/2006 | 621178.519 | 7717648.343 | 194.726 | WATER EDGE |
| 5001 | 07/31/2006 | 621193.779 | 7717670.989 | 194.544 | WATER EDGE |
| 5002 | 07/31/2006 | 621193.196 | 7717678.676 | 194.469 | WATER EDGE |
| 5003 | 07/31/2006 | 621208.644 | 7717690.839 | 194.457 | WATER EDGE |
| 5004 | 07/31/2006 | 621221.798 | 7717706.858 | 194.347 | WATER EDGE |
| 5005 | 07/31/2006 | 621231.431 | 7717721.561 | 194.409 | WATER EDGE |
| 5006 | 07/31/2006 | 621248.567 | 7717747.643 | 194.216 | WATER EDGE |
| 5007 | 07/31/2006 | 621265.997 | 7717763.446 | 194.121 | WATER EDGE |
| 5008 | 07/31/2006 | 621286.024 | 7717784.053 | 193.984 | WATER EDGE |
| 5009 | 07/31/2006 | 621289.654 | 7717807.089 | 194.087 | WATER EDGE |
| 5010 | 07/31/2006 | 621296.672 | 7717826.703 | 193.932 | WATER EDGE |
| 5011 | 07/31/2006 | 621306.798 | 7717856.662 | 193.591 | WATER EDGE |
| 5012 | 07/31/2006 | 621325.483 | 7717890.75 | 193.14 | WATER EDGE |
| 5013 | 07/31/2006 | 621329.081 | 7717914.672 | 192.904 | WATER EDGE |
| 5014 | 07/31/2006 | 621349.032 | 7717924.485 | 192.551 | WATER EDGE |
| 5015 | 07/31/2006 | 621348.476 | 7717943.296 | 192.353 | WATER EDGE |
| 5016 | 07/31/2006 | 621341.677 | 7717959.842 | 191.833 | WATER EDGE |
| 5017 | 07/31/2006 | 621338.68 | 7717974.533 | 190.599 | WATER EDGE |
| 5018 | 07/31/2006 | 621355.387 | 7717973.432 | 190.555 | WATER EDGE |
| 5019 | 07/31/2006 | 621383.509 | 7717980.099 | 190.647 | WATER EDGE |
| 5020 | 07/31/2006 | 621393.014 | 7717979.396 | 190.62 | WATER EDGE |
| 5021 | 07/31/2006 | 621396.997 | 7717974.698 | 190.712 | WATER EDGE |
| 5022 | 07/31/2006 | 621420.73 | 7717981.596 | 190.699 | WATER EDGE |
| 5023 | 07/31/2006 | 621450.922 | 7717996.105 | 190.696 | WATER EDGE |
| 5024 | 07/31/2006 | 621472.372 | 7717997.643 | 190.739 | WATER EDGE |
| 5025 | 07/31/2006 | 621506.086 | 7718000.985 | 190.652 | WATER EDGE |
| 5026 | 07/31/2006 | 621530.185 | 7717997.939 | 190.679 | WATER EDGE |
| 5027 | 07/31/2006 | 621538.744 | 7718012.691 | 190.616 | WATER EDGE |
| 5028 | 07/31/2006 | 621574.194 | 7718019.232 | 190.448 | WATER EDGE |
| 5029 | 07/31/2006 | 621602.536 | 7718021.328 | 190.378 | WATER EDGE |
| 5030 | 07/31/2006 | 621628.723 | 7718014.982 | 190.121 | WATER EDGE |
| 5031 | 07/31/2006 | 621642.024 | 7718009.617 | 189.301 | WATER EDGE |
| 5032 | 07/31/2006 | 621654.329 | 7718002.221 | 188.744 | WATER EDGE |
| 5033 | 07/31/2006 | 621682.423 | 7718011.039 | 188.341 | WATER EDGE |
| 5034 | 07/31/2006 | 621711.064 | 7718021.153 | 187.478 | WATER EDGE |
| 5035 | 07/31/2006 | 621735.793 | 7718023.426 | 186.67 | WATER EDGE |
| 5036 | 07/31/2006 | 621761.851 | 7718019.897 | 186.532 | WATER EDGE |
| 5037 | 07/31/2006 | 621790.818 | 7718017.391 | 186.37 | WATER EDGE |
| 5038 | 07/31/2006 | 621821.925 | 7718012.681 | 186.268 | WATER EDGE |
| 5039 | 07/31/2006 | 621853.866 | 7718005.361 | 186.22 | WATER EDGE |
| 5040 | 07/31/2006 | 621886.89 | 7717996.561 | 186.265 | WATER EDGE |
| 5041 | 07/31/2006 | 621913.798 | 7717989.792 | 186.227 | WATER EDGE |
| 5042 | 07/31/2006 | 621946.649 | 7717983.607 | 186.159 | WATER EDGE |
| 5043 | 07/31/2006 | 621972.775 | 7717991.414 | 185.797 | WATER EDGE |
| 5044 | 07/31/2006 | 621988.485 | 7717997.05 | 185.441 | WATER EDGE |
| 5045 | 07/31/2006 | 621997.656 | 7718007.023 | 184.886 | WATER EDGE |
| 5046 | 07/31/2006 | 622016.495 | 7717995.309 | 184.866 | WATER EDGE |
| 5047 | 07/31/2006 | 622043.621 | 7717982.09 | 184.932 | WATER EDGE |
| 5048 | 07/31/2006 | 622069.515 | 7717962.748 | 184.923 | WATER EDGE |
| 5049 | 07/31/2006 | 622090.563 | 7717943.018 | 184.763 | WATER EDGE |
| 5050 | 07/31/2006 | 622113.902 | 7717922.797 | 184.822 | WATER EDGE |